PHOTOACTIVATED FIXATION OF CARTILAGE TISSUE

A Dissertation
Presented to
The Academic Faculty

By

Valerie B. Sitterle

In Partial Fulfillment
Of the Requirements for the Degree
Doctor of Philosophy in
The George W. Woodruff School of Mechanical Engineering

Georgia Institute of Technology
[August 2004]

PHOTOACTIVATED FIXATION OF CARTILAGE TISSUE

Marc E. Levenston, Chair

David L. McDowell

Raymond P. Vito

Mostafa A. El-Sayed

Nan Marie Jokerst

Date Approved: 30 August 2004

.

DEDICATION

For Mom, Dad, and Jeff.

ACKNOWLEDGEMENT

There are many whose assistance was invaluable to the successful completion of this research. Thank you to:

- Georgia Tech Research Institute (GTRI), the GTRI Fellows Council, and my immediate supervisors over the years – Randy Case, David Parekh, Steve Cross, Robert Hyde, William Owens, George Harrison, and Ed Reedy – for supporting my education, and providing the time and resources necessary to complete this research;
- Dennis Brown and GTRI Machine Services for work on the mechanical test components;
- Lisa Detter-Hoskin and Erin Prowett in the GTRI Materials Analysis Center for their assistance with the FTIR measurements;
- Michael Knotts and Curtis Volin for help designing the optical system configurations;
- Glenn Champion and Steve Sharpe for the electronic system integration;
- David Roberts and David Gottfried for support and technical expertise;
- Wei Sun for his assistance with the ABAQUS modeling;
- The members of my thesis committee for their patience, support, and technical suggestions during what turned out to be a rather creative degree process;
- William Wepfer for his never-ending faith, support, and guidance.

Finally, thank you to my colleagues in the Levenston laboratory: Marine Amouroux, John Connelly, Crystal Hsu, Stacy Imler, Onyi Irrechukwu, Janna Mouw, Ashley Palmer, Wei Sun, Eric Vanderploeg, and Chris Wilson. I cannot say enough about their patience, training, technical assistance, support, and humor.

TABLE OF CONTENTS

LIST OF TABLES

LIST OF FIGURES

LIST OF SYMBOLS AND ABBREVIATIONS

$d\varepsilon/dt$	strain rate
λ	wavelength
μ_a, μ_s, μ_s'	absorption, scattering, and reduced scattering coefficients
μ_i	population mean
φ	fluence rate
φ^f	effective porosity
σ_i	population standard deviation
τ	time constant
ν	Poisson's ratio
A	optical proportionality constant
a	crack length or characteristic length as defined
c	statistical proportionality constant
D_{eff}	effective penetration depth
E	Young's modulus
g	anisotropy factor
h	adherend thickness
H_A	aggregate modulus
K	diffusive drag coefficient
k_p	hydraulic permeability
l	length
M	bending moment

n_{COL},n_{GS}	refractive index of collagen, ground substance
O_2^1	singlet oxygen
p	characteristic power of a distribution
P	load (axial)
r_{SC}	Fresnel surface reflection
S_i	sample standard deviation
$X_{i\bullet}$	sample mean
X_{ij}	data point of a statistical group
z	depth

AB/AM	antibiotic/antimycotic
ACI	autologous chondrocyte implantation
AGE	advanced glycation endproducts
ANOVA	analysis of variance
ATR	attenuated total reflectance
BSA	bovine serum albumin
CASPc	chloro-aluminum phthalocyanine tetrasulfonic acid
CCD	charge-coupled device
DMEM	Dulbecco's modified Eagle medium
FBS	fetal bovine serum
EDC	1-ethyl-3-(-3-dimethylaminopropyl)-carbodiimide
Eth-D-1	ethidium homodimer-1

FTIR	Fourier transform infrared spectroscopy
HG-DMEM	high glucose Dulbecco's modified Eagle medium
ICG	indocyanine green
LED	light emitting diode
NIR	near infrared
NHS	N-hydroxyly succinimide
OA	osteoarthritis
OATS	osteochondral autograft transfer system
PBS	phosphate buffered saline
pDAB	p(dimethylamino)benzaldehyde
PDT	photodynamic therapy
RA	rheumatoid arthritis
R5P	riboflavin-5-phosphate
sGAG	sulfated glycosaminoglycans
T4MPyP-tt	meso-tetra(N-methyl-4-pyridyl)porphine tetra tosylate
TBR	tetrabromorhodamine-123
TE	tissue engineered
UHMWPE	ultra high molecular weight polyethylene
UV	ultraviolet
ZNSPc	zinc phthalocyanine tetrasulfonic acid

SUMMARY

Articular cartilage degradation, whether caused by injury or arthritis, affects a tremendous number of patients worldwide. Since cartilage is an avascular tissue, it does not heal or regenerate like other tissues such as skin or bones. Therefore, after trauma to the cartilage surface, the damage continues to degrade until severe pain and inhibited mobility, especially in the load-bearing knee and hip joints, necessitate extreme treatments such as total joint replacement. New treatment options involving implants from cellular or tissue-based materials show promise for treatment of localized defects, and that the new cartilage will integrate with its surrounding host tissue if it can remain effectively secured. A critical issue for the success of tissue-based repair, however, remains the adequate initial fixation of the implant so that it remains in place until the native tissue and implant can integrate. Such fixation should not prevent any biological integration that can occur or induce substantial new trauma to the tissue.

A possible approach involves the application of a photosensitive material, which is then activated with a light source to attach the implant and host tissues together in either a photothermal or photochemical process. A combination of cartilage-specific factors, such as high collagen content and a biphasic functionality, suggests significant potential for photochemical bonding, a method that typically employs excitation wavelengths unmanageable for more vascularized tissues. The present study therefore investigates whether photoactivated bonding of a cartilage-cartilage interface can be achieved, thereby offering a viable method for more effective repair of damaged articular surfaces.

CHAPTER I.

INTRODUCTION

Articular cartilage degradation, whether caused by injury, osteoarthritis (OA), or a systemic disease such as rheumatoid arthritis (RA), affects a significant number of orthopaedic patients worldwide, resulting in pain and inhibited mobility. Traumatic injury or disease of cartilage in load bearing joints such as the knee and hip can be particularly debilitating given the incapacity of cartilage for self-repair and the lack of effective treatment options which halt further degeneration. OA alone affects an estimated 21 million Americans, with incidence expected to rise. While prevailing assumptions that OA is age- and weight-related are correct, it is also true that nearly 60% of arthritis sufferers are currently younger than 65, with incidence of traumatic cartilage injury increasing among sports-involved youth and an increasingly active population. Medical and other arthritis-associated costs have already reached $65 billion. [1]

Traditional treatment options, progressively ranging from pharmacologic pain-management to total joint replacement, are intended only to manage or replace the affected area. Newer treatment options involving implants from cellular- or tissue-based materials show promise for treating localized defects. Initial efforts using these tissue-engineered (TE) approaches demonstrate that the new cartilage will integrate with surrounding tissue if it can remain effectively secured, but current fixation methods using fibrin-based adhesives or sutures have not provided an effective solution. The critical issue in any replacement or repair of articular cartilage trauma therefore remains effective

attachment of the implant material, whether artificial or biological in nature, to the relevant joint surfaces.

The concept of attaching tissue using photothermal or photochemical methods is currently undergoing extensive study. While most efforts involve tissues other than cartilage, cartilaginous tissues are in great need of an adhesive-type of fixation that will provide an implant with adequate initial stability but not cause excessive damage to either the implant or surrounding tissue. This work examines the basic feasibility of the photochemical approach specifically as applied to cartilaginous tissues.

Investigations begin with model protein irradiation studies where collagen alone is subjected to irradiation and photosensitization, both individually and in combination. Fourier transform infrared spectroscopy (FTIR) is then used to evaluate the effects of the photochemical modification. As a potential enhancement to the process, matching the refractive index of the collagen fibrils to the ground substance in the tissue as a means to optically clear the cartilage is also evaluated. The study then reports on benchtop mechanical testing of photochemically bonded cartilage tissues and culminates with a culture test to assess viability and strength over seven days.

Some of the work in this dissertation has been previously presented and included in conference proceedings. General background review of photothermal and photochemical bonding as specifically associated with cartilage as well as a portion of the FTIR results were presented at The International Society for Optical Engineering Biomedical Optics Symposium (SPIE BiOS) in San Jose, CA in January 2003 and included in the conference proceedings.[2]

CHAPTER II.

BACKGROUND

Tissue Structure and Function

Healthy articular cartilage, a specialized form of hyaline cartilage, covers the articulating surfaces of the femoral condyles, tibial plateaus, and backside of the patella, as well as surfaces in other articulating joints. It functions primarily to ease relative movement between the surfaces with its exceptionally low coefficient of friction. Both the lateral and medial compartments of the tibiofemoral joint contain a meniscus, a crescent-shaped cushion of fibrocartilage that reduces stress on the underlying articular surfaces by increasing the contact area. Absence of (from surgical removal) or injury to a meniscus increases the stress and otherwise alters the load transmitted to the articular cartilage, thereby causing damage to the articular surface as well.

One of the differences between articular cartilage and meniscal fibrocartilage is the type of collagen that functions as the primary structural component. Particular collagens differ in their amino acid compositions that link in a linear fashion to form polypeptide chains (polymers) and are classified accordingly. The importance is that the amino acid sequence determines a protein's structure. For example, type-I collagen, the dominant type in fibrocartilage like the meniscus, consists of two identical chains and one different chain. It is the only heteropolymer among collagens. Type-II collagen, only

found in hyaline cartilage, has only one chain type. As a structural component, each collagen molecule's three polypeptide chains wind around each other in a triple helix configuration. Similar to twisted rope fibers, these chains convert a longitudinal tensile force to a more easily managed lateral compressive force exerted on the heart of the triple helix. The twist in the helix cannot be pulled out under tension because the polypeptide chains are twisted in opposite directions and covalently bonded together. Various types of collagen molecules present in a given tissue also assemble to form even larger bundles (fibrils) or sheets depending on the tissue type.[3]

In its native form, collagen consists of 33% glycine (Gly), and another 15-30% proline or hydroxyproline amino acid residues. The individual peptide chains are staggered such that the N-H group of each glycine forms a strong hydrogen bond with the carbonyl oxygen of an X residue on an adjacent chain. This ensures the triple-helical configuration described previously. The short ends on each peptide chain that are not bound into the helical configuration are then involved in crosslinking of the collagen molecule to other collagen molecules in addition to other molecular components in the surrounding environment.[3,4,5] An illustration showing how these various polypeptide chains form collagen molecules, and collagen molecules in turn form a fibril, is shown in Figure 1.

Collagen is nearly devoid of cysteine residues and so its covalent crosslinks across molecules are not disulfide bonds like those found in the skin protein keratin.[3] (Collagen III is the exception here, containing a C-terminal cysteine-cysteine sequence that form intramolecular and interfibrillar collagen III crosslinks.)[4] Instead, collagen crosslinks are derived from lysine and histidine residues in an enzyme-mediated process.

This enzyme, lysyl oxidase, creates crosslinks via two pathways: oxidizing lysine or hydroxylysine residues. Briefly the enzyme oxidizes these residues to an aldehyde form that can then react with neighboring amino groups or aldehydes to form the covalent crosslinks that result in a collagen fibril.[4,6]

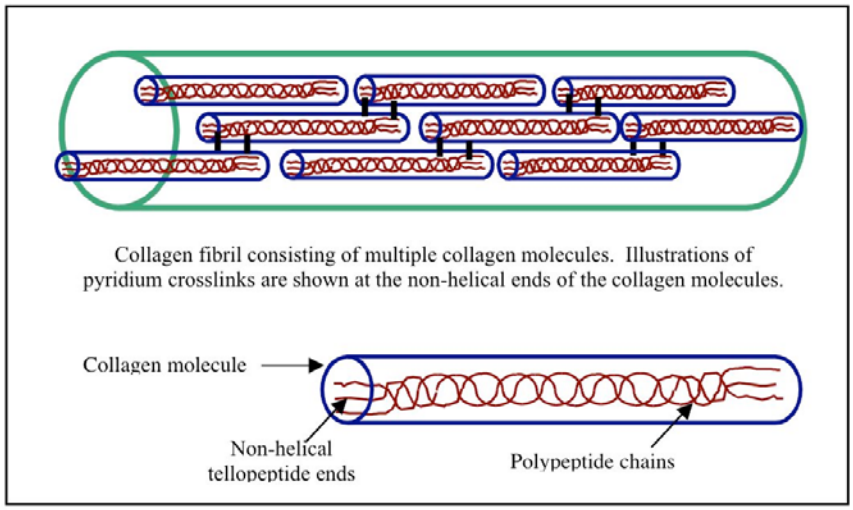

Figure 1: Illustration of collagen fibrillar and molecular architecture

One of the end products of hydroxylysine-lysyl oxidase pathway is the formation of pyridinium crosslinks. These intermolecular crosslinks account for greater than 90% of the crosslinks found in type II collagen in articular cartilage, which is nearly two-fold higher than their percentage expressed in type I collagen.[4,7] This may be expected since compared to type I collagen, collagen II contains more hydroxylysine residues.[5,8] The absence of the pyridinium crosslinks in skin and corneal collagen may be due to sunlight

exposure since the pyridinium crosslink is rapidly destroyed when subjected to ultraviolet (UV) radiation.[4]

Articular cartilage consists of chondrocyte cells embedded in an extracellular matrix that is approximately 65-80% water. It is, however, a relatively acellular material with chondrocytes comprising less than 5% of the total volume. The primary solid components are proteoglycans, an extracellular aggregate of proteins and carbohydrates, and collagen, a structural protein found throughout the body and especially prevalent in connective tissues. Proteoglycans and type-II collagen make up 15-30% and 50-73% of the dry weight respectively. Both the macromolecular organization and composition vary with depth from the surface as the collagen fibrils vary orientation and the proteoglycan content increases according to depth in the tissue. This results in heterogeneous mechanical properties. At the surface, collagen fibrils are oriented tangential to the surface, providing a tensile strength under deformation in a given contact area (not the whole surface area). In the deepest layer, the cartilage becomes calcified and the fibrils reach down perpendicularly from the cartilage to anchor into the bone. This entire structure is only 2-4mm thick in humans. [9,10] An illustration of the collagen fibril network in articular cartilage may be found in Figure 2.

Although the collagen fibrils give the tissue a tensile strength under loading, the proteoglycans and water contribute to the compressive strength of the tissue as fluid exudes upon compression and resorbs after the load is removed. In response to a compressive load, fluid in the tissue is initially pressurized and transmits the majority of the applied force down to the bone via hydrostatic pressure. The negative charge of the proteoglycans increases as they are forced closer together, and permeability of the surface

is reduced such that fluid may only exude laterally through the tissue. Frictional resistance to this interstitial fluid flow by the permeable solid matrix results in a complex, history-dependent and environmentally (temperature, pH, etc.) dependent, viscoelastic mechanical behavior. [11,12]

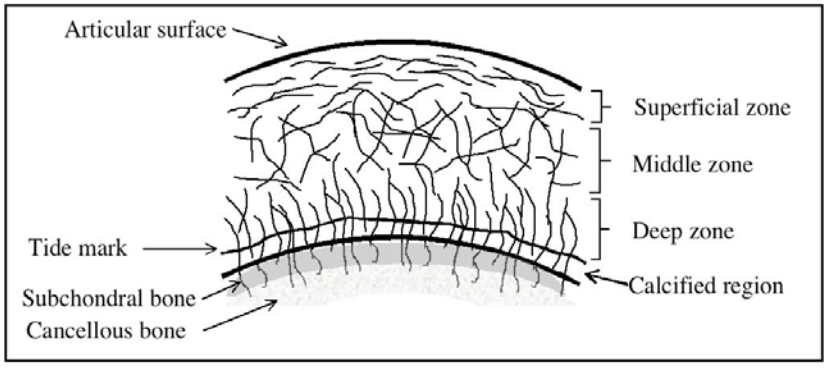

Figure 2: Schematic diagram of collagen fibril network in articular cartilage

By comparison, the fibrocartilage of the meniscus consists of approximately 60-70% water, 22% collagen, and only 1% proteoglycans. Note that unlike articular cartilage, type I collagen is dominant, comprising nearly 90% of the collagen found in fibrocartilage, and the proteoglycan content is considerably lower. A related difference is that when compared to type II collagen, type I collagen contains fewer hydroxylysine residues as well as glucosyl and galactosyl residues that mediate interaction of the collagen molecules with neighboring proteoglycans.[5] Of the semi-lunar shape of the menisci, approximately the outer third is vascularized while the inner third portion is

avascular and does not initiate healing in response to an injury. Large collagen bundles are arranged circumferentially with smaller, radially directed connective fibers providing additional structural support.[13,14] An illustration of the major zones and internal structure is depicted in Figure 3.

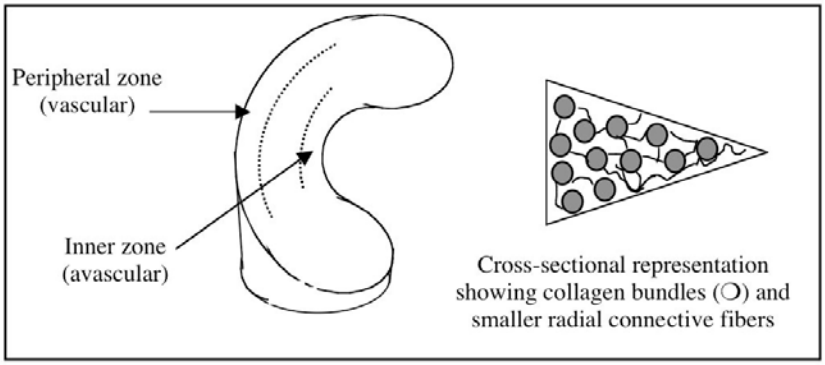

Figure 3: Schematic diagram of meniscal fibrocartilage showing vascular zones and cross-sectional fibril network arrangement

Cartilage Injury and Treatment Options

Traditional methods of treatment for cartilage degeneration beyond simple pharmacologic pain management have been articular surface debridement, surgical surface removal and/or cleansing, followed by eventual total joint replacement. Though a suitable option for older patients, the expected ten to fifteen year functionality of joint

replacements does not provide an optimal solution for younger candidates expected to outlive the implant.

Both meniscal and articular cartilage damage may require repair to prevent subsequent tissue degeneration on a larger scale. For the meniscus, its structure coupled with its fibrous attachments to the anterior and posterior of the tibial plate allows a large compressive load to be translated into a tensile stress. Tears may occur in a number of orientations, vascular or avascular regions, and may be full or partial thickness in nature. The primary meniscal tearing modes are:

a) Vertical tears: These occur in a circumferential direction and may or may not heal depending on their severity and the zone in which they occur.
b) Radial tears: These tears commonly occur after rupture of the anterior cruciate ligament and occur in the radial direction.
c) Horizontal tears: Also called cleavage tears, these tears penetrate downward into the depth of the meniscus and are difficult to repair.
d) Degenerate and complex tears: These may occur in a variety of configurations and may affect two or more planes of the meniscus.

Generally speaking, for minor trauma, meniscal repair is approached via debridement and removal of loose pieces or flaps. For more severe tears, however, sutures or various biodegradable devices such as arrows or darts are used to hold the tissue fragments together, with suturing remaining the gold standard in terms of strength.[15]

Severe articular surface degeneration, especially when it reaches the stage where bone wears on bone, will require a total surface (or at least a significant portion of the surface) replacement. Most cartilage injuries, however, begin in a manner that an

effective repair technique could potentially prevent or significantly delay future degeneration of this magnitude. Conditions such as osteochondrosis dissecans and particularly traumatic lesions or fissures tend to exhibit very localized matrix degeneration with intact surrounding cartilage tissue in their early stages of presentation and are therefore candidates for tissue repair strategies.[8] In general, cartilage defects, illustrated in Figure 4, can be classified as:

- Chondral defects limited to the cartilage tissue in terms or depth
- Osteochondral defects penetrating the underlying subchondral bone
- Fissures (cracks) and tears, which typically occur on a chondral level, but have been known to penetrate the subchondral bone; these can be horizontal, vertical, or oblique.

Attempts to stimulate cartilage repair through more biologically oriented treatments such as allograft (same species) or autograft (self) osteochondral transplantation (OATS, Mosaicplasty), subchondral drilling, microfracture, or abrasion arthroplasty have been investigated, but are still unproven or even inferior as to their long-term success or broad applicability. Many of these repair techniques are limited in the extent of the chondral lesion that can be treated due to donor site morbidity or a simple physiologic limit on the amount of graft tissue available. For example, autograft transfers have been limited to chondral lesions up to 15mm in diameter. [16,17]

Autologous chondrocyte implantation (ACI, licensed as Carticel by Genzyme Corporation), in which debridement is followed by sewing a periosteal (bone membrane) flap over the injured area and implanting cultured chondrocytes underneath, is limited to treatment of femoral condyle lesions 1 to 10 cm^2. While this has met with some success,

there has been considerable difficulty with the liquid cellular suspension staying in place. Considerable efforts have therefore been expended to modify this treatment such that a three-dimensional construct could be inserted instead: Genzyme is in preclinical development for Carticel II, a pre-formed graft that precludes the need for a periosteal securing flap [18,19]; Verigen has developed Matrix-Induced Chondrocyte Implantation (MACI), using fibrin glue (fibrin being a blood clotting protein) to secure a collagen scaffold seeded with harvested cells [20,21]; and a group at the Istituti Ortopedici Rizzoli has begun clinical trials with Hyalograft C, a scaffold based on hyaluronic acid. [22] Limited studies have shown that the implant will express a hyaline type cartilage and integrate with its surrounding tissue if it stays in place. This issue of adequate, reliable initial fixation to the relevant joint surfaces has been critical to the clinical outcomes of any implant to repair or replace damaged cartilage.

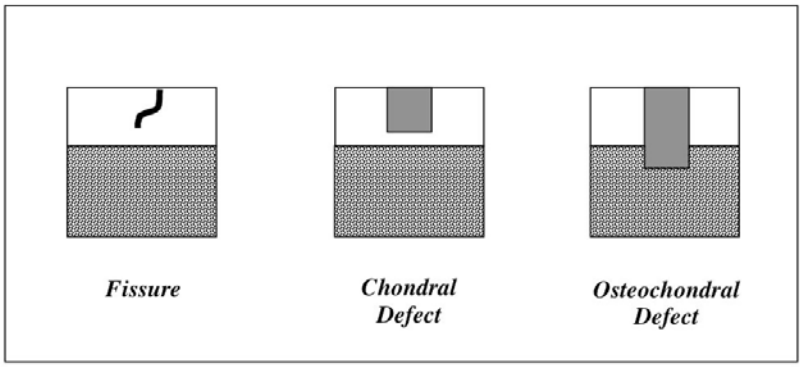

Figure 4: Illustration of defect types in articular cartilage

Soft Tissue Fixation and Repair of the Cartilage-to-Cartilage Interface

There are essentially three main methods of fixation investigated and used when one desires to attach a tissue or other implant to bone: mechanical (sutures, pins, screws, etc.), adhesive, or osseoinductive (inducing bone to grow into the tissue/implant). Of these, adhesive fixation has received the most effort in cartilage implant attachment to date. This is due in part to the desire to avoid bulk discontinuities such as those caused by even biodegradable pins or screws in a tissue that does not regenerate or heal, and partially because any osseoinductive approach requires first that the implant be securely fixed for bone ingrowth to occur. Yet years of adhesive research have yielded little or no success developing products that set rapidly in pliant tissues under physiologic conditions and have any demonstrable strength without the addition of toxic cross-linking agents such as glutaraldehyde. Methods in current clinical practice for securing the both the second generation Autologous Chondrocyte Implantation (ACI, implantation of cultured chondrocytes for focal defect repair) style products as well as chondral flap or fissure repair still rely on sutures or fibrin-based glues for fixation. [23,24] Not only are the adhesive strengths of these fibrin compounds relatively weak, as shown in Table 1, but they have also been found to have a deleterious effect on chondral repair, inhibiting cell migration and even inducing chondrocytes to exhibit a fibroblast-like phenotype. [21,24,25]

Table 1: Shear Bond Strengths of Various Adhesives to Tissue

Adhesive Type	Shear Bond Strength Order of Magnitude (kPa)	Tissue Type	Reference
Cyanoacrylate	1000	General, soft	[26]
Gelatin/Resorcinol/ Formaldehyde	100	General, soft	[26]
Gelatin/Resorcinol/ Glyoxal	10	General, soft	[26]
Fibrin	10	General, soft	[26]
Fibrin	10-20	Cartilage	[23,24]
Fibrin	1 (@ 6 weeks)	Cartilage	[27]
Tissue Transglutaminase	25	Cartilage	[24]

Generally, in repair or replacement of cartilage tissues, it is desirable for some integration to occur between the host tissue and the repair site. This allows for nutrient transport, molecular deposition that enhances integrative fixation, and eventual stress transmission across the interface. For most cartilage implants in vivo, physical apposition alone is insufficient for integration to occur. It has been postulated that integration is directly related to collagen deposition – that effective transport and crosslinking of newly synthesized collagen molecules across a repair site may be vital to the repair process.[28,29] Recent experiments correlating collagen synthesis and deposition to strength of the repair site appear to support this theory. General experimental values of adhesive strength between cartilage tissue interfaces for explants cultured in bioreactors are summarized in Table 2.

Table 2: Shear Bond Strengths of Integrated Cartilage Explants or Constructs

Interface Strength (kPa)	Test Configuration	Culture	Reference
30	Single-lap shear	2 weeks explant culture	[28]
34	Single-lap shear	3 weeks explant bovine culture,	[30]
15-69	Single-lap shear	2 weeks explant culture	[31]
64	Tensile	6 weeks fibrin glue based construct porcine explant	[27]
254	Push-out (disc)	8 weeks PGA scaffold construct calf explant	[32]

Traditionally, joint strength in non-biological systems is defined as the maximum stress at which the joint integrity can be maintained. In biological tissues such as cartilage, which is biphasic, the rate of uniaxial displacement during bond strength testing must be small enough to minimize fluid pressurization effects. However, stress in this configuration will vary over the interfacial area, and tissue strength is typically three to four orders of magnitude greater than the adhesive strength. This means that measured joint strength is primarily dependent on the adhesive properties and geometry of the repair interface. A single-lap shear test in one study is thus not directly comparable to another depending on the uniaxial displacement rate or specimen geometry differences. This must be kept in mind when comparing strength values across adhesive, integrative repair, photothermal, or photochemical tissue fixation. [29,33]

Protein Crosslinking

There has been much interest in methods to crosslink proteins, especially collagen, as a means to strengthen or fix tissue or matrices prior to implantation. Reinforcing a collagenous matrix with additional, non-native crosslinks not only increases the bulk strength of the treated matrix, but also increases resistance to enzymatic degradation. Early techniques studied included dehydrothermal treatment and exposure to UV radiation. Dehydrothermal treatment, in which the excess moisture is removed from the collagen under vacuum prior to exposure to elevated temperatures, induces the formation of interchain peptide bonds.[34,35,36] Exposure to UV radiation elicits two competing processes: intermolecular crosslinking and cleavage of peptide bonds. The latter process dominates with increasing irradiation exposure to degrade the collagenous network through free radical mechanisms and has been shown to result in a decrease in biomechanical properties.[37,38,39]

In addition to UV exposure, glycation is another "natural' treatment resulting in the formation of crosslinks in collagenous tissues. It is well known that incubation of collagen in excess glucose solutions for extended periods of time induces increased crosslinking of the protein. This result is similar to the protein damage seen in diabetic conditions where the spontaneous reaction of reducing sugars with proteins results in a collection of end products more collectively known as advanced glycation end products (AGEs). The pathological implications of AGEs, specifically as related to diabetes and aging, have been highly studied, and the non-enzymatic crosslinking of proteins by AGEs is thought to be a primary cause of stiffening of diabetic tissues. [40,41] By altering both the

biochemical and biomechanical properties of the affected proteins, AGE accumulation is also thought to contribute to incidence of osteoarthritis.[42]

While the critical nature of oxidation reactions in glucose-induced crosslinking of proteins is common knowledge, the importance of the sequence of the glycation versus oxidation reactions and the molecular mechanisms involved are not fully understood. Some previous studies have found that although the presence of oxygen increased the rate of protein crosslinking by pentose reducing sugars such as ribose, it was not required. This is in direct contrast to observed crosslinking behavior with glucose. [43,44] Similar studies have also found ribose to increase in crosslinking of collagen at a faster rate than glucose, and found evidence that varying rates of crosslinking occur for different types of collagen. [40]

Chemical Crosslinking and the Concept of Molecular Spacing as a Limiting Factor

Since nearly all proteins may be conjugated with reagents reactive to and able to couple with amine groups, such reactivity is the most common characteristic among chemical crosslinking agents. Crosslinking methods for proteins can be essentially categorized as:

a) Agents that bridge amino groups of lysine or hydroxylysine residues:

   These residues are bridged on different polypeptide chains by monomeric or oligomeric crosslinks. Examples of such agents in this classification include glutaraldehyde, epoxy compounds, and the gardenia fruit-derived natural crosslinking agent genipin.

b) Agents that enable direct crosslinking of polypeptide chains via the formation of amide bonds:

Carbodiimides are an example of this type of crosslinking agent.

These crosslinking methods may also be thought of in terms of their formation of zero-length or non-zero-length crosslinks. For instance, some agents, such as glutaraldehyde, form a molecular bridge across different polypeptide chains, forming interchain crosslinks and even polymerizing themselves to further strengthen the modified polymer structure. In contrast, zero-length crosslinkers like carbodiimides consist of small molecules able to form a bond that contains no additional atoms. In this case, there are no intermediate molecules attaching an atom of one molecule to an atom of another, and thus no polymerization of the crosslinking agent that can add to the final treated ultrastructure.[45,46]

This concept has the very critical ramification that crosslinks can only be formed between two adjacent collagen microfibrils to form interfibrillar bonds, if the distance between the two microfibrils is smaller than the length of the crosslinking agent introduced. Consider the typical architecture of collagen fibers. An individual collagen molecule is formed via the intertwining of three polypeptide chains to form a right-handed suprahelical structure. These collagen molecules may then assemble into sheets or thick fibrils stabilized by hydrophobic interactions. The individual collagen molecules assembled into this fibrillar structure contain native intermolecular (between different adjacent tropocollagen molecules) and intramolecular (within an individual molecule) crosslinks.[3] When considering the scale of the individual collagen molecules and fibrils

formed, this gives an approximate distance of 1.3-1.7 nm as the critical parameter for crosslinking across fibrils by a foreign agent.[46]

Examples of Non-Zero Length Crosslinking Agents

Glutaraldehyde reacts with the ε–amino group of lysyl residues in proteins forming activated derivatives able to then form crosslinks with other protein chains in the form of Schiff base linkages with ε- or α-amines, vinyl addition to the glutaraldehyde polymer to create secondary amine bonds, or even reaction with ε-amines from two neighboring lysine residues to form a quaternary pyridium crosslink.[45] Glutaraldehyde itself polymerizes during this process, strengthening its fixation of treated tissue by forming crosslinks of varying lengths. It exhibits both hydrophilic and hydrophobic properties, and is therefore able to penetrate both aqueous media and liphophilic cellular membranes. While this enhances its ability as a fixative, glutaraldehyde is highly cytotoxic and also known to elicit calcification of treated tissues or matrices after implantation.[46,47,48]

Genipin reacts with the free amino groups in lysine, hydroxylysine, and arginine residues found in collagen. While the specific mechanism resulting in crosslinking of collagenous tissues or matrices with genipin is not completely understood, it is thought that genipin reacts with an amino acid to form a nitrogen-iridoid (an iridoid being an oxygenated hydrocarbon derivative commonly found in plants), which in turn undergoes dehydration to form an aromatic monomer. Dimerization and additional polymerization of the genipin itself then occurs. Genipin is therefore thought to form both

intermolecular and intramolecular crosslinks within collagen molecules, as well as interfibrillar crosslinks between adjacent collagen fibrils.[46,49]

These latter crosslinks are thought to result from polymerization of the genipin prior to crosslinking with a collagen fibril, thus providing non-zero length crosslinks similar to those formed by glutaraldehyde. It has been found that crosslinking of collagenous tissues treated with glutaraldehyde and genipin exhibit significantly greater strength, resistance to enzymatic degradation, and a higher denaturization temperature than untreated tissues.[46,47,48,50] Genipin, however, has been found to elicit much less cytotoxicity than glutaraldehyde.[46,49] Diimidoesters have also been investigated as crosslinkers of collagen matrices and were similarly found to increase resistance to enzymatic degradation and strength, although not to the same extent as glutaraldehyde since diimidoesters themselves do not polymerize. Increased tensile strength was found in the collagen matrix treated with a diimidoester creating S-S (disulfide) bonds above the matrix treated with the diimidoester that created C-C bonds.[48]

The Zero-Length Crosslinker Carbodiimide and its Use in Tissue Engineering

Carbodiimides are used to mediate the formation of linkages between an amine and carboxylate or between an amine and phosphate. Their efficiency in this process enables them to form conjugates between protein molecules, peptides and proteins, and between oligonucleotides and proteins given that the distance between linked groups is on the order of the carbodiimide molecule itself. The specific crosslinking mechanism involves the formation of an adduct between the carbodiimide and the carboxylic acid

groups of glutamic and aspartic acid residues in peptides, followed by a nucleophilic substitution with an amino group, most often the ε–amino group of a lysine residue.[45,46]

Addition of N-hydroxysuccinimde (NHS), an active ester that reacts rapidly with amines, to the carbodiimide solution has been shown to increase the efficiency of the carbodiimide-mediated process by increasing the number of crosslinks formed. This enhanced efficiency is due to the NHS suppression of side reactions, one being hydrolysis, that can occur when carbodiimide is used alone.[45] Being a zero-length crosslinking agent, carbodiimide can create intermolecular crosslinks between two adjacent collagen molecules, but carboxylic acid and amino groups on two adjacent collagen microfibrils are apparently too far apart to bridge and crosslink.[46]

Carbodiimides, particularly the watersoluble form 1-ethyl-3-(3-dimethylaminopropyl)-carbodiimide hydrochloride (EDC), have been extensively investigated as a means to couple collagen and glycosaminoglycans in tissue engineering matrices. Scaffolds of collagen coupled with a chondroitin sulfate as the glycosaminoglycan were seeded with fibroblasts[51] and chondrocytes[36,52,53,54,55], and evaluated for degree of initial matrix strength, degree of matrix contraction, and matrix synthesis by the cells after time in culture. While these EDC-treated matrices show potential as a means of generating a more complex, stronger tissue engineering scaffold, the crosslinking process requires conditions such that the cells must be injected or seeded onto the scaffolds after the process is complete and the scaffolds have undergone extensive washings to remove excess crosslinking reagents. The carbodiimide treatment therefore does not appear to show much promise for an in situ crosslinking process to adhere living tissues together.

Photoactivated Tissue Bonding Methods

Basic Concepts

Use of light to initiate a chemical reaction is a common process that may be generally broken down in to three basic steps as shown in Figure 5:

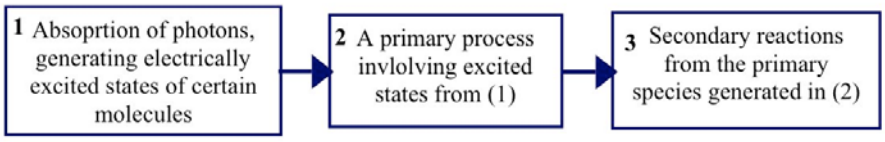

Figure 5: Photochemical process

Photothermal mechanisms, such as those in the albumin-chromophore soldering system described in the next section, rely on translational, rotational, or vibrational excitation. This means that photothermal excitation of a particular bond in a given molecular species can only be achieved by an increase in the overall energy of the molecular environment. [56,57] Photochemical excitation differs from the photothermal case in that it is characterized by the promotion of a valance electron from a σ or π bonding orbital to the corresponding σ^* or π^* anti-bonding orbital on a nanosecond timescale. Thus, the absorption of a photon can excite a specific bond or group in a given molecular

species. The photochemical process typically produces minimal thermal effects. Often the primary photochemical reaction is only a precursor to secondary reactions that actually cause polymerization or crosslinking of molecules. Type-I photochemical processes involve electron/hydrogen transfer directly from the photosensitizer, producing ions, or abstraction from a substrate molecule to form free radicals. Type II processes result from the direct interaction of the excited triplet state photosensitizer with molecular oxygen and the subsequent formation of singlet oxygen ($^1O_2$).

Photothermal Soldering and Critical Aspects that Specifically Affect Cartilage

Numerous efforts have investigated photothermal welding for vascular, urologic, or neurological applications. Studies with these tissues have found that applying a solder to help weld tissue gives superior results in terms of both strength and limiting surrounding tissue damage. Typically, these solders are based on albumin, a protein occurring in blood that becomes insoluble once denatured, mixed with a chromophore such as the cardio-dye indocyanine green (ICG). A laser diode operating around 808 nm, in the range of ICG's absorption peak, is then used to bond the tissue and solder together. This site-specific process occurs through selective absorption of the chromophore and subsequent thermal denaturation of the protein in the solder and the immediately adjacent tissue.[58,59,60,61] This particular method evolved from the initial application of tissue welding to vascular or urologic tissues. Initial attempts using CO2 lasers found the effect of water absorption in tissue severely limited penetration depth, resulting in an over-exposed outer and under-irradiated inner layer of tissue. Researchers then moved to

argon lasers, but found that haemoglobin in blood acted as a natural chromophore in this wavelength range, thereby coagulating the blood in addition to excessively heating the tissue. Efforts consequently shifted to using artificial chromophores well outside of the haemoglobin absorption bands but below the primary water absorption bands, hence the use of ICG. Further investigations have evaluated methylene blue (peak absorption at 664nm) doped albumin solders[62,63], solder reinforcement of albumin solders using polymer films[64] or other additives[65], and autologous protein solders developed from a patient's own plasma[66]. All have produced similar adhesive strengths on the order of 40-100 kPa.

There are appreciable differences between applying and refining photothermal soldering techniques for cartilage as compared to previous efforts involving vascularized tissues. For example, cartilage surgery is not subject to the same time constraints for welding tissue as that for arteries, and the treated tissue need not bear a mechanical load immediately as a consequence of its biological function. Cartilaginous tissues also do not have convective downstream heat transport due to blood flow, thereby potentially damaging other tissue and not efficiently heating the desired bond site. Optical data from septal and aural cartilage, as well as the one study on articular cartilage, show that cartilage is a highly effective scatterer at all wavelengths in the visible region with no endogenous chromophores in the visible portion of the spectrum unlike the haemoglobin peaks in vascularized tissues or melanin in dermal tissue. [67,68] With their greater tissue penetration when compared to shorter wavelength photoactive solders, photothermal solders such as the albumin solder doped with ICG (BSA-ICG) active in the NIR are therefore logical choices when striving to increase the optical penetration and subsequent

depth of treatment. Few photothermal studies have specifically investigated cartilage tissues, however. Note that results for tissue attachment of albumin-based solders vary according to weight-percent albumin, pressure applied to the weld during irradiation, and hydration post-irradiation, all in addition to the parameter sensitivity of mechanical testing mentioned previously, thereby making literature values for weld strengths not necessarily comparable.[69,70,71] Bearing this in mind, use of this approach for cartilage-to-cartilage fixation has shown mixed results, with the order of magnitude for weld strengths ranging from 10-100 kPa. Notice that bond strengths for cartilage, skin, nerves, and aorta are all within the same order of magnitude.

There are several observations reported from the studies highlighted in Table 3 that merit significant attention since they impact the clinical problem significantly. For example, live/dead viability testing utilizing calcein AM and ethidium homodimer-1 to indicate zones of cell death revealed twice the damage shown by conventional staining techniques. Cellular necrosis zones were detected up to approximately 500 μm from the weld site.[72] This region of cellular morbidity thus reaches 1 mm, where the thickness of articular cartilage in humans averages from 2-4 mm. In a tissue with limited cellular proliferation and regeneration capacity, damage of this type and extent could prove prohibitive to successful integration of a tissue engineered implant. In vivo studies using this technique, however, have not yet been reported.

The strength values for the baboon study appear noticeably higher than that achieved in other studies for several reasons. One, no specimen thickness was given; strength values in the citation were listed as force magnitudes since the authors found the fusion of solder and tissue to occur predominantly at the specimen surface and thus made

no attempt to normalize with respect to bond area. Chondral depth to calculate stress was therefore assumed as cited in the table. Also, if the strength values in terms of force are backed out of the stress values from the ovine study with similar test geometry, then the strengths are directly comparable (1.2 down to 0.7 N and 1.7 to 0.7 N for ovine and baboon respectively). Another difference is that the distracting force in the baboon study was applied perpendicular to 1 mm of tissue cut across the 5 mm width, with the remaining 4 mm being the weld length, instead of uniformly and normally across the solder area as in the other studies.

Additionally, note that with the exception of the bovine concentric disc configuration, all of these strength values were obtained from rectangular tissue specimens that were irradiated on both major sides of the weld site. In vivo, irradiating top and bottom of a tissue bond site in order to obtain more complete photothermal exposure of the solder is simply not feasible. In cartilage, for instance, one may clinically irradiate a site from the articular surface, perhaps even irradiating through the side of the tissue if there is enough penetration at the given wavelength, but cannot then irradiate from underneath the defect without drilling holes and running fibers through the subchondral bone and/or the calcified zone of cartilage-bone integration. The experimental values given in Table 3 are thus likely higher than what could be achieved in clinical situations using these parameters. These issues highlight the need for clinically relevant models, data, and controls in order to evaluate a treatment for future in vivo study.

Table 3: Comparison of Test Parameters and Bond Strengths for Photothermally-Soldered Cartilage

Species/ Location	Solder Formulation	Irradiation Parameters	Test Configuration/ Method	Approx. Strength (kPa)	Reference/ Notes
Baboon; femoral condyle	0.5g BSA +15mg ICG per ml H2O in gap; 2.25g BSA +5mg ICG per ml H2O on surface	525mW, 67W/cm^2, 30J per side	Tensile; applied to cut edge; rectangular strips; 0.75N tare, 2.5N/min	280	73 a
		240mW, 31W/cm^2, 30J per side		120	
Ovine; shoulder	45% w/w BSA + 2.4 mg/ml ICG	1W, 75J per side	Tensile; applied to area; rectangular strips; 5mm/min	82, 72	74 b
		1W, 37.5J per side		52	
		4W, 75J per side		54	
		4W, 37.5 J per side		49	
Bovine 4 mo. calf condyle	25% BSA, 0.5% hyaluronic acid, 0.1% ICG	1.5W, 61J total	Tensile; applied to area; concentric disc pullout; 23mm/min	20	72 c
		1.5W, 61J per solder treatment		65	

NOTES: (a) Strength values assume a specimen thickness of 1.5mm. (b) All strength values for ovine specimens are for tissue at a distance of 10mm from optical fiber tip except 72 and 52 kPa values are at 5mm from fiber tip. (c) Solder values not specified as % w/w or % w/v though formulation appears to be same as that given by Chan [75] and attributed to Pohl and Bass; 20 kPa specimen utilized one solder treatment of cavity with implant inserted and subsequently irradiated; 65 kPa specimen first treated cavity with solder and irradiated, then treated again with solder, inserted implant, and irradiated again.

While no decrease in bond strength was found in the bovine study when the double solder treatment was hydrated in PBS for 48 hours, another study, which included the baboon cartilage tissue and primary author of the previous citation, found significant detachment of albumin-based solders from articular cartilage after hydration times of only one hour [75]. This discrepancy may be attributed to the geometrical differences, open-faced strips compared to cylindrical plugs, and the barrier effect created by the double solder treatment technique. (See Note (c) in Table 3.) The use of two separate solder treatments may well have added to the press-fit effect in addition to creating a photothermal weld between the solder material and the tissue.

One must also consider the interaction of the cartilage matrix constituents and fluid during normal function. A critical clinical issue to consider is the use of photothermal soldering for focal defect repair, attaching cartilaginous repair material to native cartilage laterally around the perimeter of an implant. Albumin solders form a watertight seal once denatured, so, physiologically, the weld site is located precisely where fluid must exude laterally throughout the tissue under loading. Thermally soldering cartilage to cartilage in this manner may create a bulk discontinuity in a non-regenerative tissue and/or interfere with the nutrient transport via fluid flow to/through the new tissue. The effects of this would need to be assessed in vivo to determine if the technique could be suitable with a sufficient period of non-weight bearing by the patient, or if the effects of the thermal damage coupled with the barrier to fluid flow produced a deleterious effect on tissue healing and health over the near- or long-term.

Photochemical Bonding Approaches

Some photosensitive molecules such as riboflavin undergo both types of photochemical processes when excited, although the Type-I mechanism is highly dominant for flavins. Excitation of riboflavin (λ_{max1}=375 nm, λ_{max2}=447 nm [76]), usually in the form of riboflavin-5-phosphate (R5P), has been used to stiffen the cornea by inducing more collagenous crosslinks [77,78], seal ureteral tissue [79], and seal scleral and corneal incisions in vitro [80,81]. These latter studies illuminated the weld site using argon laser illumination with results on the order of 20 kPa for closure strength, failure being defined as initiation of fluid leakage. Interestingly, one study used R5P-doped fibrinogen while the other used only R5P in a physiologic buffered saline solution (PBS) and obtained similar results.

In contrast, most sensitizers used for photodynamic therapy (PDT) rely on Type-II singlet oxygen generation and are under development for treatment of cancerous tissue. Many of these sensitizers are able to excite at longer wavelengths in the visible spectrum and thus achieve greater tissue penetration. One such sensitizer, tetrabromorhodamine-123-bromide (TBR) is a cationic, hydrophobic dye more typically employed as a mitochondrial probe. Its singlet oxygen quantum yield production of 0.65-0.7 is roughly the equivalent to that of a 1,8-naphthalimide dye used for some cartilage studies described in the following paragraphs. However, TBR absorbs at 514 nm, a standard argon line, instead of 430 nm. It has been minimally investigated for its bonding potential, used only in conjunction with solubilized collagen as a ureteral sealant. [79]

More recently, skin adherence has been achieved using rose bengal. Rose bengal has a strong absorption coefficient near 514 nm, a primary argon laser wavelength. Partial thickness porcine skin grafts were cryopreserved, and then bonded together using 560 mW/cm^2 at 514 nm and 0.01-1.0 % weight/volume rose bengal solubilized in PBS. Results showed a dose-dependent relationship between the irradiance and the adherence established. Peel tests yielded strength values ranging from 0.078 N/cm^2 to 0.657 N/cm^2 at fluences of 126 to 504 J/cm^2 respectively for the 560 mW/cm^2 irradiance. Histological evaluation showed that collagen organization and cellular viability were preserved.[82]

The one group that has investigated photochemically bonding cartilage and meniscal tissue used a patented, bromiated 1,8-naphthalimide dye. In vitro results for meniscal and articular cartilage tissue yielded bond strengths for cartilage and meniscus roughly on the order of 50 kPa for cartilage and 100 kPa for meniscus.[83] Excitation at 458 nm was required because the dye absorption actually peaks at 430 nm and does not overlap the higher argon bands, thus necessitating a 20 W argon laser system. While such a requirement may be clinically prohibitive for large-scale treatments, the potential for this technique was demonstrated. However, strength assessments were performed by hanging washers off the end of a lap specimen resulting in an uneven, impulse-type loading profile and thus preventing direct comparison with strength assessments performed at a constant rate or load. In addition, specimens were wet frozen prior to thaw and use. The specimens were also debrided prior to bonding, yet no information on the debridement method or scope was given. This also makes direct comparison with fresh or cryopreserved tissue with no extra physical debridement above the scalpel or microtome blade used to cut the tissue difficult.

Subsequent study by this group evaluated in vivo healing of meniscal flap tears and partial thickness incisions in femoral articular cartilage of adult sheep. Defects were irradiated at 458 nm and 800 mW/cm^2 for 7.5 minutes, immobilized for 24 hours, and evaluated at intervals up to six months post-treatment. Results showed wound closure along with cellular recruitment and active matrix deposition at the weld sites, and a return to normal surface texture.[84,85] However, no controls, histological, or ultrastructural characterizations were performed.

CHAPTER III.

OBJECTIVES, HYPOTHESIS, AND SPECIFIC AIMS

Clinical Significance

Cartilage repair and/or replacement is necessary for many orthopaedic conditions including cracking of cartilage as seen in early OA, fissures from blunt trauma, and replacement of damaged areas with biological or synthetic constructs. These issues extend to other sites in the body as well, such as the temporomandibular joint, spinal discs, and cartilage reinforcement of ureteral tissue. The common need is for a method to achieve sufficient initial cartilage bonding at the repair site without interfering with the natural processes or inducing even more trauma. Current practice utilizing fibrin-based adhesives and sutures has not provided an adequate solution to date. Similarly, standard chemical crosslinking methods and photothermal soldering approaches do not lend themselves to adhesion of living cartilage tissues due to either process or results that cause excessive cellular necrosis for tissue.

This study aims to address effective initial fixation of the cartilage with minimal trauma to adjacent host tissues in such a manner that biological integration in vivo may be enhanced. Successful initial fixation and subsequent biological-mechanical integration of a cartilage implant will provide an alternative means of treatment for patients suffering from cartilage injury, potentially avoiding or delaying more extreme

solutions such as a total joint replacement. Findings and methodology will be applicable all cartilaginous tissues.

Objectives

This study's objective is to investigate and test the in vitro attachment of cartilage-to-cartilage via laser-mediated photochemical methods in order to evaluate the potential effectiveness of such methods for initial fixation of tissue- or cellular-based cartilage repair implants for focal defects or for cartilage tissue tears.

More generally, in terms of success of biological constructs for cartilage repair or even cartilage bonding for repairing fissures, many issues result from a lack of integration of the implant with the host tissue and neither fibrin-based adhesives nor sutures have adequately solved the problem. It is known that chondrocyte necrosis occurs and/or cell density decreases within a radius of approximately 100 μm from a cut cartilage surface [86]. Zones of necrosis surrounding sutures are known to occur in other tissues [87], and it has similarly been found that persistence of a suture track and damage to the surrounding tissue exists through 18 months in cartilage [88]. Consider that a fissure from blunt trauma already has a zone of damage adjacent to the defect. Similarly, debridement or coring is required to create an implant site for biological-style implants. The complete absence of damage due to bonding technique should not then be the goal, but rather to not expand upon the damage already present in current practice or due to injury. It would also be ideal if the bonding technique itself enhanced the healing by offering a tissue-fixation or fixed scaffold with which to guide the natural healing response. In theory, and according

to the ocular and cartilage studies previously cited, photochemical bonding should provide such a mechanism by enabling covalent crosslinks between collagen fibers with no thermal or other denaturization damage.

Toward this end, the potential of reducing the scattering inherent in cartilage tissues with the addition of a high refractive index fluid will be investigated. With no intrinsic chromophores in the visible portion of the spectrum, cartilage tissue with reduced scattering would increase the penetration depth of light in the visible range. This could offer improved bonding by increasing the total light exposure that is capable of being delivered to all the relevant surfaces of a defect.

In addition, Fourier transform infrared spectroscopy (FTIR) will be used to evaluate collagen gels doped with the photosensitizers being investigated to determine if there is indeed a change in the collagen bonds. Since collagen type I is well known to spontaneously form a gel at physiological pH and temperature, simple gellation alone will not elucidate whether a given photosensitizer has created crosslinks within the matrix. FTIR is able to isolate certain key bond signatures and changes from one state to another may then be seen. This preliminary bulk photogellation will be used to down-select photosensitizers as well as determine intensities and irradiation times necessary for the tissue bonding experiments themselves. An understanding of how photosensitizers affect different collagen types and how this translates into the possible bonding of cartilaginous tissues where the dominant collagen is of a given type would provide foundations that could guide the next generation of photoactivated cartilage adhesives.

Finally, experiments will be conducted to determine if actual cartilage-to-cartilage bonding may be effected via photodynamic means. Benchtop strength tests will be

performed and culture tests will be conducted to assess longer-term stability of the bonds as well as viability.

The encompassing goal of this effort is to determine if a photochemical bonding approach can be used to achieve cartilage-to-cartilage adhesion, withstand hydration, and provide reproducible results a under controlled testing environment. If the above conditions are met, the next goal will be to determine if these bonds are stable under a culture environment and whether or not the method results in excessive cellular necrosis at the bond interface. The studies conducted in this work aim to determine not only if the photochemical method can be reproducibly effective for cartilage tissues, but also whether the immediate after-effects of such treatment are prohibitive to use of this method for these tissues in future or clinical application.

Hypothesis

Photoactivated attachment of cartilaginous tissues can provide initial fixation of implanted cartilage repair tissue to surrounding host tissues for focal defects.

Specific Aims

1. Evaluate the potential of optically clearing cartilage tissue by using a high refractive index fluid in order to increase the optical penetration depth into the tissue.

2. Using collagen gels as a model system, evaluate the ability of select photosensitizers to affect both collagen type I and type II using FTIR analysis.
3. Using the collagen gels as a model system and the FTIR results as a guide, determine initial irradiance and exposure parameters to be used for the tissue bonding experiments.
4. Design and evaluate a mechanical test configuration that will enable an effective assessment of the shear strength of a photochemically bonded cartilage interface.
5. Design, test, and evaluate a cartilage-to-cartilage photochemical bonding method via benchtop mechanical testing.
6. Evaluate the viability and bond stability of a photochemically bonded cartilage interface over seven days of in vitro culture.

CHAPTER IV.

GENERAL PROCEDURES

Common procedures used throughout most of the studies found in the subsequent sections will be described here. Methods specific to a given experiment will be discussed in the relevant section. Materials and their sources are listed in Appendix A-1.

All references to Phosphate Buffered Saline (PBS) in this work refer to 1X PBS with no calcium or magnesium. All references to Dulbecco's Modified Eagle's Medium (DMEM) throughout this study refer to high glucose DMEM (HG-DMEM).

Tissue Harvest and Culture

All cartilage tissue was harvested from the femoral condyles, patellofemoral groove, and from the medial menisci of immature (1-3 week old) calves. Leg sections were shipped overnight on wet ice from an abbatoir, so that harvest took place within 36 hours of sacrifice. The bulk of extraneous tissue was removed on the benchtop while taking care not to puncture the joint capsule. The knee section was then transferred to a sterile tissue culture hood for completion of the harvest. Careful incisions were made, first bisecting the inferior patellar tendon, then continued with transverse, short incisions to bisect the stifle, followed by resection of the collateral ligaments. Complete separation

of the femur from the tibia was then achieved by cutting the cruciate ligaments and any remaining posterior connective tissue.

The medial meniscus was harvested whole by carefully cutting through the ligamentous material attaching the outer edges of the meniscus to the tibia, and then cutting through the short ligaments attaching the anterior and posterior horns of the meniscus to the tibial surface.

The method of tissue harvest from the femoral condyles and the patellofemoral groove depended on the particular experiment being conducted. Each particular tissue section taken for the given experiment will be described again in the relevant section. However, for the sake of describing a common tissue treatment procedure, they will be described in detail here:

- For all of the optical scattering reduction viability studies, cylindrical tissue cores were taken with the core axis perpendicular to the articular surface using 4 mm biopsy punches (Miltex). A number 22 scalpel blade was then used to undercut the tissue near the tidemark and lift the cores from the joint.
- For all of the single-lap shear specimen cartilage-to-cartilage photo-bonding studies, the tissue was taken in bulk sections for future precision cutting on a microtome. In this case, tissue was sliced using a number 22 scalpel blade transversely across the joint such that tissue sections were approximately 12 mm thick. Tissue was removed along the periphery joint surfaces by making secondary cuts lengthwise along the condylar (or patellofemoral groove) surface, and then removing these sections in wedge shaped pieces with subsequent cuts until the bone was exposed on the sides of the joint. The

scalpel blade was then used to undercut the section near the tidemark approximately one-third of the way through the thickness of the tissue section from each side. Due to the young age of the animals, tweezers could then be used to grasp and remove the complete tissue section. This process is illustrated for clarity in Figure 6.

- For the culture photo-bonding studies, cylindrical cores were removed by the same general method as described for the optical scattering reduction studies. For these experiments, however, cores were created using both 8 mm (Miltex) and 4 mm (Miltex) biopsy punches.

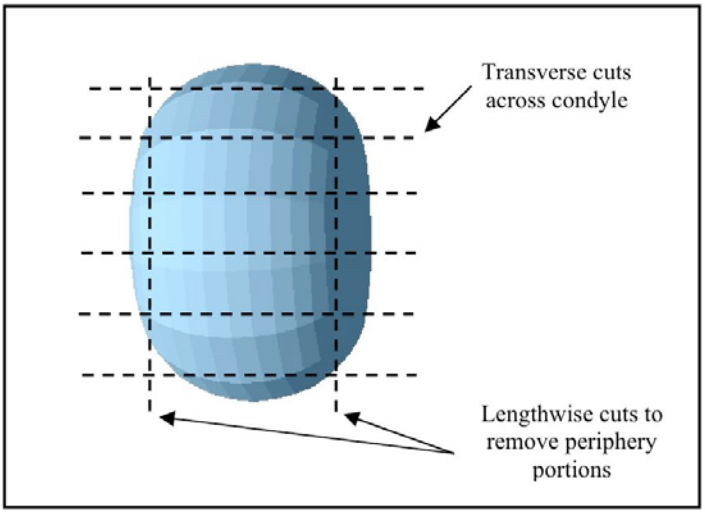

Figure 6: Illustration of tissue sectioning on a condylar surface for the shear specimen cartilage photo-bonding studies

All tissues were wetted often during harvest with sterile Phosphate Buffered Saline (PBS) without calcium or magnesium and containing antibiotic/antimycotic (AB/AM) to prevent tissue dehydration (5 ml of 100X AB/AM per 500 ml PBS). Immediately after removal from the joint, all tissue specimens were immersed in a wash solution consisting of 500 ml high glucose Dulbecco's Modified Eagle's Medium (HG-DMEM), 0.5 ml gentamicin (1000X), 5 ml kanamycin (1000X), and 5 ml AB/AM (100X).

After soaking in the wash solution for approximately one hour, subsequent treatment depended on the particular experimental use for the tissue, and will be detailed in the relevant sections to follow. For instance, some specimens were immediately sectioned for a live/dead assay, while some were sectioned and stored in the wash solution for 12 hours in an incubator at 37 °C prior to being transferred to media. Again, this will be detailed where relevant, but for all tissue, the culture media consisted of the same formulation and was changed at the same frequency of every other day. Specifically, the culture media was comprised of 450 ml HG-DMEM, 50 ml fetal bovine serum (FBS), 5 ml non-essential amino acids (NEAA), 5 ml HEPES buffer solution, 0.5 ml gentamicin, and 1 ml ascorbate.

Live/Dead Assay

Live/Dead assays were conducted using the LIVE/DEAD Viability/Cytotoxicity Kit (Molecular Probes, L3224) for animal cells. This method employs two fluorescent

probes, calcein AM and ethidium homodimer-1 (EthD-1)). Calcein is a polyanionic, green-fluorescent dye that serves as an indicator of cells having esterase activity as well as an intact membrane to retain the esterase products, thereby staining only live cells (excitation/emission: 494 nm/ 517 nm). As such, calcein AM is retained within live cells. EthD-1 is a red-fluorescing nucleic acid stain that is only able to pass through the compromised membranes of dead cells (emission/excitation: 528 nm/ 617 nm).

Treatment specific to a given experiment performed prior to the live/dead assay will be described in the relevant section. The common protocol followed for conducting the live/dead assay on cartilage specimens was as follows:

a) All tissue specimens were washed in PBS under gentle agitation three times for ten minutes per wash. (All agitation for all steps in this protocol is conducted in an incubator at 37 °C.)
b) Calcein AM and EthD-1 were diluted in PBS to concentrations of 4 μM each.
c) Tissue was sectioned with a number 22 scalpel blade to expose the face to be evaluated for live/dead staining immediately prior to incubating and then covered with the Calcein AM/EthD-1 solution under gentle agitation for 45 minutes.
d) The Calcein AM/EthD-1 solution was aspirated and replaced with PBS. Tissue specimens were washed in PBS under gentle agitation three times for ten minutes each.

All specimens were then evaluated using a Zeiss LSM 510 confocal microscope using a 10X objective. Excitation was performed using line switching to avoid fluorophore crosstalk by argon and helium-neon lasers at excitation lines of 488 nm and

543 nm respectively. The corresponding emission filters were a band pass 505-550 nm for the 488 nm excitation and a long pass 560 nm filter for the 543 nm excitation.

Hydroxyproline and sGAG Assay

For collagen and proteoglycan content analysis, samples were collected and frozen until the end of the study. They were then thawed, weighed, lyophilized, and reweighed. The samples were then digested at 55 °C in 0.5-0.7 ml of 2 mg/ml proteinase-K until completely digested. Sulfated glycosaminoglycan (sGAG) content, which indicates the amount of proteoglycans present in the tissue, was evaluated according to the DMMB dye-binding assay of Farndale[89]. Hydroxyproline content, indicative of the total amount of collagen present, was determined using the p-DAB/choramine-T assay of Woessner[90] and as described by Reddy and Enwemeka.[91]

CHAPTER V.

OPTICAL SYSTEM CONFIGURATIONS

Argon Laser

A 5W, water-cooled argon laser system (SpectraPhysics) was assembled on an optical table such that the major argon wavelengths of 458 nm, 488 nm, and 514 nm were prismatically separated. The lines were then sent through a blocking aperture such that experiments could be conducted using only one argon line or all lines concurrently. Once a line (or all lines) were passed through the aperture, the beam was allowed to expand to a diameter of 6.5 mm and then reflected down using a mirror. In this manner, all photogellation experiments could be conducted with the beam incident straight down on the substance, most often a viscous liquid, to be irradiated. An illustration of this concept is depicted in Figure 7.

667 nm System

A fiber-coupled laser diode system was purchased from Edmund Optics (E55-370, manufacturer BWF). The off-the-shelf system integrated a laser diode with a thermoelectric cooler, heatsink, fan, power supply, and component electronics in a single unit measuring 152.4 mm x 76.2 mm x 254 mm height, width, and depth respectively.

The system came supplied with a high brightness glass fiber, 1 m in length with a 100 μm core diameter, coupled to the diode output by a non-epoxy high-powered connector and an SMA-905 termination. This class IIIb system supplied 0-300 mW of continuous wave output at a peak wavelength of 667 nm with a bandwidth of less than 3 nm. Input power was a maximum of 1A at 110V AC.

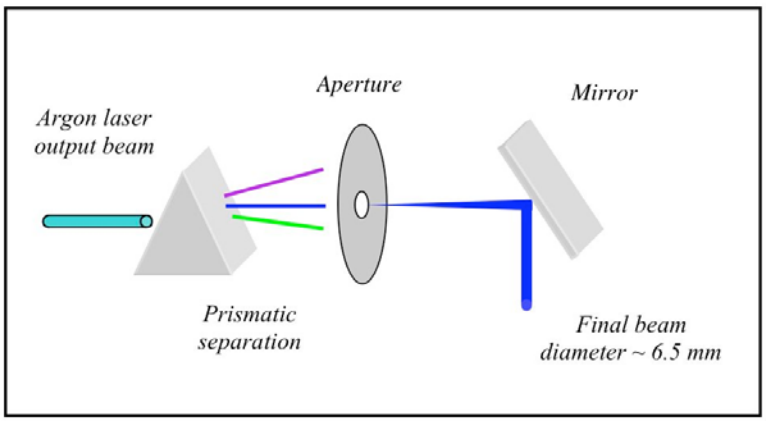

Figure 7: Schematic illustration of argon irradiation setup

In order to expand the spot size of the emanating beam and maintain a degree of uniform irradiance across the spot diameter, the fiber was coupled to a 40X objective to directly image the fiber face. The fiber was fitted through an x-y translation stage (HPT1 ±1 mm XY Cage Translator; SM1A3 RMS to SM1 Thread Adaptor; SM1SMA SM1 Series Fiber Adaptor; Thor Labs) in order to center the fiber face on the objective, and the objective was in turn coupled to a z-translation stage (SM1Z Z Translator, Thor Labs)

to control distance from the fiber face after positioning. A 165 mm distance from the objective was found to achieve a 4 mm diameter focused spot.

To validate the beam irradiance profile, the focus spot from the 40X objective was imaged directly onto the focal plan of a CCD camera (Princeton Instruments, RTE/CCD-768-K/1, 768 x 512 pixels) after passing through an absorptive neutral density filter with an optical density (OD) of 2. Wintest software for the CCD camera was used to collect an image of the spot given a 0.01 second exposure time. The resulting image was then analyzed using MATLAB to provide an irradiance profile as shown in Figure 8. The final system used for photochemical bonding is as described and shown in Figure 9.

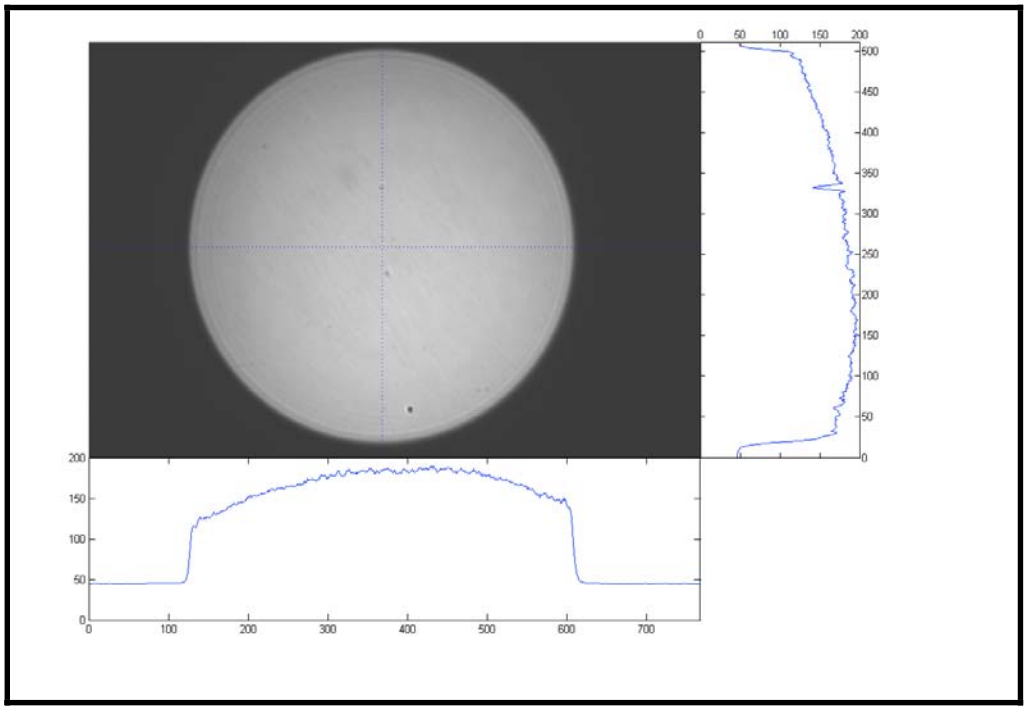

Figure 8: Irradiance profile of fiber output for 667 nm diode system

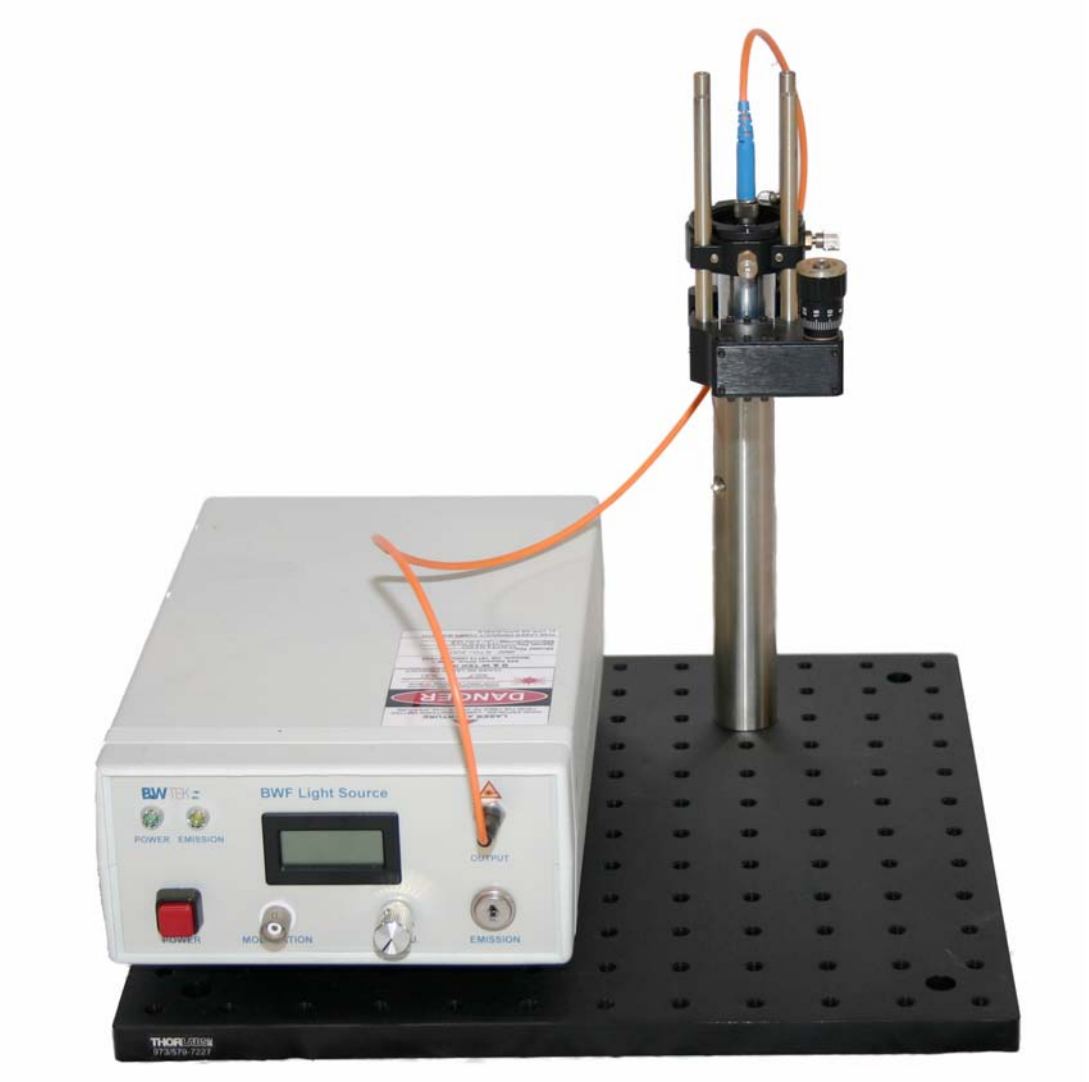

Figure 9: Experimental configuration for 667 nm diode system coupled to 40X objective

420 nm System

The 420 nm system was configured around light emitting diode (LED) lamps obtained from Uniroyal Optoelectronics. The LEDs were the standard T-1-3/4 configuration, having a 5 mm diameter for the main body of the lamp, and capable of running with a continuous forward current of 30 mA. The typical radiant intensity per lamp (rated at 25°C) was 13 mW/Sr across a 20° viewing angle. LEDs emitted light around a 23 nm bandwidth with a peak emission wavelength of 420 nm.

To configure an illumination system, an hexagonal array was constructed from 55 LEDs with the LED rim trimmed off and arranged in close proximity. Two Fresnel lenses were placed in series to capture the light emanating from the LEDs, collimate it to a degree, and then focus. Fresnel lenses have a series of concentric grooves molded into a thin plastic sheet instead of the curved surface and bulk of conventional lenses, and thus little light is lost by absorption. The lenses used in this configuration gave a 92% transmissivity across the range of 400-1100 nm. These grooves then act as individual refracting surfaces to bend parallel rays to a common focal length. Both lenses used here were 170 mm square with an effective size of 152 mm. Lenses NT32-686 and NT32-593 (Edmund Optics) had effective focal lengths of 305 mm and 76 mm respectively. A schematic of the 420 nm system configuration is shown in Figure 10.

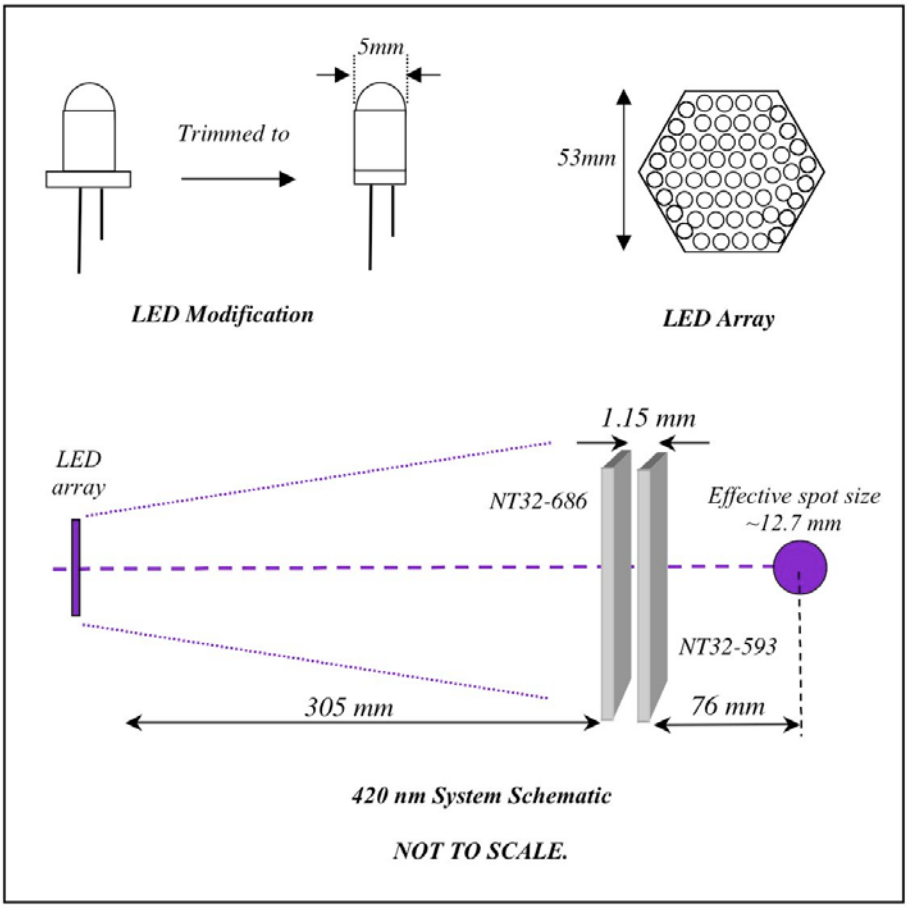

Figure 10: 420 nm Optical System Configuration

Due to the close packing of the LEDs, a thermoelectric cooling device and electronics to control the current were added to the system. A picture of the array is shown in Figure 11, and the complete system is shown in Figure 12.

Figure 11: 420 nm LED array and associated electronics

Figure 12: 420 nm optical system

CHAPTER VI.

OPTICAL SCATTERING REDUCTION IN COLLAGENOUS TISSUES

Introduction

Optical Properties of Cartilage

Generally speaking, a collimated beam of light normally incident on a tissue will have some portion reflected at the surface, with the rest of the light penetrating the tissue being attenuated by absorption and scattering with increasing depth. This concept is Beer's Law and may be written:

$$\varphi(z)= \varphi(0)*(1-r_{sc})*\exp[-(\mu_a + \mu_s)z]$$

where:

$\varphi(z)$ is the fluence rate of collimated light at a position z (depth)

$\varphi(0)$ is the collimated irradiance incident on the surface

r_{sc} is the Fresnel surface reflection (specular)

μ_a and μ_s are the absorption and scattering coefficients, and represent the probability of an absorption or scattering event within an infinitesimal distance.[92]

D_{eff} is the effective penetration depth of the light through the tissue. For the penetration depth of a collimated beam:

$$D_{eff}=1/(\mu_a+\mu_s')$$

and is described as the mean free path for an absorption or scattering event such that D represents the depth where the intensity of light transmitted into the tissue is reduced to 37% of the incident intensity at the surface.[92] Here, μ_s' is the reduced scattering coefficient, given by $\mu_s'=(1-g)\mu_s$, and g represents the anisotropy factor. In tissue, scattering is generally not isotropic, but is instead strongly directed forward. The anisotropy factor g is defined as the mean cosine of the scattering angle, representing this scattering bias. Values of g range from –1 to +1 where g=0 is the isotropic case and –1 and +1 correspond to complete backscattering or forward scattering respectively.[93] Most mammalian tissues have g values that fall into the range 0.7 to 0.97.[94]

Note that $D_{eff} = (1/\mu_{eff})$ is often used where $\mu_{eff} = [3*\mu_a*(\mu_a + \mu_s')]^{1/2}$ is the effective attenuation coefficient as described by transport theory.[95,96,97] This derivation is more relevant to photodynamic therapy (PDT) where the spot size of the incident radiation is fairly large, to cover as much of a given area as possible. In this case, most of the scattered light remains within the "collimated" irradiation cylinder, and so the large irradiation area maximizes the effective penetration depth. The fluence rate at the center of the irradiation area may then be described by one-dimensional transport theory, hence

the relation for μ_{eff}. Note that this relation is really an estimation that considers fluence where:

$$\varphi(z)=A*\exp[-\mu_{eff}z]$$

represents the fluence rate as a function of penetration depth, z. (The fluence rate is the integral of the radiance over all directions with typical units of Watts per unit area.) Therefore, the equation $D_{eff}=(1/\mu_{eff})$ is only valid if the constant A represents the simple magnitude of the irradiance at the surface, which may not necessarily be true.[95]

Typically an integrating sphere or double-integrating sphere setup is used to directly measure the reflectance, diffuse transmittance, and collimated transmittance of a sample. The remaining optical properties, the absorption and scattering coefficients μ_a and μ_s, are then estimated by a light propagation model such as Monte Carlo estimation or the inverse-adding doubling method. The specific method employed in a given study depended largely on what level of accuracy the authors desired or what precedent and validation had already been associated with using a particular algorithm given a specific measuring setup. Since the different light propagation models and their advantages and limitations have been detailed previously[93,94], that effort will not be repeated here. For a better understanding of the literature results shown in Table 4, however, a few key methods will be described briefly:

- Kubelka-Munk theory models absorption and scattering based on the propagation of a uniform, diffuse irradiance through a one-dimensional isotropic layer of medium with no reflection at the boundaries. These assumptions are often not

representative of the behavior of light interaction with tissue when that light emanates from a laser. Note that the Kubelka-Munk scattering and absorption coefficients are not directly comparable with the transport scattering and absorption coefficients (as given in the table).

- Monte Carlo estimation simulates the random walk of photons in an absorbing and scattering medium using a purely statistical approach.
- The adding-doubling (and inverse adding-doubling) method assumes transmission and reflection knowledge for a thin, homogeneous layer of tissue. The reflection and transmission of a layer of double the thickness is found by juxtaposing an identical layer, and summing the contributions from each. The adding component then extends the doubling method to dissimilar slabs, thereby allowing simulation of tissue with different layers.
- Diffusion theory approximates light as particles absorbed or scattered by structures imbedded in a turbid media.[93,94]

Cartilage is a very effective light-scatterer at all wavelengths in the visible and near infrared portions of the spectrum. This behavior is demonstrated by its whitish color, which is due to its non-wavelength selective scattering behavior. Many studies of cartilage optical properties have already been conducted, with selected results shown in Table 4. However, it is important to note that optical properties measured by different studies are difficult to compare due to differences in materials used (animal for tissue source, tissue harvest site, animal-to-animal variation), method of tissue treatment/storage prior to making the optical measurements, and the light propagation model used to

approximate the absorption and scattering coefficients. For example, some studies have already demonstrated significant effects of freezing and associated tissue storage methods on the measured optical properties of tissues[94,98], and data from the previous literature studies with cartilage has been collected after freezing[67] or refrigerating in saline[68], or cryopreservation [96].

Table 4: Optical Properties of Cartilage Tissue near 630 nm

Tissue	**Optical Setup/ Estimation Method**	**λ (nm)**	**μ_a (cm^{-1})**	**μ_s (cm^{-1})**	***g***	**μ_s' (cm^{-1})**	**Ref.**
Rabbit cartilage	Double integrating sphere/ inverse adding-doubling	632.8	0.33 ±0.05	214 ±0.2	0.909 ±0.005	19.4 ±1.1	97
Porcine nasal cartilage	Integrating sphere & collimated transmittance/ Monte Carlo	632.8	0.14 ±0.05	304 ±47	0.973 ±0.005	8.2 ±1.3	96
Porcine nasal cartilage	Integrating sphere/ inverse adding-doubling	630	0.22 ±0.06	-	-	5.6 ±1.3	68
Porcine shoulder cartilage	Integrating sphere/ Kubelka-Munk	632.8	0.17 ±0.02	-	-	10.6 ±2.0	99
Equine articular cartilage	Integrating sphere/ Kubelka-Munk	630	0.5 ±0.1	-	-	17.0 ±1.0	67

Taking these properties and approximating an effective penetration depth for an incident beam of radiation, a comparison can be made between the approximation of penetration depth for a collimated beam versus a large, more diffuse incident spot of

light. This comparison for differing wavelengths is given in Table 5. Looking at the quite different values given by the two relations, the importance of proper estimation for a given system of light-tissue interaction becomes obvious.

Table 5: Effective Penetration Depth of Light in Cartilage at 420 and 670nm

Tissue	**λ (nm)**	**$D_{eff}=(1/[3*\mu_a*(\mu_a+\mu_s')]^{1/2})$, For large irradiance spot (mm)**	**$D_{eff}=1/(\mu_a+\mu_s')$, For collimated beam (mm)**
Porcine nasal cartilage[68]	420	2.16	0.60
	670	5.66	1.92
Equine articular cartilage[67]	420	0.84	0.23
	670	1.95	0.68

Consider scattering as a phenomena that may be loosely classified as Rayleigh or Mie scattering. Rayleigh scattering refers to media in which the intensity of the scattered light is roughly proportional to $1/\lambda^4$ and typically involves particles smaller than the wavelength of incident light (specifically, smaller than $\lambda/15$). In contrast, scattering is only weakly dependent on wavelength as particle size begins to approach the incident wavelength, referred to as Mie scattering.[100] With collagen fibers in articular cartilage on the order of 25-300 nm in diameter (and larger in fibrocartilage), and proteoglycan aggregates around 600 nm in effective diameter[9,13], Mie theory is obviously the better descriptor of cartilaginous tissues.

With respect to cartilage in the visible portion of the spectrum, scattering is constantly and gradually increasing as the wavelength decreases from 800 nm to 400 nm.[67,68] This is expected since Mie theory predicts the strongest scattering will occur when the radius of the scattering particle approaches the same order of magnitude as the incident wavelength.[101] Absorption is nearly constant throughout this same region, but increases sharply in the UV with a local absorption peak around 340 nm.[67] Absorption also sharply increases due to the presence of water at 980 nm and 1180 nm.[68] Unless the tissue retains some vascularity, as is the case with the outer third of the meniscus and with tissue from very young animals, there are no local absorption peaks corresponding to haemoglobin at 540 nm and 577 nm.

Physically speaking, in Mie theory, the anisotropy factor (g) represents the decreased scattering as the index of refraction of the scatterers (n_s) in a medium approaches the index of refraction of the ground substance (n_o). As the ratio of n_s/n_o approaches unity, g reaches a maximum.[101] Holding other coefficients constant, this means the effective penetration depth of the incident light increases as g increases. This concept leads us to the idea of reducing the refractive index mismatch as a means of increasing the penetration depth of the light.

Physical basis for Transparency of Tissues

Some portion of the turbidity of a highly scattering matrix such as cartilage is caused by a mismatch between the index of refraction of the matrix fibrils, in this case

collagen, and the interstitial medium enveloping those fibrils. In general, the reduced scattering coefficient of a tissue (μ_s') is dependent to a large degree on the index of refraction mismatch between the extracellular membranes, the cytoplasmic organelles, and extracellular fluid. For a more fibrous tissue like cartilage or sclera, this mismatch occurs between the collagen fibrils and the ground substance (n_{col}=1.474 and n_{gs}=1.345, values for scleral tissue). Also, for most normal tissues, the absorption coefficient is much less than the scattering coefficient, $\mu_a << \mu_s$. Therefore, to the degree that the indices of refraction may be brought closer together, coupled with the degree of the scattering caused by the mismatch, the turbidity of that tissue can be reduced. [101]

Application of osmotic agents such as glycerol, propylene glycol, or glucose, has been a recent development in this area. The solutions are used to bind the water present in the interstitial matrix, diffusing throughout the tissue, reducing scattering as the tissue becomes permeated with the agent. Glucose in particular came under investigation as a clearing agent after work in near infrared (NIR) diagnostics found a correlation between scattering decrease and tissue glucose concentration. [102,103,104] There appears, however, to be little consensus or understanding of the exact physical and biochemical mechanisms behind the vast change in optical properties exhibited by immersed tissues. It is well understood that to the degree an osmotic agent dehydrates the water present in a tissue, there will be some physical shrinkage of that tissue, thereby packing the scattering fibrils more closely together. The combination of water loss and matrix packing will together alter the optical transparency of a tissue, which can be seen from studies where tissue was compressed to alter its turbidity. [98]

This does not, however, appear to be the dominant mechanism for the effectiveness of osmotic immersion solutions. It has been postulated that matching refractive index of the osmotic solution itself to the refractive index of the scatterers is an additional primary means for scattering reduction in the tissue. Results with anhydrous glycerol (n_{GLY}=1.47) and 7M glucose (n_{7M}=1.46) for skin appear to support this concept.[105] Other studies, however, appear contradictory. There has been some work to suggest that if the osmolarity of a given immersion fluid (specifically, glucose) is too high for the given tissue, the dehydration effect will tend to increase the refractive index of the scattering fibrils, and no great reduction in turbidity will be observed. Experiments with scleral tissue found better transparency resulted from 2.1M (n_{2M}=1.391) than for 3M (n_{3M}=1.398) glucose solutions, and even show an optimal time window for maximum transparency. [106]

This could have a significant effect on the molarity of solution necessary for optical clearing of cartilage, and therefore the clinical potential of such a method. It is possible that the osmotic clearing agent acts in some way to alter the index of refraction of the interstitial medium in fibrous tissues, instead of simply matching that of the scattering fibrils. Noting the similarity between scleral tissue and cartilage tissue as listed in Table 6, the osmotic solution parameters for cartilage will likely be similar as well.

Table 6: General Physical Comparison of Scleral and Cartilage Tissue

Tissue	Collagen Fiber Diameter	Collagen Fibrillar Thickness (associated fibers)	Collagen % by Dry Weight	Proteoglycan % by Dry Weight	Hydration	Ref.
Sclera	30-300nm	0.5-6 μm	75%	10%	68%	[101]
Cartilage	30-200nm	0.2-1.2 μm	50-73%	15%	65-80%	[9,10,13]

Due to some basic similarities of tissue collagen, it is possible that the optical agents used to reduce scattering in the previously mentioned studies involving skin and sclera could be used to achieve the same effect in cartilage and meniscal tissues. While the ability to take a highly scattering tissue and render it essentially transparent may have great potential ranging from cellular imaging (organization throughout an entire construct) to cartilage reshaping, the key here will be its effect on the wavelengths of interest to photochemical bonding.

The Potential Biological Effects of Sugars and Other Osmotic Clearing Agents

Sugars, more specifically called carbohydrates or saccharides, are one of the most prevalent biological molecules with roles ranging from energy sources to structural materials. Monosaccharides are the simplest carbohydrates, consisting of either aldehydes or ketones with two or more hydroxyl groups. Their basic formula is $(C\text{-}H_2O)_n$, where $7 \geq n \geq 3$. Monosaccharides can also join to alcohols and amines through

glycosidic bonds. In these cases, the anomeric carbon of the sugar, that of the carbonyl group in the aldose or ketose, forms a bond with the hydroxyl oxygen in an alcohol (O-glycosidic bond) or the nitrogen of an amine (N-glycosidic bond).

For example, nucleosides are formed by the reaction of sugars such as ribose and an amine base unit. These glycosidic bonds, much like peptide bonds, are cleaved by hydrolysis extremely slowly under physiologic conditions. The products of these sugar-alcohol or amine reactions, termed glycosides, do not have the same reactivity as the parent sugar, however. Typically, sugars bearing anomeric carbons that have not reacted to form glycosides can readily reduce mild oxidizing agents, and are hence referred to as reducing sugars. This is because the parent monosaccharide in open chain form has an open aldose or ketose residue to react with oxidizing agents; modified sugars have their anomeric carbon glycosidcally linked, and are thus not free to react. Glucose, ribose, and fructose are all reducing sugars. In terms of their biological significance: glucose is the principle food compound, or energy source, of many cells; ribose forms the backbone of ribonucleic acid; and fructose principally a fruit sugar, also forms phosphate intermediates in glycolysis and glucogenesis processes.[3,107]

Sugars and other high-osmotic solutions have been used extensively in cryopreservation techniques where maintaining a high percentage of cell viability is a primary concern. This is especially important for a structural tissue with a low cellularity such as cartilage since structural tissues have been shown to be more failure-prone post-implantation if the cell population is not viable. Cryoprotectants are often added to the media during the freezing process to minimize intercellular ice formation and reduce cell injury by mediating electrolyte concentrations and stabilizing cell proteins. These

protective agents include those that can permeate through cell membranes like glycerol and dimethyl sulfoxide (DMSO), and those that cannot, including various polymers and sugars. There is, however, a delicate balance of cryoprotection offered by these additives versus cellular toxicity from their exposure, often due to the high osmotic forces they exert on the cells. A cell will initially contract when exposed to a higher-osmotic protective solution as water exits the cell faster than the cryoagent permeates into the cell. Although the cell will eventually regain its initial volume, these volumetric changes often put the cells though fatal stresses. Toxicity may be reduced by reducing time of exposure or concentration of the protectant, or by adding the protectant in a stepwise fashion to minimize the cell volumetric extremes. Unfortunately, this last method often induces more toxicity due to the prolonged exposure time.[108]

For instance, work investigating the motility of mouse sperm found that even without the freezing protocol, when exposed to various sugar solutions, cellular motility steadily decreased in a linear fashion beginning at solution osmolalities of 500 mOsm.[109] Previous cryopreservation studies involving cartilage have also found that duration of exposure and concentration of the cryoprotectant (and hence, its osmotic pressure) were critical parameters affecting the survival of chondrocytes.[110,111] Further studies unrelated to cryopreservation have shown that when exposed to a hyper-osmotic medium at 450 and 550 mOsm, chondrocytes only recovered to 83% and 75 % of their original volume respectively.[112]

Considering the issues associated with sugar oxidation and crosslinking, coupled with the effects of osmotic stress on the cells, it becomes apparent that one of the first consequences of optically clearing cartilaginous tissues that needs to be investigated is

the effect on cell viability. Throughout all of the tissue scattering reduction studies mentioned above, including an investigation into clearing of gastric tissue describing the osmotic agent as biocompatible[113], none of them included any assessment of viability. Yet for the purposes of this study, maintaining cell viability is a necessary requirement if we are considering implanting a tissue engineered construct or allograft.

Methods

It was first necessary to determine the correct concentration of sugar solutions necessary to match the refractive index of the tissue, especially given some of the wide-ranging values cited in the literature. In this way, viability testing could be performed using a reasonable spread of concentrations that would encompass the refractive index range. Since refractive index values of 1.474 and 1.43 have been estimated/determined for scleral collagen and hydrated type I collagen films respectively, it was assumed that for cartilage collagen the refractive index of an osmotic agent must also fall into that range. Once the sugar solutions had been correlated with their respective refractive indices, a viability test was conducted to determine if the chondrocytes could withstand that magnitude of short-duration osmotic stress.

Refractive Index Measurements

Measurements of the index of refraction (n_D) for various sugar solutions as well as collagen solutions and hyaluronic acid were carried out on an Abbe-3L refractometer (Spectronic Instruments), which employs a standard lamp operating wavelength of 589.3 nm, the sodium-D line. Calibration was verified using an NIST Certified Test Piece (glass, 1.5125 n_D nominal). Accuracy for this instrument is specified at ±0.0001 for refractive index values.

Solutions of three different sugars, glucose, ribose, and fructose, in PBS without ions were made. The highest molarity solution was made first (target of 7 M), brought into solution by stirring on low heat. The lower molarity solutions were then arrived at by dilution of the high molarity stock. Three readings were collected per aliquot of sample, with two aliquots measured. Data given below represent the average of these readings across both aliquots. All data were collected for samples at room temperature.

Viability Studies

Cylindrical cartilage cores 4 mm in diameter were harvested from the femoral condyles and patellofemoral groove of calf stifles shortly after sacrifice as described in Chapter IV. The cores were incubated in the wash solution for approximately two hours, at which time the wash solution was aspirated off, replaced with culture media, and

specimens were incubated overnight. Immediately prior to beginning the treatment with the osmotic sugar solutions, a custom cutting jig was used to slice the cores into sections 2 mm thick taking care to remove both the superficial and calcified zones.

The first viability study investigated shock immersion testing and used fructose solubilized in PBS without ions as the osmotic solution. All solutions used during this process were first brought to 37°C by immersing them in a water bath. All control specimens had their bath solution aspirated and changed at the same frequency as the specimens receiving sugar treatment. However, the control specimens always received a bath solution of high-glucose DMEM. In this experiment, all groups of specimens were placed in a high-glucose DMEM solution and gently agitated at 37°C for 30 minutes. The bath solution was aspirated off and replaced with the respective solution according to treatment group: high-glucose DMEM (control), 0.5, 1, 2, 4, and 8 molal fructose solutions. The specimens were again gently agitated at 37°C for 30 minutes. This bath solution was then aspirated off and replaced with high-glucose DMEM for all specimens for another 30 minutes of gentle agitation at 37°C. Specimens were then returned for incubation in culture media for 48 hours. At this point, the live/dead assay protocol was followed as described in Chapter IV. Four specimens were obtained in each group.

The second viability test harvested, incubated, and sectioned cylindrical cores as before. Both a shock and a step-wise immersion test were performed using 0.5, 1, 2, 4, and 8 molal ribose-PBS solutions. In this procedure, controls again received the same frequency of bath changes, yet always received high-glucose DMEM. Again, the test began with all groups of specimens were placed in a high-glucose DMEM solution and gently agitated at 37°C for 30 minutes. The shock immersion test protocol was identical

to that using fructose and described above. The only difference is that specimens were assed for viability both immediately after immersion testing and after culture for an additional 48 hours (as was done with fructose). In addition, one group immersed in glycerol was included in this test. Four specimens were obtained in each group for the immediate viability testing, and three specimens per group were kept for the 48-hour testing.

For the step-wise viability test, all specimens again began with gentle agitation in high-glucose DMEM solution at 37°C for 30 minutes. For the sake of brevity, note that all solution immersions described in this process from this point forward are under gentle agitation at 37°C for 20 minutes. All specimens other than the controls were then placed in a 0.5 molal ribose solution as described. At intervals of 20 minutes, specimens were put in increasing molality solutions in a stepwise fashion: 1, 1.5, 2, 2.5, 3, 3.5, 4 molal steps. At each interval, controls received new high-glucose DMEM. Some specimens were removed and placed back into high-glucose DMEM after the 1, 2, 3, and 4 molal immersion points. All specimens removed and placed back into the DMEM received changes of DMEM at every step from that point forward in a similar fashion to the controls. In this way, all groups endured the same amount of solution changes. Groups were obtained that had been ramped up to final ribose molalities of 1, 2, 3, and 4 molal. Four specimens were obtained in each group for the immediate viability testing, and three specimens per group were kept for the 48-hour testing.

Results

Refractive Index Measurements

The refractive index of PBS, the solvent for all sugar solutions, was measured to be 1.336± 0.0001. Tabulated refractive index data for the sugar solutions are given in Table 7.

Table 7: Refractive Index Measurements of Various Sugars in PBS

Glucose							
Molarity	1M	2M	3M	4M	5M	6M	7M
Molality	1.1 m	2.6 m	4.6 m	7.5 m	12 m	20 m	38 m
Refractive Index	1.361 ± 0.0005	1.388 ± 0.0005	1.415 ± 0.0005	1.441 ± 0.001	1.465 ± 0.001	1.485 ± 0.001	1.5044 ± 0.001
Fructose							
Molarity	1M	2M	3M	4M	5M	6.3 M	-
Molality	1.1 m	2.6 m	4.5 m	7.3 m	11.5 m	22 m	-
Refractive Index	1.362 ± 0.0005	1.389 ± 0.0005	1.413 ± 0.0005	1.438 ± 0.001	1.461 ± 0.001	1.482 ± 0.001	-
Ribose							
Molarity	1M	2M	3M	4M	5M	-	6.8 M
Molality	1.1 m	2.4 m	4.1 m	6.3 m	9.2 m	-	18 m
Refractive Index	1.359 ± 0.0005	1.378 ± 0.0005	1.396 ± 0.0005	1.420 ± 0.0005	1.435 ± 0.0005	-	1.464 ± 0.0005

Viability Studies

Plates showing the viability results from the experiments in this section are included in Appendix A-3. Recall that red and green signify dead and living cells respectively. All images represent 921 μm by 921 μm areas. For illustration here, Figure 13 shows images for 1 molal, 2 molal, and 4 molal fructose solution immersion at 48 hours.

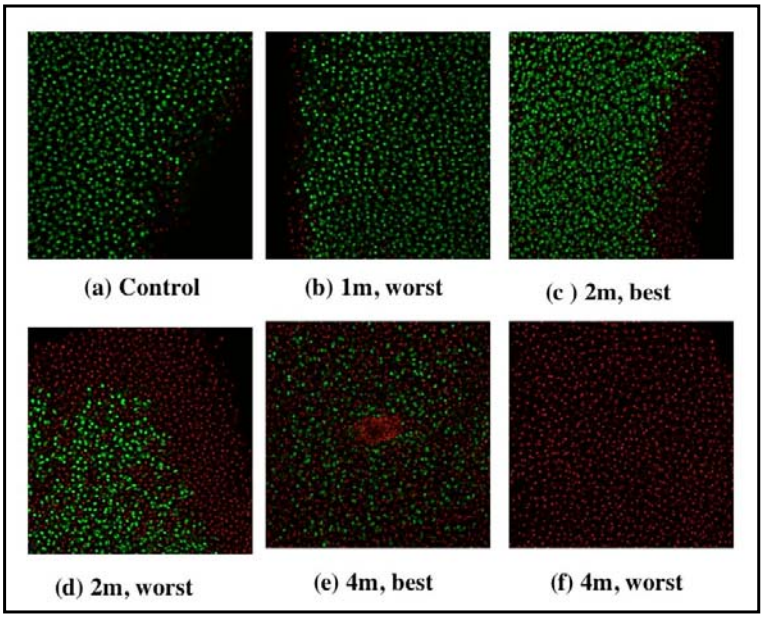

Figure 13: Selected viability results after shock immersion in hyper-osmotic fructose solutions: (a) Control, no immersion; (b) Immersion in 1 molal fructose, worst case; (c) Immersion in 2 molal fructose, best case; (d) Immersion in 2 molal fructose, worst case; (e) Immersion in 4 molal fructose, best case; (f) Immersion in 4 molal fructose, worst case

In summary, total cell death occurred after shock immersion in 8 molal fructose, 8 molal ribose, or glycerol. Near total or total cell death resulted from shock immersion in 4 molal fructose and ribose solutions. For shock immersion in fructose, 48 hours later, 70 μm and 180-180 μm necrosis zones were found for 1 and 2 molal exposure respectively. By comparison, control samples had an average necrosis zone of approximately 60 μm.

Similar results were found for shock immersion in hyper-osmotic ribose solutions, but the outcomes were slightly worse in terms of cell death. For instance, 0.5 molal exposure produced a necrosis zone 50-130 μm thick in the best cases and 250 μm deep in the worst at day zero. Specimens exposed to 1 molal ribose had cell death ranging from 300 to 600 μm deep; 2 molal solutions caused excessive cell death, though not on the scale as the 4 molal solutions. After 48 hours of culture, similar necrosis zones were seen as those present at day zero. Only the innermost 600 μm of cells were alive in tissue exposed to 2 molal ribose.

Step-wise increases of the solution molarity did not reduce the cell death at all. Tissue exposed to peak concentrations of 3 and 4 molal ribose in this manner showed near-total cell death, while those with 2 molal peak exposure exhibited 500 μm necrosis zones. Only cells exposed to a peak of 1 molal ribose appeared to fare better than the shock-immersed counterparts. In this case, shock immersion at 1 molal produced cell death averaging 500 μm across both time points. Stepping the molality first to 0.5 and then to 1 molal reduced the death to an average of 200 μm deep.

Discussion

In short, the viability results proved that reduction of scattering in articular cartilage via hyper-osmotic agents resulted in excessive if not total cell death at molalities high enough to make any optical difference. There was a visible translucency to the specimens exposed to 4 molal solutions, and transparency for those exposed to 8 molal solutions. This was seen to a greater effect for fructose than for ribose. (In light of this method's exclusion as a complement to tissue bonding, transmittance spectra were not taken.) Noting from the data that fructose exhibited a higher refractive index than ribose, this might be expected. Fructose was investigated because it had similar physical properties in terms of refractive index and molecular weight as glucose, but would not be as biologically active since fructose must be broken down prior to its use by cells. Interestingly, ribose elicited more cell death than fructose at corresponding molalities.

While there was not an osmometer nearby with a range on the order of the sugar solutions used here, the osmolarities may be estimated. The PBS without calcium or magnesium averages 297 mOsm and the high-glucose DMEM approximately 450 mOsm. Osmolarity is the concentration of a solution expressed in terms of its osmotically active particles, that is, those particles that contribute to the concentration gradient. NaCl has two, Na^+ and Cl^-; glucose, and similarly ribose and fructose, have one. Therefore, the osmolarity of a sugar-PBS solution may be considered as additive. For example, a 1M (1 molar) glucose-PBS solution will have an osmolarity of approximately 1297 mOsm (1.297 Osm = 1 Osm from glucose and 0.297 Osm from PBS). Obviously, even a 0.5

molal sugar solution, which in this range is approximately equivalent to a 0.5M solution, produces an 800 mOsm solution that is well above physiologic values.

One point of note is that a few papers by the same group cite 7M (7 molar) glucose as the osmotic agent being used.[105,114] The refractive index cited, however, is more in line with 4M glucose, which would correspond to the 7 molal solution measured in this study. Also, the refractive index data determined here correlates well with data found elsewhere[106], and a 7M sugar solution was too viscous to attain much permeation into a tissue.

Perhaps this optical clearing approach will be of use for imaging collagen architecture, given the tissue could be cleared while the collagen fibrils could be selectively stained. It is not, however, a potential enhancement that could be used in concert with photochemical bonding given the near-total to total cell death that occurs at "clearing" molalities.

CHAPTER VII.

PROTEIN IRRADIATION STUDIES

Introduction

Photo-Oxidation of Proteins

Type I processes are characterized by the direct photo-oxidation of protein side chains or bound chromophores. UV induced protein crosslinking and degradation is an example of this process. A type I process results in the generation of excited singlet or triplet states of biomolecules, leading to the formation of highly reactive radicals. In contrast, a type II process is characterized by the indirect photo-oxidation of a substrate via formation of singlet oxygen ($^1O_2$). In this case, a chromophore (whether intrinsic or exogenous in nature) is excited by incident radiation. The excited state of this chromophore in turn generates $^1O_2$ by the transfer of energy from the excited photosensitizer to the ground state, in situ molecular oxygen. Protein oxidation in a type II process is thus a secondary effect and not the primary event.[115,116] Because proteins typically have no functional groups with absorbance peaks greater than about 320 nm, they are inefficient at generating $^1O_2$ by direct sensitization and require the presence of an exogenous photosensitizer.[115,117]

Singlet oxygen generated outside of cells is inefficient at inducing cellular toxicity, a primary goal of Photodynamic Therapy (PDT), when compared to singlet oxygen generated inside of the cellular space. Thus, quantum yields for cellular inactivation are often ten times larger for lipophilic sensitizers that penetrate the cellular lipid bilayer than for hydrophilic sensitizers that stay localized in the surrounding extracellular medium. Many of these dyes, however, have similar yields of singlet oxygen. The biological effects are therefore dependent on the preferential localization of the dye.[118] A dye excluded from PDT for being inefficient at inducing cellular destruction may work well for targeting effects to extracellular proteins. In addition, the degree of hydrophilicity can also affect which proteins are affected as more hydrophobic sensitizers tend to associate with lipoproteins, while the more hydrophilic photosensitizers tend to associate with serum albumin and other high molecular weight proteins such as the structural proteins.[119]

The amino acids cysteine, histidine, methionine, tyrosine, and tryptophan are known to be affected by photo-oxidation, and are, in fact, the only amino acids that react with $^1O_2$ at physiological pH at rates fast enough to be significant.[115,116,120] Typically, however, the products formed by this photo-oxidation depend on the class of photosensitizer – type I or type II – used as the excited chromophore. Generally, while the side chain amino acid residues are affected or even damaged by photo-oxidation, the peptide bonds are not damaged.[116]

Consequences of $^1O_2$ exposure of proteins have included the formation of aggregates and crosslinks.[115,116] These may include oxidizing cysteine to form intermolecular disulfide bonds or crosslinking reactions that are byproducts of the initial

oxidized product. For instance, products formed from oxidized histidine residues can react with lysine, cysteine, or even other histidine residues to form crosslinks.[115,117,121] It is important to note, however, that reactions and reaction rates with constituent amino acid groups, and even denatured proteins in solution, are not necessarily (and are often not) indicative of the reactivity and consequences of oxidation of a large polypeptide.[122] Even the very nature of the crosslinking mechanisms and which side groups are involved has been debated.[123,124]

Many studies have investigated the effects of photo-oxidation on collagen[125,126,127,128,129], which lacks cysteine and tryptophan. Studies have shown that increased molecular weight aggregates and crosslinks are formed[126,127,128], but also that singlet oxygen treated collagen behaves very similarly to pepsin treated collagen when solubilized in that it can no longer associate into physiologic fibrils. No denaturation of the collagen molecule itself was seen, however.[130] It has also been shown that porphyrins bind to collagen, causing aggregation behavior prior to irradiation. Binding was found to a greater extent with acid soluble collagen than it was for insoluble collagen.[131] Different studies have used riboflavin[126,132], methylene blue[125], hypericum[133], or porphyrins[131]. Still other studies have found that standard photosensitizers rose bengal and methylene blue had an effect on collagen, but not to any great extent with respect to the ability to form crosslinks and higher molecular weight aggregates.[134]

Photosensitizers

In photodynamic therapy (PDT), which aims to destroy cancer cells by oxidizing them from within via a type II process, a wide range of photosensitizers have been extensively investigated. These include porphyrins and the related compound classes of phthalocyanines and chlorins. Porphyrins are planar aromatic compounds exhibiting a characteristic absorbance peak near 400 nm (called the Soret band) and multiple smaller absorbance peaks in the 500-650 nm region (called Q bands). Porphyrins are typically hydrophobic, but when synthesized they may be made hydrophilic by sulfonation at the p-positions of the benzene rings. In general, the greater degree of sulfonation a porphyrin is subjected to, the greater the degree of hydrophilicity. Phthalocyanines are larger planar compounds than porphyrins, generated when all four meso carbon bridges are replaced by nitrogen and benzo rings are fused the ββ'–bonds of porphyrins. These changes shift the absorbance spectrum such that the strongest absorbance peak now occurs in the 670-700 nm region. Increasing hydrophilicity can again be achieved with sulfonation.[119] Porphyrins typically act via a type II process[135], while phthalocyanines may sensitize biomolecules via type I and type II processes.[116]

Other photosensitizers, while not prime candidates for PDT, are also photochemically reactive when excited with wavelengths in the visible spectrum. Tetrabromorhodamine-123 (TBR) and riboflavin-5-phosphate (R5P) have been investigated for ureteral and corneal sealing as described in Chapter II. Recall that TBR is a cationic, hydrophobic dye that operates via a type II process and exhibits an absorbance peak at 514 nm. In contrast, riboflavin-5-phosphate is a hydrophilic

photosensitizer with a secondary absorbance peak at 447 nm. R5P is predominantly a type I photosensitizer.

Fourier Transform Infrared Spectroscopy to Investigate Proteins

Fourier Transform Infrared Spectroscopy (FTIR) is a widely used method to study proteins and their conformation. FTIR instruments are based on the Michelson interferometer and employ the fast Fourier transform algorithm to obtain a sample spectrum. Complete reviews of FTIR instruments, their development, and applications are widely available, and thus will not be repeated here.[136]

Attenuated Total Reflectance (ATR) is a method used in conjunction with FTIR that exhibits relative insensitivity to sample thickness. ATR is a reflectance method where samples are held in close contact with a high refractive index crystal (usually Germanium or Zinc Selenide). The incident infrared beam is incident on one face of the trapezoidal, prismatically shaped ATR crystal. At each point of internal reflection, there is an evanescent electromagnetic wave that penetrates the crystal surface into the sample material of lower refractive index. If there are no absorbing species in the material of lower refractive index, the interface will reflect 100% of incident light. Therefore, the difference in the intensity of light due to internal reflection gives information on infrared absorbing species in the sample material. Considering a typical refractive index for proteins to be approximately 1.5 in the dry state and a Germanium crystal, this gives a penetration depth of roughly 430 nm into a protein sample.[137] Single-bounce FTIR-ATR

methods such as those employed in this study, however, are not as sensitive as multiple-bounce methods that require a larger sample size.

The infrared spectra of proteins exhibit a number of bands, called amide bands, which represent different vibrational modes of the peptide bond. An investigation of these bands can therefore provide insight as to the secondary structure of proteins, as these modes are very sensitive to hydrogen bonding and coupling between adjacent peptide bonds. Amide I bands centered around 1650-1658 are generally considered to be typical of alpha helices such as those that make up collagen molecules. Water also has a strong IR band in this region, however, and attempts to simply subtract the water signal often induce artifacts. To overcome this issue, proteins are often dehydrated and incorporated into KBr pellets or placed into deuterated water (D_2O). Yet proteins in the physiological state are most often in an aqueous environment, and so such techniques usually result in a non-ordered conformation of the protein.

Collagen has several characteristic amide bands arising from peptide bond vibrations that are visible with FTIR:

- Amide-I (C=O stretch, ~1650-1665 cm^{-1}),
- Amide-II (C–N stretch and N–H bend vibrations, ~1530-1550 cm^{-1}),
- Amide-III (C–N stretch, N–H bend, C–C stretch, ~1250 cm^{-1}),
- Amide-A (N=H stretch, 3330cm^{-1}), and
- Amide-B (N–H stretch, ~3080 cm^{-1}).[138,139]

Shifts in the frequency of these bands and/or the ratios of peak magnitudes or area under the curves represent a structural change in a protein's peptide bonds such as would be seen in a photochemically induced covalent bonding between different amino acids. It is

not, however, the absolute value of a given peak in one sample as compared to an irradiated version of that sample that defines a change, but instead the change in the ratio of the amide peaks (or the area under the Gaussian amide curves) between the two samples.

Methods

Collagen is well known to self-associate into fibers in solution at physiologic pH and temperature. This entropy-driven process has been frequently used to create bulk gels for various biomedical or tissue engineering applications. Yet while collagen type I readily self-associates to form a gel in this manner, type-II collagen does not.

This portion of the study used bulk collagen as a model system to qualitatively assess the ability of various photosensitizers and irradiation to crosslink the collagen fibers FTIR/ATR was used to evaluate the amide bands characterizing the peptide linkages of both non-irradiated and irradiated collagens doped with the photosensitizers. The variations seen in the collagen amide bands with differing photosensitizers and irradiation protocols were used to assess which photosensitizers could affect a given collagen type and which irradiation protocols were necessary to induce crosslinking. The collagens used in this study were:

- Collagen, type I from calf skin (MP Biomedical) – acid soluble
- Collagen, type I from calf skin (MP Biomedical) – insoluble
- Gelatin, type A (MP Biomedical)
- Collagen, type II from calf articular joints (Elastin Products) – acid soluble

All solutions derived from acid soluble collagen were first solubilized in 0.1M acetic acid to a concentration of 10 mg/ml at 4°C. After dissolution was complete, and immediately prior to irradiation experiments, the solutions were brought to a pH between 7.0 and 7.4 with 1 M sodium hydroxide (NaOH) and a photosensitizer solution such that the final collagen and photosensitizer concentrations were approximately 8 mg/ml and 1 mM respectively. The acetic acid, NaOH, and photosensitizer solutions were all brought to the specified molarity using PBS with no calcium or magnesium in order to maintain a NaCl concentration close to the physiologic level.

All FTIR/ATR spectra were conducted on a Magna 550 FTIR (Thermo-Nicolet) with a Germanium crystal, single-bounce ATR accessory (ThunderdomeTM, Thermo-Nicolet). Final absorbance spectra were automatically differenced, subtracting out the background spectrum that included any residual water vapor. All spectra were collected over 100 scans at a resolution of $4cm^{-1}$.

Preliminary Investigations with Riboflavin-5-Phosphate and Tetrabromorhodamine

Riboflavin-5-Phosphate (R5P) (Sigma) and tetrabromorhodamine-123-bromide (TBR) (Molecular Probes) were used as sensitizers due to their use in prior efforts by other researchers as already described. Recall that riboflavin-5-phosphate is predominantly a type I photosensitizer while TBR photo-oxidizes via a type II process. Bulk photogellation studies were performed by irradiating the solutions within coated aluminum wells. Well area was approximately 4 mm in diameter and 2 mm in depth.

A 5 W argon ion laser system (SpectraPhysics) was used as described in Chapter V. Wavelengths of 458 nm, 488 nm, and the combination of all lines (458, 488, and 514 nm) were investigated for R5P photogellation. Only the 514 nm wavelength was used for TBR-doped samples, corresponding to maximum absorbance for TBR. A range of concentration values and irradiation parameters were used for each photosensitizer. The beam diameter was approximately 6.5 mm; irradiances and exposures are given in the *Results* section that follows.

All irradiated and control samples were stored in a desiccator in the dark immediately after irradiation for approximately 48 hours prior to evaluation. Control samples consisted of the same collagen-photosensitizer mixture with no irradiation and were stored in the same manner.

Photosensitizer Selection and Absorbance Spectra

The purpose of R5P and TBR photogellation experiments was to determine whether a type I or type II photochemical process was necessary to affect type I and/or type II collagen. It was desired to use photosensitizers such as porphyrins or phthalocyanines that exhibited a known affinity for collagen, and had a range of absorbance peaks in the visible portion of the spectrum depending on the specific compound selected. Recall that porphyrins photosensitize via a type II process and phthalocyanines via both type I and type II pathways.

In this portion of the study, various porphyrin and phthalocyanines photosensitizers were investigated for their degree of hydrophilicity and wavelength of

peak absorbance. Hydrophilic sensitizers were desired since collagen solutions are aqueous and ethanol or other organic solvents required to solubilize hydrophobic sensitizers are known to modify collagen as well as induce cellular toxicity. One porphyrin and two phthalocyanines were investigated:

- Meso-tetra(N-methyl-4-pyridyl)porphine tetra tosylate (T4MPyP-tt) (Frontier Scientific) is a cationic, essentially hydrophilic porphyrin with a molecular weight of 1363.6.
- Chloro-aluminum phthalocyanine tetrasulfonic acid (CASPc) (Frontier Scientific) is an anionic, hydrophilic phthalocyanines with a molecular weight of 895.2
- Zinc phthalocyanine tetrasulfonic acid (ZNSPc) (Frontier Scientific) is an anionic compound with a molecular weight of 898.2 that is less hydrophilic than CASPc.

Absorbance spectra were run on a Varian Cary 500 spectrophotometer using quartz cells with a 2 mm path length. A blank cuvette (air only) was used as the baseline. Photosensitizers were solubilized in ethanol and PBS to evaluate their relative hydrophilicity in terms of an absorbance peak shift. Concentrations were diluted until absorbances were within the range of the instrument. Final absorbance spectra were normalized against the peak absorbance for the given spectral curve such that all spectra displayed a peak absorbance of 1.0.

Bulk Collagen Photogellation Experiments using CASPc and T4MPyP-tt

Two photosensitizers, CASPc and T4MPyP-tt, were selected from the previous set of experiments due to their hydrophilicity and absorbance peaks corresponding to portable laser emitting diode systems. Acid soluble collagen type I and type II were brought into solution as described previously. Final collagen and photosensitizer concentrations were approximately 8 mg/ml and 1.1 mM respectively at a pH between 7.0-7.4. All irradiations involving CASPc were conducted with the 667 nm diode system described in Chapter V at 1110 mW/cm^2 and 666 J/cm^2 (corresponding to 10 minutes) using a 5 mm spot size. Similarly, all irradiations involving T4MPyP-tt were conducted with the 420 nm system at 57 mW/cm^2 (the maximum achievable with that system) and either 34 J/cm^2 or 68 J/cm^2 (corresponding to 10 or 20 minutes, respectively).

Both collagen solutions exhibited increased viscosity instantly with the addition of photosensitizer though perhaps to a slightly greater effect with CASPc. Small portions of collagen/photosensitizer solutions were therefore scooped onto a microscope slide with a small spatula such that the diameter of the portion to be irradiated did not exceed the spot size for a given system. Samples were irradiated in open air and then immediately stored in a desiccator in the dark for 48 hours prior to conducting the FTIR/ATR analysis. Control specimens included the photosensitizer but were not irradiated, since the photosensitizer altered the solution kinetics and the FTIR spectra. Separate photosensitizer spectra were also taken, both non-irradiated and irradiated cases. Native cartilage spectra were taken as well.

Spectra were also taken for insoluble collagen and gelatin in addition to the acid soluble collagens type I and II in order to help elucidate differences in spectra due to denaturation. Spectra were taken for these substances in their supplied form. Specifically, the acid soluble collagens were not solubilized, but instead taken in their solid, supplied form with no additional treatment.

Results

Preliminary Investigations with Riboflavin-5-Phosphate and Tetrabromorhodamine

Preliminary experiments using R5P and TBR were conducted to determine if a specific photochemical pathway, type I or type II, was necessary to affect a given collagen type. Type I and type II collagen were evaluated due to their relevance for the meniscal fibrocartilage and hyaline cartilage tissues that are predominantly type I and II collagen respectively.

First it was found that a lower concentration of R5P than commonly used for photochemical tissue bonding (12 mM) allowed better optical penetration through 2 mm collagen solution thicknesses, and thus better gellation. For the final well size selected (4 mm in diameter by 2 mm in depth), it was determined that a 1 mM photosensitizer solution offered the best penetration while maintaining sufficient photodynamic activity to affect the collagen as detectable by FTIR/ATR. By visible inspection, pure collagen type I irradiated with R5P formed a gel with the same degree of firmness as the

physiologic temperature and pH method. There was some visibly apparent, though minor viscosity increase for the collagen-II/R5P solutions. However, collagen type II irradiated with R5P did not form a coagulated gel. It was further observed that physical coagulation was possible for a 1:1 mixture of collagen-I to collagen-II. An argon laser producing 1 W/cm^2 (spot size 6.5 mm) at 488 nm was used at an average exposure of 900-1000 J/cm^2 for the R5P/collagen solution irradiations.

Increasing the power density to 6 W/cm^2 and using all argon lines (458nm, 488nm, 514nm) simultaneously resulted in a decrease in the collagen/R5P solution viscosity for all cases. Additionally, leaving the collagen-I/R5P sample to be gelled under irradiation at 488nm (1 W/cm^2) for exposures on the order of 1800 J/cm^2 resulted in first a visible gelling, and then a drastic viscosity decrease. There appears, therefore, to be a limit to the type I photochemical process with respect to its radical formation and collagen crosslinking before the protein has been so affected that it can no longer maintain its structural characteristics. There was no discernable effect for type II collagen with R5P for the range of irradiation parameters investigated as determined by visible inspection of coagulation or by FTIR evaluation.

While the collagen-I/TBR solution also gelled upon irradiation, it coagulated much faster than the R5P samples. Irradiances ranging from 0.9-1.7 W/cm^2 at 514nm and exposures ranging from 500-1000 J/cm^2 were investigated. TBR concentrations were held at 1 mM for all collagen solutions. Unlike the R5P samples, the irradiated collagen-II/ TBR specimens formed a coagulated three-dimensional gel with the same apparent firmness as the collagen-I samples. Subsequent immersion of the collagen-II/TBR gels in

PBS and stored at 5ºC for four days showed only minor deterioration of the matrix by visible inspection.

Figure 14 (a) shows the FTIR results for the collagen-II/TBR system, with a visible increase in Amide II with respect to Amide I. Spectra in the Amide A and B regions did not yield enough signal to be conclusive and are therefore not shown. Variations of the Amide I and II bands with respect to the amount of exposure are seen in Figure 14 (b) for collagen-I/TBR, again showing an apparent irradiance/exposure limit with respect to the effect on collagen. For the collagenI/R5P solutions, Figure 14 (c) shows a complete reversal of the Amide-I and –II peaks with irradiation. Additional control samples that were irradiated identically to the photosensitizer-doped samples, but contained only collagen were similar to the controls shown in Figure 14 and exhibited no changes in the amide peaks such as those seen in the protein-sensitizer irradiated samples.

Photosensitizer Selection and Absorbance Spectra

Both CASPc and T4MPyP-tt maintained their absorbance characteristics when solubilized in PBS. ZNSPc did not and its absorbance peak demonstrated a pronounced decrease and blue-shift when PBS was used as the solvent instead of ethanol. ZNSPc also exhibited a lower absorbance when compared to the same concentration of CASPc. Figure 15 shows absorbance spectra for each of these photosensitizers in ethanol and PBS.

(a)

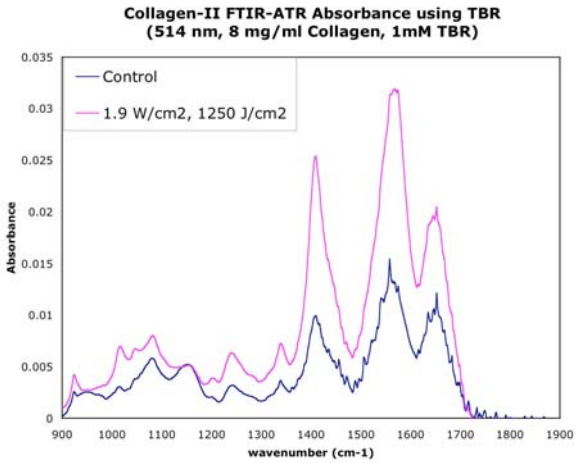

(b)

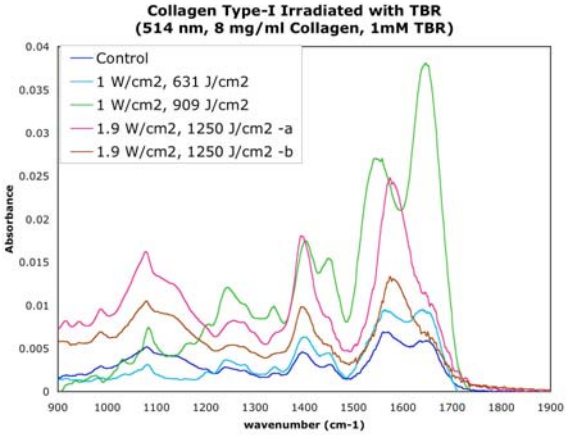

(c)

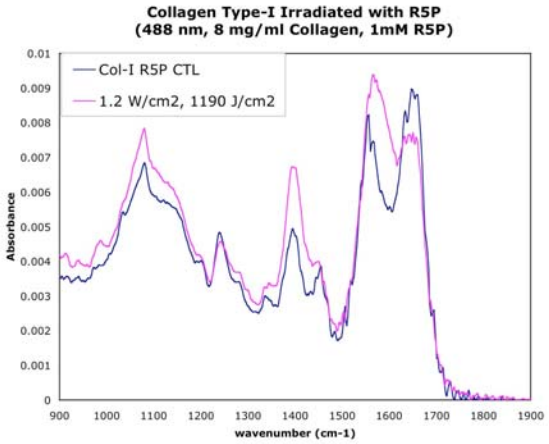

Figure 14: Preliminary collagen photogellation FTIR results using R5P and TBR

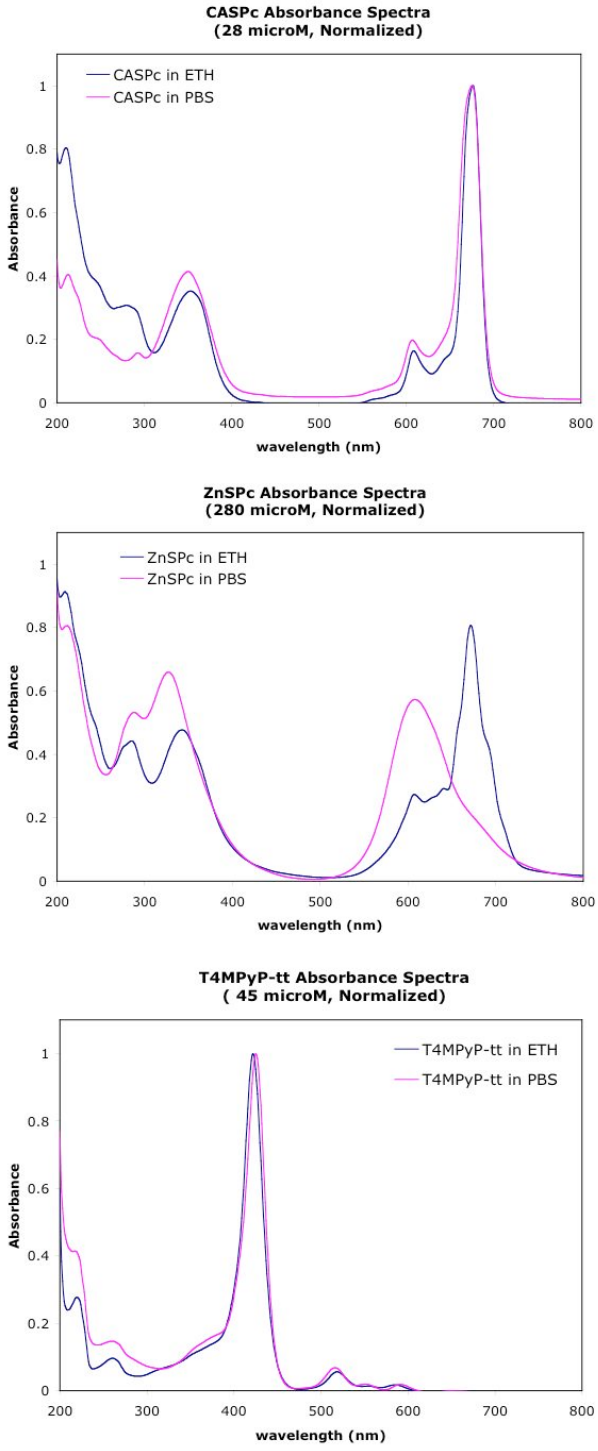

Figure 15: Absorbance spectra for CASPc, ZNSPc, and T4MPyP-tt

Bulk Collagen Photogellation Experiments using CASPc and T4MPyP-tt

Spectra for photosensitizer and native calf cartilage are shown in Figure 16, while spectra for the photosensitizers and collagens as supplied are shown in Figure 17. A clear dominance of the Amide I peak over the Amide II band was seen for native articular cartilage (hyaline cartilage). The CASPc photosensitizer exhibited a peak at 1030 cm^{-1}, but only minor absorbance in the Amide I and II regions and is thus not a contaminating factor with respect to evaluating these bands. Also, the CASPc spectra did not exhibit any significant alteration upon irradiation. In contrast, T4MPyP-tt presented slightly shifted peaks and the appearance or increased prevalence of peaks below 1250 cm^{-1} upon irradiation, and there was a minor absorbance peak at 1641 cm^{-1} that overlaps the Amide I band in proteins.

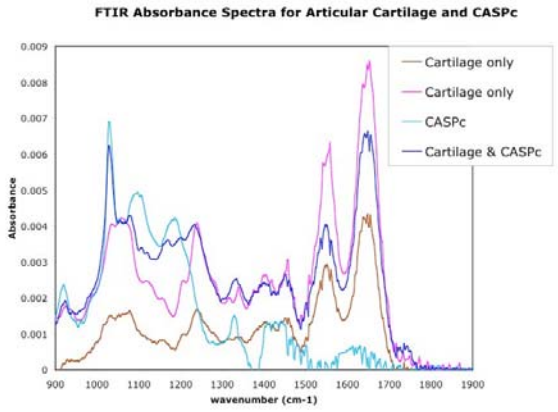

Figure 16: FTIR absorbance spectra for native calf cartilage with and without CASPc

Similar to the native cartilage, spectra for the untreated/unsolubilized collagens also exhibited a dominance of the Amide I band over that of the Amide II band, as shown in Figure 17. No change in this characteristic was seen for the gelatin sample where the collagen was known to be denatured. However, a small, downward spectral shift in the Amide I band was seen for the gelatin as compared to the other collagen samples. This potential significance of this will be covered in the *Discussion* section of this chapter.

Bulk collagen irradiations with both CASPc and T4MPyP-tt were conducted for acid solubilized collagen type I and type I. Selected spectra for collagen type I are shown in Figure 18, and for collagen type II in Figure 19. Specific ratios of Amide I and II peaks are detailed in Appendix A-4.

Irradiated collagen solutions did exhibit a clear difference in the ratio of the Amide I and Amide II peaks, and the precise nature of that difference depended on the type of collagen and how long a sample had been irradiated. For example, collagen type II with T4MPyP-tt showed the Amide I peak increasing with respect to the Amide II peak when compared with controls, and then decreasing below the ratio seen in controls with longer exposure. This likely indicates an increase in structural crosslinking, followed by a decomposition as the increasing degree of oxidation breaks down the molecular integrity. This has important ramifications for photocrosslinking of tissue – there will be a temporal limit on effectiveness prior to degradation of the very bond(s) it is desired to effect.

Collagen type I and type II irradiated with CASPc also showed increasing importance of the Amide I peak with respect to Amide II when compared to non-irradiated controls, again demonstrating a change in structural conformation. Results for

collagen-I treated with T4MPyP-tt are less conclusive, but given the photosensitizer peak around 1641 cm^{-1}, this may or may not be an artifact of localized photosensitizer concentration in a viscous solution.

All controls shown in the FTIR/ATR spectra include the photosensitizer but were not irradiated. Presence of the photosensitizer altered the solution viscosity prior to irradiation and the photosensitizer spectra showed some peaks that overlapped those of the collagen, the peak around 1330 cm^{-1} for example. Non-irradiated controls that included the photosensitizer were thus necessary for comparison. Collagen alone has no absorbance at either 420 nm or 667 nm, but instead absorbs only in the UV region. Irradiances were low enough that no thermal effects were induced for collagen alone at these wavelengths and other, preliminary investigations showed no differences in irradiated versus non-irradiated collagen without photosensitizers.

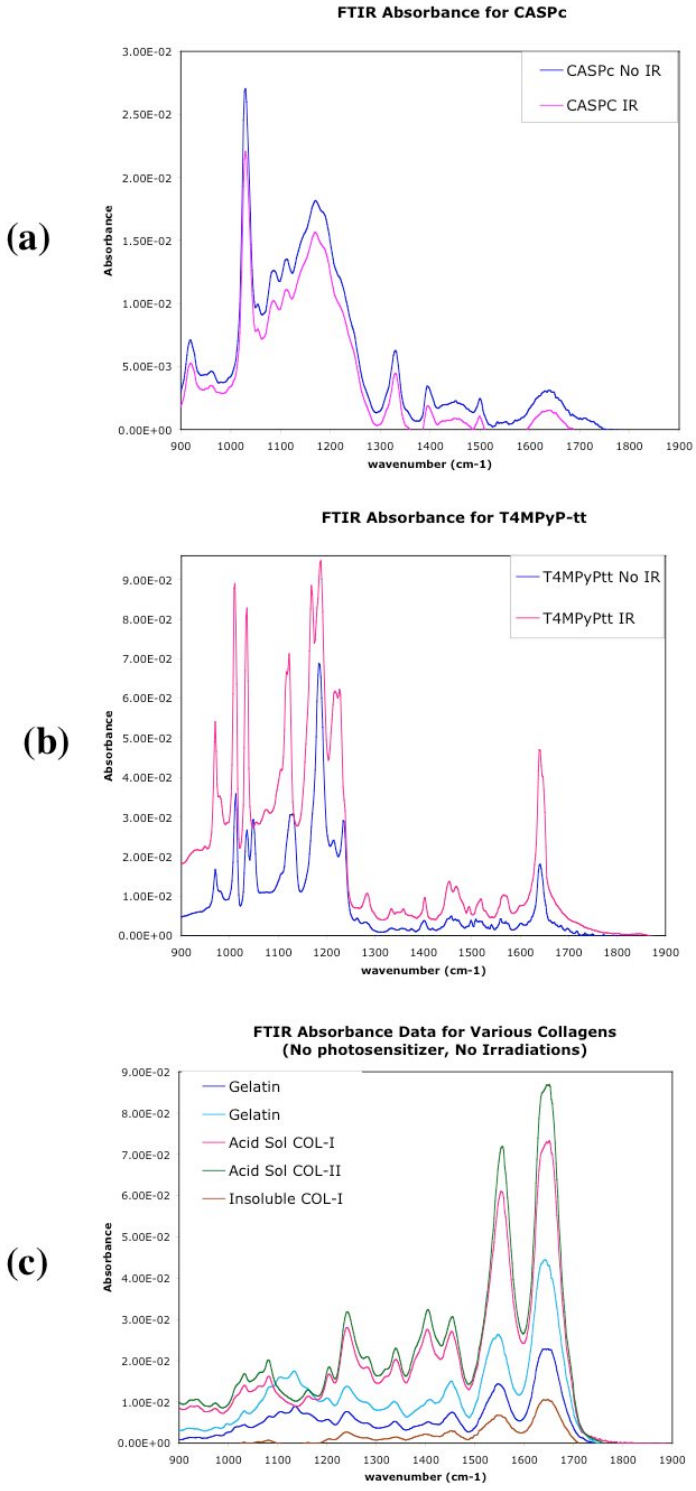

Figure 17: FTIR absorbance spectra for the photosensitizers CASPc and T4MPyP-tt and for different collagens. (Collagens as supplied, with no additional treatment.)

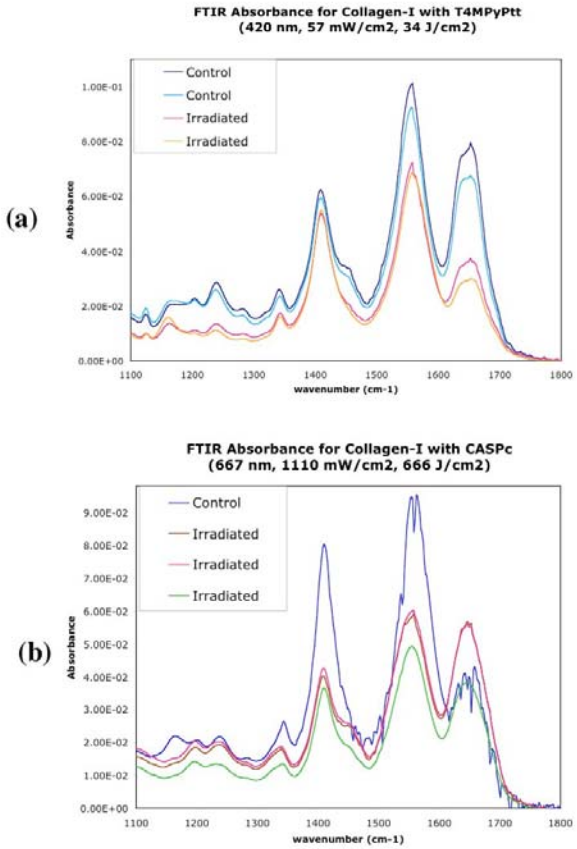

Figure 18: FTIR absorbance spectra for acid solubilized collagen type I irradiated with CASPc and T4MPyP-tt

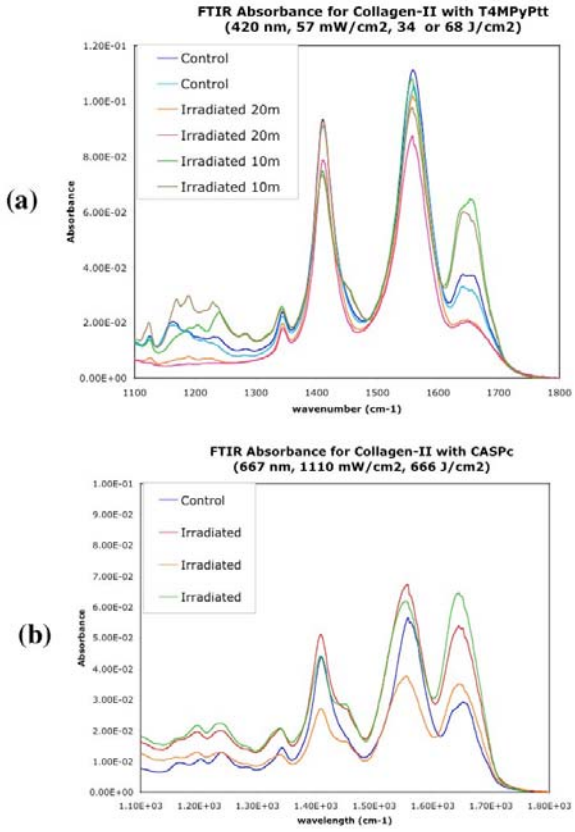

Figure 19: FTIR absorbance spectra for acid solubilized collagen type II irradiated with CASPc and T4MPyP-tt

Discussion

The preliminary bulk gellation and FTIR studies show that different mechanisms of photochemical processes, type-I versus type-II, have differing abilities to affect different collagens. For example, TBR, a type-II photosensitizer, was able to affect coagulation of collagen-II under irradiation while R5P, a type-I sensitizer, was not. This has significant implications with respect to cartilage tissues. Recall that the articular cartilage matrix is predominantly collagen-II while meniscal fibrocartilage is comprised primarily of collagen-I. Given the results of the R5P and TBR experiments, a method of photochemical bonding effective for one of these tissues may thus be expected to have different results for the other. These experiments demonstrated that to affect collagen-II in a manner that enhances structural coagulation and causes an alteration in amide bands as detectable by FTIR/ATR, a photosensitizer that operates via the type II photochemical pathway is likely necessary.

Previous investigations into vitreous liquefaction seem to support these results. Like articular cartilage, the vitreous is comprised mainly of collagen type II. It was found that riboflavin caused vitreous liquefaction, while a porphyrin derivative, a singlet oxygen generator (type II photochemical pathway), caused extensive crosslinking of the tissue collagen as manifested by aggregation and insolubilization.[127]

In order to move away from the highly hydrophobic TBR photosensitizer and the larger argon laser system, porphyrins and phthalocyanines were then investigated. The porphyrin and phthalocyanine photosensitizers operate via type II and combined type I/II photochemical pathways respectively. Therefore, both photosensitizers had the potential

to affect the type II collagen. Bulk gellation studies of acid soluble collagen with T4MPyP-tt (the porphyrin compound) and CASPc (the phthalocyanine) showed that these photosensitizers were indeed able to effect structural changes in the collagen molecule for both types of collagen investigated.

Many previous studies in the literature have investigated collagen via FTIR. The Amide I peak is found to be greater than the Amide II peak for undenatured, untreated collagens [140,141], which correlates well with the results seen here for the acid soluble collagens when the spectra were run prior to any acid solubilization. Noting that the Amide I peak is lower than that of the Amide II in the control collagen samples, those that have been acid solubilized, it becomes obvious that the acid acted to alter the conformational state of the collagen. Since any photosensitizer artifacts would only serve to increase the Amide I and not the Amide II band, additive photosensitizer spectra can be discounted (i.e. – the presence of the photosensitizers used in these studies did not serve to increase the Amide II band). The post-irradiation results seen in these experiments, where the Amide II band increased with respect to the Amide I band, are therefore most likely due to the radicals released during the photochemical process.

Although the comparison of the collagens themselves (insoluble, acid soluble, and gelatin) did not appear to be conclusive with respect to spectral differences detected in this study, it has been shown in the literature that the Amide I peak decreases in magnitude with denaturation. It has also been shown that the Amide I component bands centered at 1660 and 1633 cm cm^{-1} decrease and increase in magnitude respectively with denaturation. This results in a downward shift of the peak Amide I frequency.[139,142]

Looking at the CASPc treated collagens in this study, the Amide I peak shifted from 1653-1657 cm^{-1} to 1647-1649 cm^{-1}. In these cases, however, the Amide I peak was increasing with respect to the Amide II peak with irradiation in apparent contrast to the Amide I magnitude attenuation that should be seen with denaturation. A possible explanation is that the structural integrity is broken down by the acid solubilization process (decreasing the Amide I from the non-acid solubilized samples), and then followed by the increased crosslinks formed intra- and/or intermolecularly by the photochemical process, thus beginning to increase structural order/level seen in the Amide I region.

The many results of this section highlight a few key points with respect to photochemical bonding of cartilage, namely:

- In a system that contains many biological components, as cartilage is comprised of proteins, glycosaminoglycans, proteoglycans, etc., it is difficult if not impossible to determine precisely which components were affected by the photodynamic process to contribute to any formed crosslinks. By evaluating collagen alone as an isolated system, these experiments showed that the photosensitizers used here were able to affect the collagen, the structural component of the tissues it is desired to bond, and that they were able to do so within the power levels available from the given optical systems.
- In order to affect collagen type II, as found in articular cartilage, a photosensitizer that can operate via the type II photochemical pathway, producing singlet oxygen, was needed. Results showed that a photosensitizer operating via both type I and II pathways, specifically the phthalocyanine CASPc, was also able to affect type

II collagen. Therefore it was the presence of a type II photochemical pathway and not the absence of a type I pathway that appeared to be the critical requirement to affect the type II collagen for the photosensitizers studied.

- The structural effect on the collagen crosslinking seen as changes in the relative levels of the Amide bands could reverse itself with too much exposure. Therefore, there will be a temporal limit to the cartilage bonding process or the very bond formed may be degraded by the same radical species that helped to create it.
- Various experimentation with lesser powers and times than those shown here did not induce any discernable change in the FTIR spectra, and so this serves as a power and exposure guide for the tissue bonding experiments.

CHAPTER VIII.

BIOMECHANICAL TESTING OF THE TISSUE-TISSUE INTERFACE

Introduction

Recall from the previous discussion on cartilage injury in Chapter II that the cartilage injury may present itself in the form of intra-tissue tears or fractures. Potential repair sites may be between cartilage-to-cartilage tissue in the cases of tissue fractures, tears, or osteoarthritic fissures. Or, if a larger defect is to be repaired, the construct-cartilage interface becomes critical. This interface, between the implant, whether allograft or scaffold-based (the scaffold which may, in turn, be biological or synthetic or some combination thereof) and the host tissue, may be limited to the cartilage in depth or may include both cartilage and bone interfacial contact as an osteochondral repair. These concepts are re-illustrated here in Figure 20.

Given its importance, many efforts have been undertaken to assess the strength of the repair interface. The interface may consist of nothing but biological repair material as in the case where two tissue specimens are held together in apposition until some biological integration has occurred. Conversely, the interface may include an exogenous adhesive intended to hold the tissue sections together. For adhesives, failure may then be either adhesive, in which failure occurs between the adhesive and adherend, or cohesive where failure occurs within the adhesive itself.[143] Approaches to determine the

interfacial strength of two surfaces in apposition vary with the expected loading environment of the actual specimen and hence the probable failure mode. Some efforts are more concerned with the ultimate strength in a given configuration while others are more concerned about failure characteristics at a certain rate or in combined loading situations. All of this tends to be reduced simply to methods using a strength of materials approach or a fracture mechanics approach.[29]

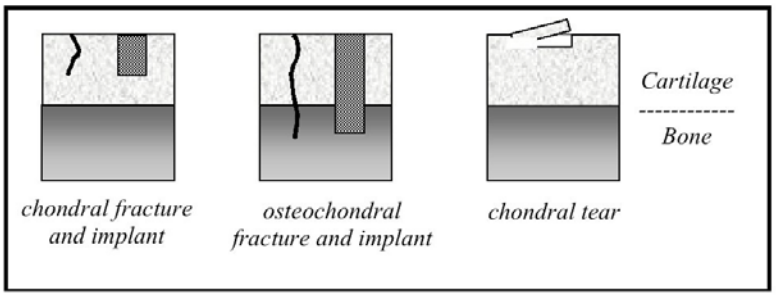

Figure 20: Examples of cartilage repair sites – defects limited to the chondral depth; defects penetrating the subchondral bone; and cartilage tear

Briefly, the strength of materials approach characterizes mechanical failure of a bonded region by determining the maximum normal or shear strength sustained immediately prior to failure. Examples of this testing approach include push-out and single-lap shear tests. Strength is typically defined as the maximum load applied prior to failure divided by the total area of the bonded joint, the maximum stress at which joint integrity can be maintained. Methods for testing these joints have been applied in various

adaptations to determine cartilage integrative repair strength[27,28,30,32,144] or the strength of adhesives applied to cartilage tissues.[24]

In contrast, the fracture mechanics approach assumes there are flaws in the materials being tested, and that it is the propagation of these flaws that cause failure. This propagation behavior is dependent on the applied stress, the applied stress rate, the specimen geometry, and the fracture toughness of the material.[145] Peel or tear tests are the most common means to investigate cartilage fracture mechanics. These tests investigate Mode I failure: failure due to tensile stresses normal to the crack plane. For comparison, Mode II and Mode III failures in fracture mechanics represent in-plane shear or transverse, out-of-plane shearing of the crack interface respectively.[29,145]

Peel or tear tests estimate the energy dissipation at the crack tip during fracture propogation, and offer the advantage that a direct comparison of native tissue to a repair or bonded tissue region can be made. Accurate analysis of results requires that the energy dissipated at the fracture tip be differentiated from the storage and dissipation of energy occuring elsewhere in the tissue test specimen. However, the amount of elastic energy stored and the energy dissipated through the solid-fluid interaction in the cartilage tissue matrix has not yet been estimated.[29,30]

Potential Strength of Materials Test Methods and Associated Considerations for Cartilage

Direct Tension or Shear of Opposing Surfaces

One commonly used method is to create a butted joint, that is, a bond between two surfaces in direct apposition such that the entire surface of one side of each adherend comprises the bond area. An example of this technique in cartilage testing is two osteochondral cylindrical dowels that are attached cartilage-to-cartilage as shown in Figure 21 (a). When testing in pure uniaxial tension, there will be some bulk deformation of the cartilage complicating the measurement of adhesive bond strength, an effect that becomes more significant with increasing interfacial strength. The advantage of using osteochondral plugs instead of pure cartilage specimens in this situation is that by virtue of gripping the bone, one does not induce potential alteration of the bulk mechanical properties by leaching of a specimen-fixing glue or resin such as cyanoacrylate into the tissue, thus potentially inducing test-to-test uncertainty related to the bulk deformation during testing. This approach is, however, limited to articular cartilage rather than fibrocartilage testing. Uniaxial tension of cartilage apposed in culture with fibrin has been performed at rates of 5 mm/min[146] and 0.9 mm/min.[27] Direct shearing using this configuration has also been performed, in this case for exogenously bonded cartilage using tissue transglutaminase as the adhesive and employing a linearly increasing force of 0.29 N per 12 mm/s.[24]

Push-out Tests

When investigating cartilage or construct integration with surrounding cartilage, a concentric ring/disc geometry is common. Push-out testing appears to be preferred in the literature over pull-out methods due to the need of the latter to actively grip the ring, or the potential corruption of the interfacial region itself with a cyanoacrylate-type adhesive. Even in push-out approaches, however, non-uniformities of the geometry or interface region complicate the idealized stress distribution.[147] Extremely tight tolerances of specimen and gripping geometries are required to negate physical deformation or bolstering of the specimen or interface region. Also, results are specimen geometry dependent.[29]

Push-out tests of cartilage cylindrical cores surrounded by a supporting annulus as shown in Figure 21 (b) are a common means to evaluate cartilage integration and/or adhesion in a clinical-style configuration. Tests have been performed on cultured cartilage in this configuration using rates of 0.5 mm/min[32] and 0.5 mm/s[148] for bovine cartilage specimens in conjunction with different scaffold materials and with differing internal and external annulus radii. Ultimate strength was taken to be the force at ultimate failure per unit of the interfacial area.

Torsion of a Concentric Disc/Ring Specimen

Torsion of a concentric disc/ring configuration, or disc/annulus model, illustrated in Figure 21 (c), is another common means of assessing strength, although non-

uniformities of the geometry or interface region may complicate the idealized stress distribution. Gripping of cartilage specimens is difficult without using cyanoacrylate or applying axial compressive forces on the specimen, thereby potentially either corrupting or compressing the interfacial region.[30]

Single-Lap Joint in Tension

A single-lap shear specimen modeled off of ASTM D-3983[149] is another common means of assessing interfacial strength.[28,30] In this configuration, shown in Figure 21 (d), two thin, rectangular specimens are bonded together in an overlap region and then pulled apart in tension. Though a simple enough geometrical design, the stress behavior of the single-lap joint depends on the properties of adherends and the bond between the adherends, in addition to geometrical parameters such as specimen length (l), adherend thickness (h), crack length (a), etc. Failure of a bond interface in this configuration is actually due to a combination of axial load (P) and bending moment (M). If both adherends have an equal thickness, the bending moment is proportional to $P*h$, but the constant of proportionality (k) is geometry and load dependent such that:

$$[M/P*h] = k\,(\,P/Eh,\ l/h,\ L/l).^{33,150,151,152,153}$$

True shear strength of the adhesive can only be determined if normal stresses are completely absent. In most cases for this configuration, tensile stresses in the adhesive, manifested in the form of peel stresses, determine joint failure. Therefore, the single-lap test is not a true measure of shear strength. Both normal and shear stress concentration

factors increase towards the ends of the overlap area. The tensile component of the normal stress is usually much higher than the compressive component as the specimen deforms under the bending moment and has a dominant effect. Therefore, the peel stresses cause failure, not the average tensile shearing stress across the interface. In other words, the apparent strength of a single-lap specimen is simply the average shear stress that happens to exist in the joint when the stress concentrations reach a critical level and the joint fails. It is not the true shear strength of the adhesive.[30,33,153,154]

The single-lap configuration has been used in integrative cartilage repair studies due to ease of application and ability to replicate sample dimensions and tensile rates across multiple experiments. Similar strength results from 30-34 kPa were found across studies using specimens 9 by 5 by 0.5 mm^3 with an applied displacement rate of 0.5 mm/min after two to three weeks of culture[28,30], and another study found 15-70 kPa at the same test rate using 8 by 2.5 by 0.25 mm specimens[3,31].

Effects of Hydration on Adhesive Strength

The presence of a liquid can alter the initiation kinetics and development of defect sites responsible for fracture in adhesive-adherend systems. Therefore, the measured adhesive strength may also be altered when testing identical specimens in air as opposed to immersed in a liquid. One potential explanation is that a liquid sufficiently able to penetrate into a crack tip can produce a pressure that adds the stresses already acting on that interface. Thus, failure would occur at loads lower than when testing the same configuration in air. Such an added debonding pressure would be controlled by the

liquid's surface tension and ability to wet the joint surfaces. Another possible explanation, however, is adsorption of the liquid into the adhesive crack, thereby reducing the work of creation for new crack surfaces. The interplay of these possibilities has been previously examined for an experimental interface between an epoxy adhesive and steel wire. [155]

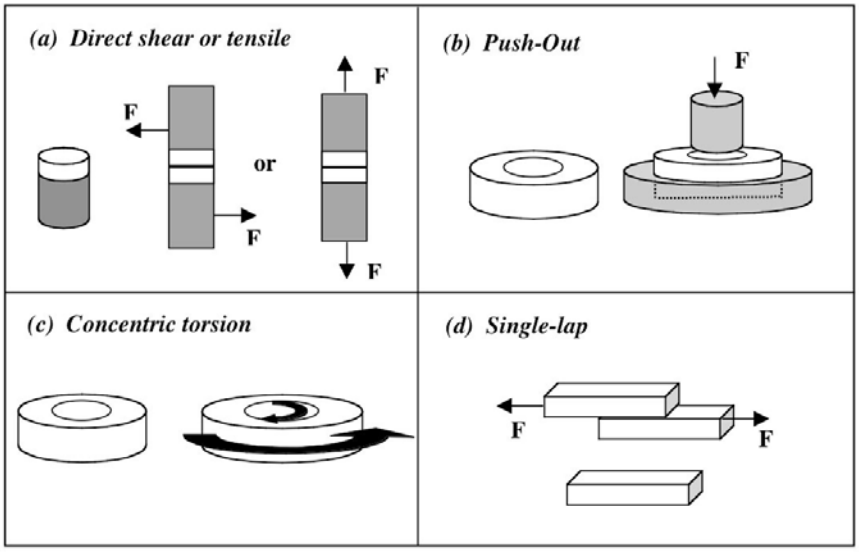

Figure 21: Specimen geometry and test configuration for (a) shear and tensile testing of surfaces in direct apposition (butted joints), (b) push-out, (c) torsional testing of interfacial bond strengths, and (d) single-lap shear.

In general, all organic adhesives absorb water, and swelling of the adhesive layer within a joint may also result in additional internal stresses. The situation is more complicated for adherends with a large surface free-energy, where adhesion is primarily due to physical interaction resulting from van der Waal's forces. In this case, the penetrating water may literally displace the adhesive. Even covalently bonded interfaces are not immune. Depending on their chemical nature and temperature, these bonds may be cleaved by hydrolysis.[156] Whichever the dominant mechanism or combination thereof, the result will be a decrease in the measured strength of the bond.

Most of these studies have involved metal adherends and synthetic adhesives for structural applications. There are, however, mentions in the literature of how hydration affects the measured strength of adhesively bonded tissue. In one study on various adhesives and tissues, special mention was made that while dehydration had no discernable effect on fibrin bond strength with skin and bone, tissue drying caused significant increase of measured bond strength with cartilage. Measured fibrin bond strength was increased from approximately 5 kPa to 15 kPa with dehydrated cartilage in a butt-joint configuration tested in tension at a displacement rate of 5 mm/min. [26] These previous observations highlight the necessity of keeping the cartilage hydrated during testing.

Methods

Many of the non-uniform stress distributions across the bond interface of single-lap joints are removed using a double-lap joint that effectively removes the bending moment associated with the adherend deformation in the single-lap case.[153] A double-lap joint is really not feasible for investigating photochemical bond strength of cartilage, however. This would require increased exposure during bonding and imposing incident radiation for the duration of ten minutes or so to each side. Since this method exhibits unknown reliability and repeatability, using a double-lap specimen might produce a joint where the bond on one side is substantially weaker than the other. Yet there are advantages associated with double-lap joints that might be extrapolated to the single-lap case by making some structural modifications.

Specifically, in finite element analysis of double-lap joints, only the top half of the joint is modeled, employing a roller support for the center-line.[157,158] Figure 22 illustrates this concept. Borrowing from this concept, it may be possible to reinforce the single-lap joint. By reinforcing to either side of the bond area with a rigid barrier, rotation of the bond that occurs as the single-lap specimen deforms under the induced moment would be reduced. This could help to mitigate the tensile stresses occurring normal to the bond interface, thus evening out the stress distribution across the length of the bond. To evaluate this concept, a simple finite element model of a single lap was analyzed using ABAQUS/Standard 6.4-1 with the assistance of Dr. Wei Sun. Two cases were considered: the standard single-lap configuration, and the case where the bond area is supported on either side such that bending of the specimens in the bond area is

minimized. The supports were modeled with contact elements such that the specimen material could deform away from them (pull away in toward the bond center), but not penetrate their boundary (not cross the boundary set by the supports).

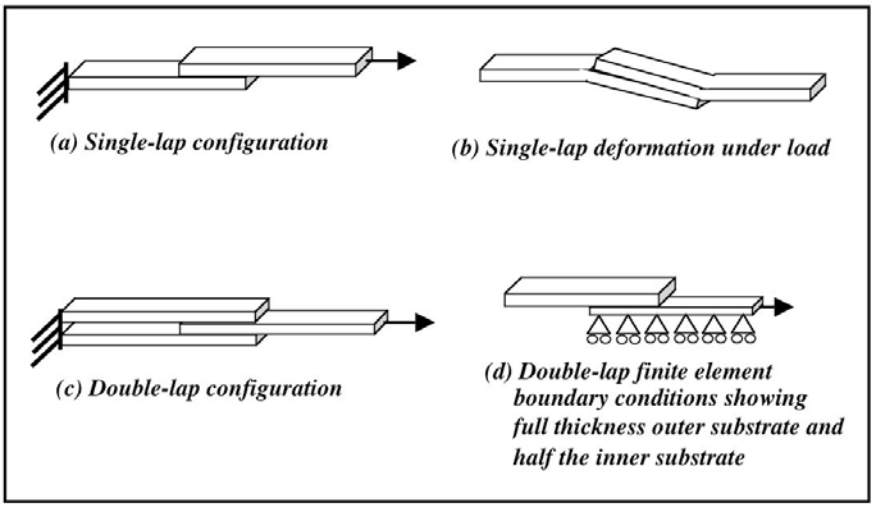

Figure 22: Comparison of single-lap and double-lap tensile configurations

The ABAQUS model considered only the isotropic, linear elastic case. A Young's modulus (E) of 0.467 MPa and a Poisson's ratio (ν) of 0.16667, similar to calf tissue properties[159] were used. A non-linear geometric model was constructed using a 20-node quadratic, reduced integration brick element for all simulations. The end of the first lap was kept fixed, while the end of the second received a 0.5 mm displacement in the axial direction. The model consisted of 3040 C3D20R elements for the tissue laps describing a lap geometry 5 mm long, 3 mm wide, and 0.5 mm thick as shown in Figure

23. The bond overlap length was modeled as 3 mm. The total length per lap of 5 mm was modeled assuming a 10 mm long test coupon for which the grip area would be 5 mm. This would leave 5 mm in length free to deform with the test. In the case of adding external support to the bond overlap, the supports were modeled as finite sliding contacts with a friction coefficient of zero.

For normal cartilage, the tensile stress-strain relationship is linear up to strains of 15%.[13] For the model in this study, a displacement of 0.5 mm with a total geometrical length of 7 mm generated an axial strain of roughly 7%, thus the linear analysis was a reasonable first order approximation.

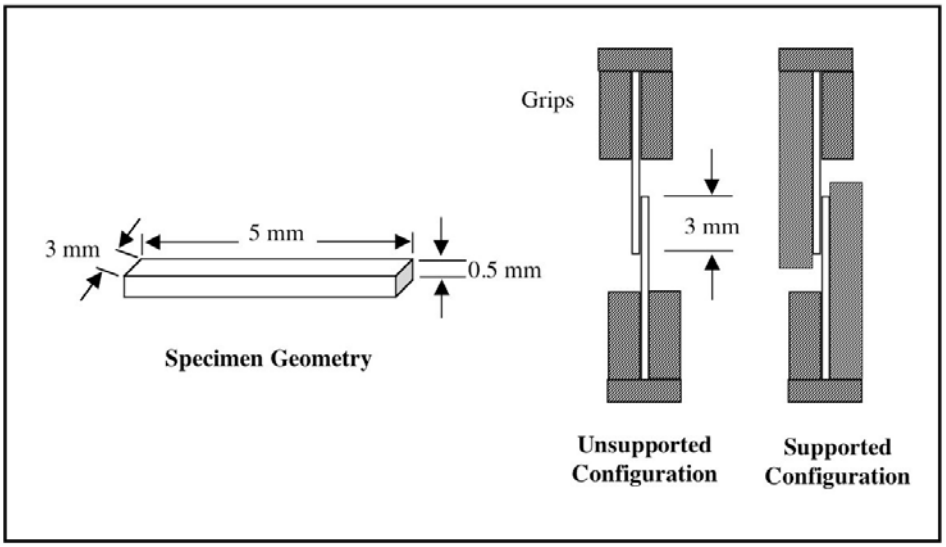

Figure 23: Schematic of the single-lap specimen geometry used for the ABAQUS model

Results

An ABAQUS depiction showing the elements and specimen configurations for the unsupported (free) configuration in the undeformed and deformed (by the applied displacement) states is shown in Figure 24. For comparison, an ABAQUS depiction of the supported case in the deformed state is shown in Figure 25. Shear and peel stress distributions across the normalized bond interface length are shown in Figure 26. Clearly, the addition of supports to prevent rotation of the bond area served to mitigate the tensile stresses seen by the bond during this test. The maximum shear and peel stresses occurring at each end of the bond interface for the supported case was reduced to 48% and 24% of the values for the unsupported case, respectively.

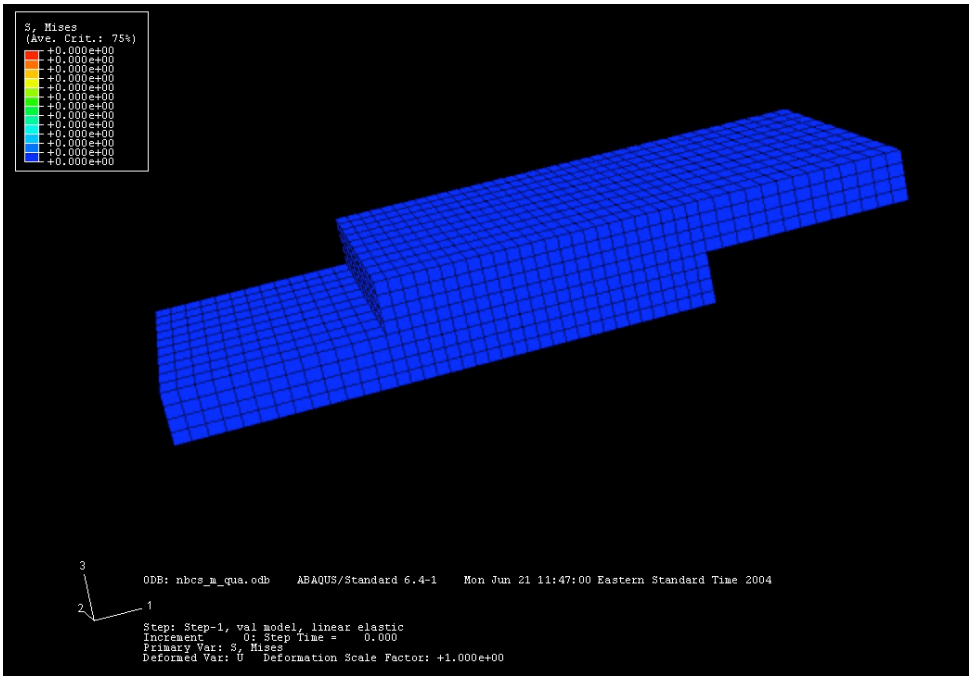

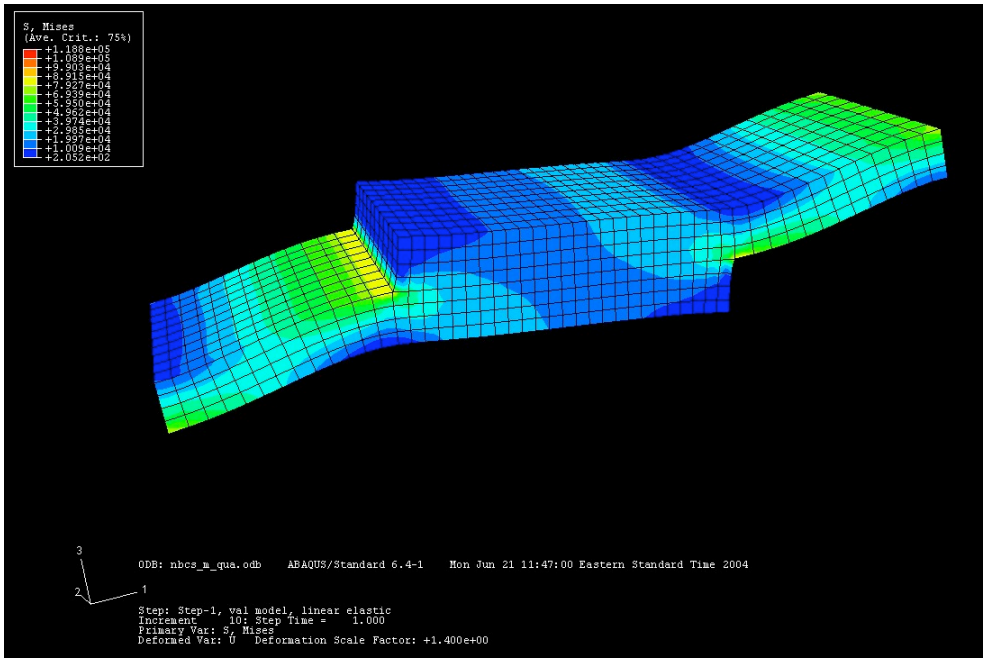

Figure 24: ABAQUS output showing the undeformed (top) and deformed (bottom) geometries for the non-supported, classical single-lap case

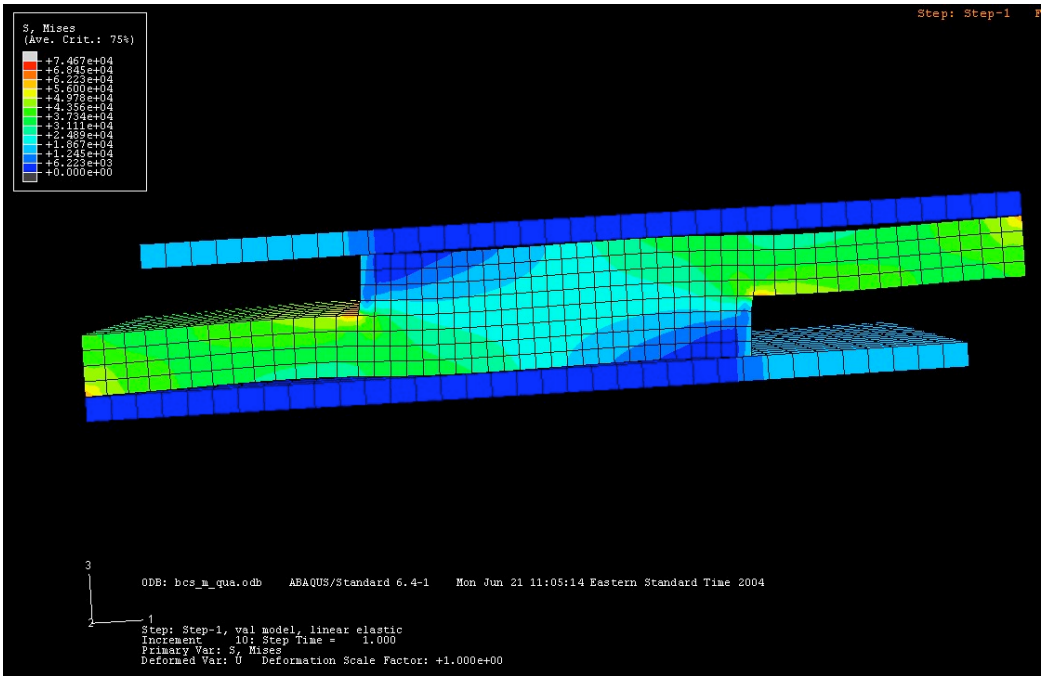

Figure 25: ABAQUS output showing the deformed geometry for the non-supported single-lap case

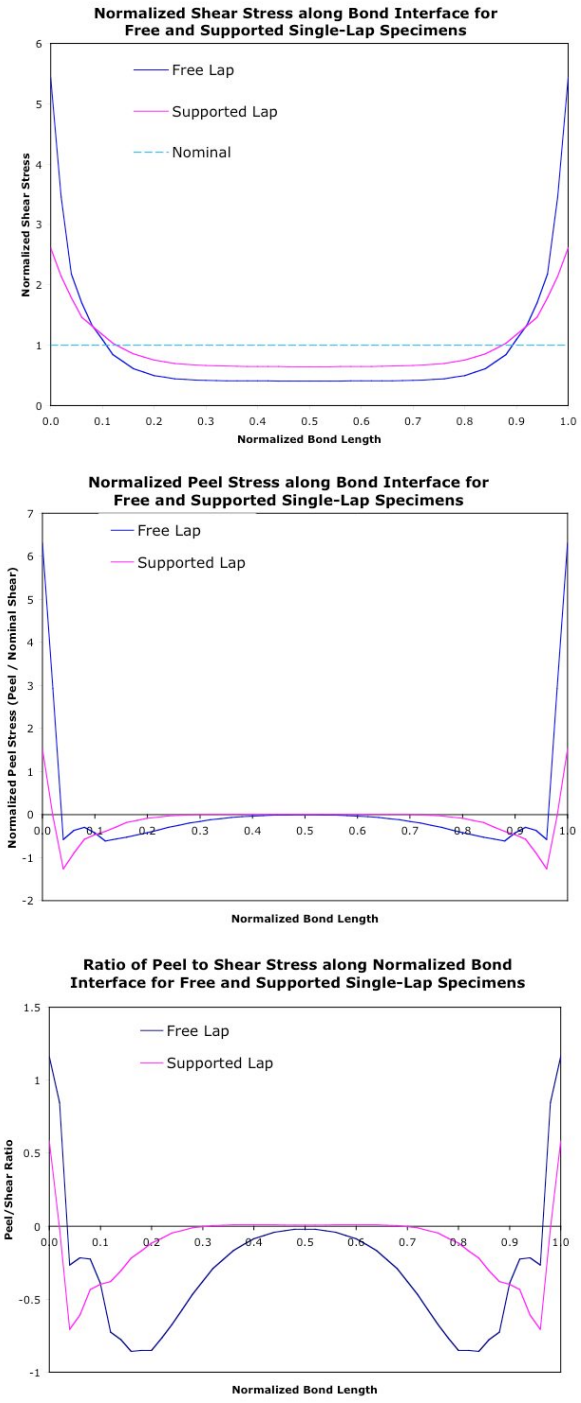

Figure 26: ABAQUS output data for shear, peel, and the ratio of peel to shear stress for the non-supported and supported single-lap configurations.

Discussion

The ABAQUS results show a significant reduction in peel stress at the edges of the lap interface, which manifests as a more uniform shear distribution across the interfacial length that is more representative of the nominal shear stress, calculated as the applied or failure force divided by the interfacial bond area. Taking the ratio of the peel to shear seen by the joint, the supported case exhibits a peel-to-shear ratio of very nearly zero across nearly 40% of the bond length, compared to less than 10% for the non-supported lap configuration. This means that effectively 40% of the bond length for the supported case is experiencing a shear stress, while only a small portion of the bond in the non-supported case is in a simple shearing environment. Furthermore, the ratio of peak peel to shear stress at the edges on the bond was reduced from 1.2 in the unsupported case to 0.6 in the supported lap configuration.

These results show that peel will still be an issue for the supported lap test. There will still be peel stresses on the edges of the bond and thus our prediction of shear failure stress will not be directly representative. The supported case does, however, reduce the peel and hence shear at the lengthwise edges of the bond by approximately 24% and 48% respectively. So, while the modified test will still not result in a pure shear of the specimens, calculating the failure shear stress as the peak force divided by the bond area is a much closer estimate using the supported configuration.

The specimen geometry and test rate selected in this study were governed partially by previous efforts investigating integrative repair in order to provide some degree of similarity and thus basis for comparison. The specimen length, width,

thickness, and bond overlap dimensions used here fall approximately into the middle of the geometrical ranges cited in these previous studies.[28,30,31,144] Another factor influencing the specimen geometry was the spot size and corresponding irradiance capable of being generated by the 667 nm diode system. When considered in conjunction with the necessary irradiance values and exposures estimated from the FTIR analysis, it was determined that a 4 mm diameter irradiance spot was needed. This, in turn, limited the selected specimen width and bond overlap dimensions to those used here.

Considering the applied displacement rate, it is well known that the rate of a test affects the measured adhesive strength as it does the measured material properties of any viscoelastic polymer like cartilage. Though cartilage may be approximated as a viscoelastic material, it is also a biphasic tissue.[13] As such the fluid pressurization within the tissue can contribute to the total tissue stress if tested at a rate sufficiently high as to cause significant interaction in the form of frictional drag between the interstitial fluid and the solid matrix. The degree of this contribution can be estimated from specimen geometry and the biphasic model.[160]

Repeating the analysis performed by Reindel[30] and originated by Armstrong, Lai, and Mow[160], if we assume the poroelastic behavior for cartilage in tension is analogous to unconfined compression, the contribution of interstitial fluid pressure to load may be related to the dimensionless quantity:

$$\tau \bullet d\varepsilon/dt$$

where:

- [$\tau = a^2/(H_A \bullet k_p)$] represents the time constant, often called the gel diffusion time,

- $d\varepsilon/dt$ is the strain rate,
- a is the characteristic length of the test specimen, defined as $^1/_2$ the thickness of the test structure
- H_A is the aggregate modulus, and
- k_p is the hydraulic permeability[13,30]

This is relates the properties of the solid matrix to the fluid component via the hydraulic permeability term. The hydraulic permeability represents the ratio of the tissue porosity to the drag coefficient:

$$k_p = (\phi^f)^2 * K$$

where:

- ϕ^f represents the effective porosity of the tissue matrix, approximately 0.75 for cartilage, and
- K is the diffusive drag coefficient.

The time constant τ is therefore proportional to the ratio of the frictional drag coefficient to the compressive aggregate modulus.[13] So, taking material property values representative of calf cartilage:

- H_{AO} = 0.27 MPa in compression[161] to 4.3 MPa[159] in tension (equilibrium), where H_A is related to the Young's modulus and Poisson's ratio by:
  - $H_A = E(1-\nu) / [(1+\nu)(1-2\nu)]$[13]
- k_{po} =1 E-14 $m^2/(Pa \bullet s)$[161]
  (an intermediate value for patellofemoral groove and condylar tissue)

and:

- *a* in the geometry employed in this study ranges from 0.25-0.5 mm

then:

- $d\varepsilon/dt$ = (displacement rate) / (extensible specimen length)

So, if we consider the same rate employed in the previous single-lap tests for integrative repair of cartilage of 0.5 mm/min[28,30,144], then:

- $d\varepsilon/dt$ = (0.5 mm/min)/(7 mm) = (0.00833 mm/s)/(7 mm) = 0.012 s^{-1}

and this gives us:

- $\tau \bullet d\varepsilon/dt$ value that ranges from 0.002 to 0.111

This range includes the minimum and maximum values found using both the compressive and tensile aggregate moduli since the specimen will experience both loading environments as it deforms. The calculated $\tau \bullet d\varepsilon/dt$ value is also likely an overestimate of the magnitude seen by the bond due to the larger area bearing the stress.

Recall that the time constant τ is proportional to the ratio of the frictional drag coefficient to the compressive aggregate modulus. Therefore, for the strain rate of 0.5 mm/min, since $\tau \bullet d\varepsilon/dt$ is significantly less than unity, the contribution by the interstitial fluid pressure is minimal in this case and the stress distribution throughout the test is governed by the properties of the solid matrix. This is, however, only a first order

approximation dependent on loading mode and boundary conditions and not a precise guiding value. Though to maintain some degree of comparison to previous efforts and to the level of approximation provided for the specific geometry and values in this study, all single-lap tests performed in the experiments to follow will employ a tensile rate of 0.5 mm/min.

CHAPTER IX.

PHOTOCHEMICAL CARTILAGE BONDING

Introduction

The overall goal of this study is to qualify and test a tissue bonding method that has not been successfully demonstrated on many tissues, but has great potential to enhance integrative cartilage repair without, in theory, much added tissue damage. Photochemical sensitizers, most of which have absorbance peaks in the 400-700 nm range[135], are limited in their potential to effect protein crosslinking in very cellular, and hence vascularized, tissues. These tissues absorb heavily in the 400-600 nm region due to the presence of oxygenated and de-oxygenated haemoglobin.[162] Cartilage, however, is an avascular tissue with limited cellularity. So, one of the primary reasons for its incapacity for repair allows it to be a candidate for photochemical bonding. Water absorption also is a minimum in this portion of the spectrum, and mature cartilage tissues tend to lack any other intrinsic chromophores in the visible region. The exception here will, of course, be the vascularized portions of meniscal fibrocartilage. These meniscal regions retain intrinsic porphyrin chromophores that increase their absorbance from 400 to 600 nm. Given also that it is believed the events initiated by the photochemical

process rely on species that react to intrinsic amino acid groups in structural collagen proteins, cartilage would appear to be an ideal tissue for this technique.

Up through this point, the efforts in this study have been directed toward determining the most effective means of bonding cartilage photochemically through the use of sensitizers and then testing that bond. The FTIR evaluations using collagen solutions as model systems presented guidelines for power density and exposure time for the photosensitizers in this study in addition to verifying that the collagen molecule is, in fact, demonstratably affected by this process. Recall that CASPc and T4MPyP-tt were selected as photosensitizers due to their hydrophilicity and affinity for collagen, and both were able to produce a photodynamic effect on collagen as seen in the FTIR studies. The optical scattering reduction experiments, however, proved that enhancement of optical penetration via exposure to osmotic agents was highly cytotoxic and thus not feasible for the goals of this study.

The concept of how to test the adhesive strength of any photochemical bond formed was then investigated in Chapter VIII. The single-lap test was chosen for several reasons, but primarily for its ease of use within the constraints of how to irradiate the tissue and for its comparability to other studies investigating integrative cartilage repair mechanisms. A rough, first-order analysis was performed to verify that the tensile test rate used for these other studies would still be applicable for this study.

In addition, the ability of supports on either side of the bond area for this test configuration to reduce the peak edge stresses and thus even out the stress profile was theoretically validated via finite element analysis. The difference in the measured failure strength for the photochemical bond technique tested with both the supported and the

non-supported single-lap configurations is experimentally investigated in this chapter. Finally, the encompassing purpose of this portion of the study is to synthesize all of the above considerations and findings to produce and test a photochemical cartilage-to-cartilage bond.

Enzymatic Modification of Cartilage Surfaces for Enhanced Integration

In light of the poor intrinsic repair capability of cartilage following injury, many tissue engineering studies have focused on the ability of cartilage or tissue engineered constructs to integrate with the surrounding tissue once inserted into a defect. A brief review of these efforts was included in Chapter II. Two leading thoughts on why long-term repair at an injury site might be inhibited include the loss of cells at the interfacial region and the presence of proteoglycans in the matrix. It is known that chondrocyte necrosis occurs and/or cell density decreases within a radius of approximately 100 μm from a cut cartilage surface[86]. Therefore, one theory is that the loss of matrix-producing cells at a repair interface, one that has been injured or surgically smoothed for implantation, contribute to the lack of native repair.[163,164] Another hypothesis is that the anti-adhesive nature of the intrinsic proteoglycans inhibits integration of two apposed cartilage surfaces[24,164], potentially due to their inhibitory effect on cell adhesion.[32]

Several studies have therefore investigated the concept of mild enzymatic degradation of the cartilage surface as a means of enhancing repair. This idea has been bolstered by complementary findings showing that the removal of extracellular matrix induces chondrocytes to proliferate.[32] Of these studies, several have investigated repair

after enzymatic degradation alone[164,165,166] while another investigated enzymatic proteoglycan removal as a means to enhance the strength of an adhesive interface.[24] Protocols have been relatively similar: 1 U/ml of chondroitinase-ABC for 5-15 minutes[24,164,165], 2.5% trypsin for 5-20 minutes[164,165,166], 1% trypsin for 10-20 minutes[32], 0.5 % trypsin for 5 minutes[167], or 1 U/ml of hyaluronidase for 15 minutes.[24] Yet another study used longer durations of enzymatic exposure with 0.3 % hyaluronidase or 30 U/ml collagenase for 48 hours.[163]

In all of these studies except for the one employing collagenase, enzymatic treatment was found to remove surface proteoglycans without significant disruption of the collagen matrix. Of those that investigated the depth of this removal, two related efforts determined that 1 U/ml of chondroitinase-ABC for five minutes removed proteoglycans to a depth of only 1 μm.[164,165] Another determined that trypsin at 2.5% for 10 or 20 minutes resulted in a harsher effect, removing proteoglycans to a depth of 300 μm or 600 μm respectively.

In general, results across these studies were not consistent with respect to the intended effect of increasing cellularity near to the repair site[163,164,165]. In addition, while the one study investigating enzymatic treatment to enhance the bond of a tissue adhesive found the treatment did indeed increase the bond strength[24], studies investigating native cartilage integrative repair were not so conclusive. One of these found no increased adhesive strength between enzymatically treated cartilage surfaces cultured in apposition over two weeks.[166] A more extensive study then found that there was no increase in repair strength when more mature constructs (5 weeks) were used to fill an annulus and cultured, but that immature constructs (5 days) did see an increased integrative strength

with enzyme treatment. This was postulated to be due to the presence of still-proliferating cells in the immature construct.[32] Whatever the strength result, all of these studies found no long-term negative impacts due to the enzymatic treatments. This was seen in both an *in vitro* culture model over eight weeks[32], and in a rabbit model over a period of six months.[164,165]

Protein Modification

As previously discussed, collagen has only three amino acid residues that are susceptible to singlet oxygen. Specifically, cartilage lacks a cysteine residue and is thus incapable of forming disulfide-type crosslinks. It was also mentioned in Chapter II that increased strength was found in a collagen matrix treated with a diimidoester creating disulfide bonds above that treated with a diimidoester creating only C-C bonds.[48] While there are many methods for modifying amine residues with functional groups depending on the application, many of the agents used either require an organic solvent for solution or conditions that are not conducive to maintaining cellular viability. A few of these, however, are water-soluble and able to react with the amide residues at physiologic pH. One such compound is Traut's Reagent (2-Iminothiolane-HCl), a cyclic imidothioester that reacts with primary amines to leave a free sulfhydryl group. One of the difficulties with modifying agents of this type is that the free sulfhydryl groups are highly susceptible to oxidation and the subsequent formation of disulfide crosslinks.[45] While Traut's Reagent may not be the most effective or least cytotoxic means of introducing these groups to cartilage collagen molecules, it will provide a means to test the concept of

functional collagen modification as a means of enhancing the bond formed by photo-oxidation.

Methods

Photosensitizer and Traut's Reagent Viability Evaluation

The viability of cartilage tissue exposed to photosensitizers and Traut's Reagent was assessed immediately after harvest. Cartilage cylindrical cores 4 mm in diameter were harvested from the patellofemoral groove of an immature calf and soaked in the wash solution of high-glucose DMEM, gentamicin, kanamycin, and AB/AM at 37°C for one hour. Tissue cores were then trimmed to a thickness of 2 mm as described in Chapter VI. Photosensitizer solutions were comprised of 10 mM CASPc or TMPyP-tt in PBS. Traut's Reagent was solubilized to 1.5 mg/ml in PBS.

Cartilage discs were washed three times for ten minutes each in PBS at 37°C under gentle agitation. Discs were then soaked in either photosensitizer solution or Traut's Reagent solution for ten minutes. Controls were soaked in high-glucose DMEM for ten minutes. All samples were then washed in PBS four times for ten minutes each at 37°C under gentle agitation. The live/dead assay procedure from this point is identical to that described in Chapter IV.

Optical Penetration Evaluations

In order to evaluate what degree of irradiance would actually reach the bond interface, tissue sections 0.5 mm thick were prepared as described. These specimens were not trimmed down to the rectangular dimensions of the lap specimens, but instead maintained as a full-thickness cross-section of the tissue. Power was then measured with a detector calibrated for the peak wavelength of the given optical system for the following cases:

- no interfering substrate (detector only),
- microscope slide,
- microscope slide and one 0.5 mm thick cartilage slice,
- microscope slide and one 0.5 mm thick cartilage slice painted on one side with a 14 mg/ml photosensitizer solution (15 mM for CASPc, 10 mM for T4MPyP-tt).

The detector face was 8 mm in diameter. The 667 nm system produced a 4 mm spot size, while the 420 nm system produced an illuminated area 12 mm in diameter. The detector face was centered underneath the spot for all measurements. Both meniscal fibrocartilage and articular cartilage tissues were investigated using the 667 nm system, while articular cartilage alone was investigated using the 420 nm system.

A Coherent Lasercheck handheld power meter was used for these measurements. This device can measure power for 0.5 μW to 1 W within ±5% calibrated accuracy from 400-1064 nm.

Sample Preparation: Procedures and Testing

Single-Lap Specimen Preparation

Cartilage was harvested in full-thickness slabs from the patellofemoral groove, femoral condyles, and medical menisci of immature calves as described in Chapter IV. Tissue was soaked in the wash solution for two hours prior to being transferred to culture medium and incubated at 37°C. All tissue was cultured overnight at a minimum and for a maximum of four days prior to use in bonding experiments. Care was taken to randomize strength assessments across protocol groups such that for a given protocol group (n=8) no more than half the specimens came from the same animal and, further, that no more than half of the samples came from tissue with the same amount of time in culture.

Harvested cartilage was removed from culture immediately prior to testing and sectioned into full-thickness slices 0.5 mm thick with a Microm HM 450 sledge-type microtome. Slices were immediately immersed in PBS, and then cut to dimensions of 3 mm wide and 10 mm long using custom cutting jigs, taking care to remove the superficial layer and calcified zone as illustrated in Figure 27. Cartilage harvested from immature calves provided 6-8 mm of full thickness depth, so isolating a center portion 3 mm wide was not difficult. Slices were kept in PBS until photosensitizer or enzymatic treatment and used within three hours. Slices were then selected at random as pairs to be bonded with no attempt to match adjacent tissue sections.

Meniscal fibrocartilage was sliced in a similar manner. Cross-sections as shown in Figure 2 were sliced to 0.5 mm thick prior to cutting to the same dimensions as for the articular cartilage samples above, keeping all tissue treatment the same.

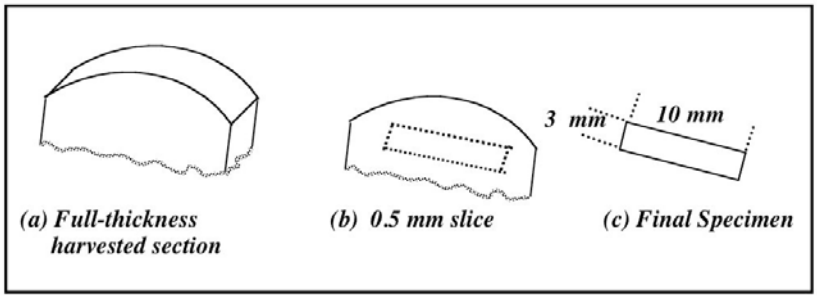

Figure 27: Cartilage sectioning for photochemical single-lap bonding

Enzymatic Modification

Enzymatic protocols were derived directly from those described in the introduction to this chapter. Specifically, enzymes, their concentrations, and protocols were used as detailed in Table 8. All enzymes were first reconstituted and then frozen in aliquots, to be used within three weeks of reconstitution/freezing. Aliquots were thawed in a water bath at 37°C immediately prior to use and used within three hours of thawing.

Experiments were first conducted at room temperature (approximately 25°C) to determine an effective and consistent protocol for modification prior to photochemical bonding. For tissue treatment, 150 μL of a given enzyme solution was pipetted in to a single well of a standard, 96-well plate. The solution depth was roughly 3.5 mm within the well. Tissue subjected to enzymatic modification was placed into the well for the amount of time specified by the specific protocol and covered with PBS dampened gauze to prevent dehydration of the portion of the lap specimen not immersed in solution. Treated tissue specimens were then removed and immersed into a well completely filled with PBS, covering the entire piece of tissue, for ten minutes prior to the photosensitizer

treatment. Specific details of the photosensitizer treatments will be described in the following section.

Table 8: Enzymatic Treatments

Treatment Designation	Enzyme	Concentration/ Solvent	Time (min)	Temperature
CH15 or CH20	Chondroitinase-ABC	1 U/ml 0.01% BSA in PBS	15 or 20	25°C or 37°C
HY15	Hyaluronidase	10 U/ml in PBS	15	25°C
CHHY	Chondroitinase-ABC /Hyaluronidase In Sequence	1 U/ml Ch-ABC, 10 U/ml H-dase (solutions/solvents same as for CH15 and HY15)	4 min Ch-ABC, 4 min H-dase, 4 min Ch-ABC, 4 min H-dase	25°C
CHYBRID	Chondroitinase-ABC /Hyaluronidase In Combination	1 U/ml Ch-ABC, 10 U/ml H-dase (solvents for each as above)	15	25°C
COLT2	Collagenase, type 2	50 U/ml in PBS	15	25°C

Photosensitizer Treatment, Lap Specimen Assembly, and Irradiation Procedures

Rectangular lap specimens were obtained as described and placed in PBS. Specimens were either treated with a photosensitizer solution or enzymatic treatment followed by the photosensitizer solution. For enzymatic treatment, 150 μL of a given enzyme solution was pipetted into a single well of a 96-well plate, resulting in a solution depth of 3.5 mm as described. Each lap of a given sample pair were placed into different wells of enzyme solution with no agitation for the time specified by the enzymatic

protocol. Lap specimens were then removed and placed into separate wells filled with PBS, thus covering the entire lap length for ten minutes, again with no agitation. A single specimen from each pair was then immersed in a 150 μL photosensitizer solution for approximately thirty seconds. The specimen was removed and the photosensitizer-stained end was blotted dry before the specimen was placed on moistened tissue paper on top of a standard microscope slide. The other specimen was then removed from the PBS and similarly blotted dry before being positioned on top of the photosensitized area of the bottom specimen such that the overlap length was 3.5 mm as measured with digital calipers. Moistened tissue paper was placed across each end of the now combined specimen, which was then covered with a piece of moistened sandpaper having a 4 mm by 4 mm rectangular cutout. The sandpaper served to avoid specimen slippage and provide an irradiation mask for the rest of the specimen outside the bond area. A piece of saran wrap was then placed over the specimen before the final microscope slide was added on top.

This sandwich-style construction contained moistened layers and saran wrap to prevent any excessive dehydration during the irradiative bonding treatments. The assembly was then secured between two rubber-faced miniature clamps to compressively hold the laps in apposition. This dual clamp force was measured using an Enduratec ELF 3200. One microscope slide was fixed to each actuator of the ELF 3200 before applying the spring clamps in the same manner used to constrain the lap specimens. A 1 mm displacement between the slides was maintained and the resulting axial actuator force recorded. Assuming the bond area bears the entire load and that none is distributed to the

layering materials surrounding the lap specimens, the resulting normal stress on the bond interface was calculated to be approximately 1083 kPa.

The optical setup for the 667 nm and 420 nm systems was as described in Chapter V. The radiation was incident normal to the bond area of the top lap, penetrating the 0.5 mm thickness to reach the actual bond area. In order to maintain a more clinically possible approach, the entire duration of exposure was in this configuration, with no repositioning of the sample.

Specimens not undergoing enzymatic modification were prepared by dipping one lap into the photosensitizer solution and then assembling the overlap as described. Control specimens subjected only to ambient light were constructed and clamped identically to the above procedure and then placed on the benchtop for the same amount of time as the experimental irradiations. Similarly, controls undergoing enzymatic modification and no photosensitizer exposure or irradiation were subjected to enzymatic treatment/PBS wash, blotted dry, and then assembled in the same manner to sit on the benchtop for the prescribed amount of time. Immediately following irradiation or ambient only exposure, all lap specimens were removed from the microscope slide-clamp assembly and immersed into a PBS filled petrie dish for 10 minutes prior to mechanical testing.

Mechanical Testing

Mechanical testing was performed on an Enduratec ELF 3200 test machine using a 25 N load cell (Interface, SMT1-5.6) in tension. The upper tissue grip was fixed to the actuator used to apply the displacement to the lap specimen. Horizontal positioning of

this grip was controlled with a miniature, linear translation stage (Thorlabs, T12X). The bottom grip was fastened to the load cell and included a catch tray for saline used for specimen hydration during testing. Wire-cut portions of a steel file 5 mm high and 5 mm wide were inserted to grip the tissue. Miniature springs held the file grips in place prior to tightening with screws. The complete assembly is shown in Figure 28.

Specifically, the lap specimen was secured in the upper grip before the lower grip was carefully actuated into place such that the tissue specimen just touched the grip's bottom face. The lateral position of the top grip was then adjusted with the translation stage until the specimen was in complete contact with both support faces. The file grip screws were tightened to firmly hold the tissue, and PBS was continuously dripped onto the specimen via a transfer pipette during testing. The final configuration for this procedure is shown in Figure 29.

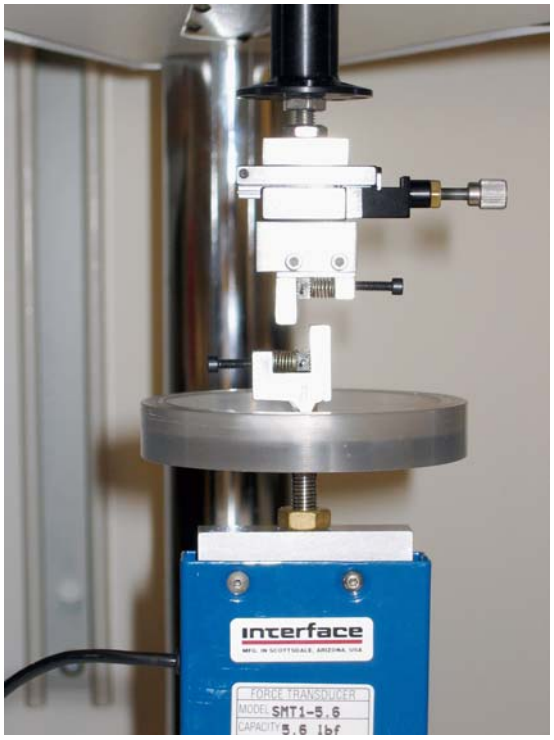

Figure 28: Supported single-lap test grips and configuration

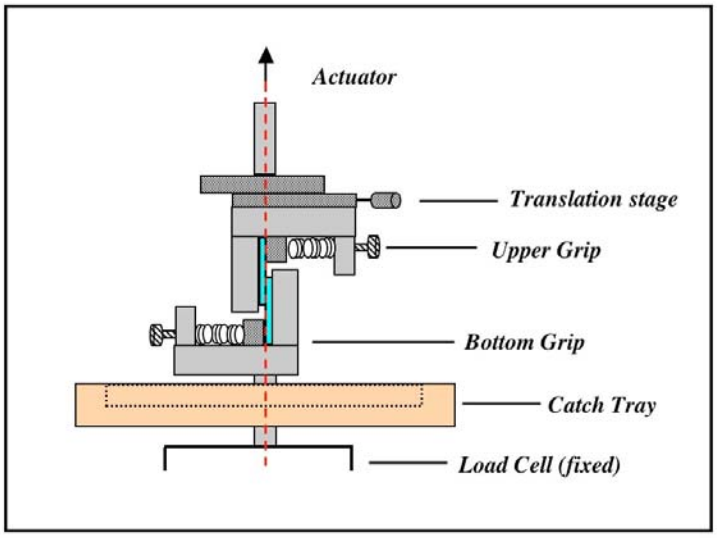

Figure 29: Tissue placement in the supported single-lap configuration

Photochemical Bonding Experiments

Room Temperature Experiments

Experiments were first conducted at room temperature (approximately 25°C) to determine which protocol(s) would actually produce a photochemical bond between the tissue pieces and yield the most consistent results. Experiments were conducted as given in Table 9. Briefly, the table illustrates that bonding was attempted first with no enzymatic treatment; just the photosensitizer CASPc and/or 667 nm irradiation were used. Enzymatic treatments were then investigated using chondroitinase-ABC, hyaluronidase, and collagenase (type 2) as previously described. Articular cartilage from the femoral condyles (CAC), articular cartilage from the patellofemoral groove (FG), and meniscal fibrocartilage (MFC) were investigated as tissue substrates.

For this set of experiments, only the 667 nm system was used along with a 15 mM CASPc solution. All irradiances and exposures were 1.7 W/cm^2 and 1022 J/cm^2 (corresponding to an irradiation time of ten minutes) respectively. Controls were collected (not shown in Table 9) for enzymatic treatments with no photosensitizer or irradiation, and for the photosensitizer with only ambient light exposure. A sample size of eight per group (n=8) was collected except for those cases where no bonding occurred. In those cases, a sample size of 4 or 6 was deemed sufficient.

Samples from tissue harvested adjacent to the sections tested were saved and frozen for later assay for sGAG and hydroxyproline as described in Chapter IV.

Table 9: Bonding Experiments Conducted at Room Temperature

Treatment Designation	Tissue	Enzyme Treatment	15 mM CASPc	W/cm2
Control Groups: Irradiation Only and Photosensitizer Only (No Enzymes)				
MFC-NoEnz	MFC	none	Yes	1.7
CAC-NoEnz	CAC	none	Yes	1.7
FG-NoEnz	FG	none	Yes	1.7
MFC-IRonly	MFC	none	No	1.7
CAC- IRonly	CAC	none	No	1.7
Chondroitinase-ABC Only				
CAC-CH15-RT	CAC	CH15	Yes	1.7
CAC-CH20-RT	CAC	CH20	Yes	1.7
FG-CH20-RT	FG	CH20	Yes	1.7
MFC-CH20-RT	MFC	CH20	Yes	1.7
Chondroitinase-ABC Sequenced with Hyaluronidase				
CAC-CHHY-RT	CAC	CHHY	Yes	1.7
FG-CHHY-RT	FG	CHHY	Yes	1.7
MFC-CHHY-RT	MFC	CHHY	Yes	1.7
Other Groups: Hyaluronidase Only, Collagenase Only, and Chondroitinase-ABC+Hyaluronidase				
CAC-HY15-RT	CAC	HY15	Yes	1.7
CAC-COLT2-RT	CAC	COLT2	Yes	1.7
FG-CHYBRID-RT	FG	CHYBRID	Yes	1.7

Notes:
CAC= condylar articular cartilage, FG- patellofemoral groove articular cartilage, MFC= meniscal fibrocartilage, RT=room temperature (approximately 25°C). All irradiances and exposures were 1.7 W/cm^2 and 1022 J/cm^2, respectively.
All photosensitizer treatments used 15 mM CASPc.

37°C Experiments

Experiments were conducted at 37°C, where enzymatic activity is greater and more representative of the physiologic environment, using the CH15 enzymatic treatment from the room temperature experiments as a baseline for comparison. All enzymatic treatments at 37°C were performed by floating the 96-well plate in a covered water bath at 37°C. All aliquot volumes and general procedures were as described for the room temperature treatments.

In this set of protocols, photosensitizer concentration, irradiance, and exposure, were varied. Other groups included incorporation of ribose in the photosensitizer solution, use of a hydrophobic phthalocyanine photosensitizer (zinc phthalocyanine tetrasulfonic acid as discussed in Chapter VII) analogous to the CASPc used for all the other groups, and 320 grit sandpaper to debride the tissue surface in place of enzymatic treatment.

Due to the lack of hydrophilicity of the ZNPc, the ZNPc-PBS mixture became highly aggregated and did not completely go into solution. The group using CASPc in a ribose solution was examined to see if an active reducing sugar had a measurable effect on the photochemical process. However, due to the viability results for sugar solutions in the optical scattering chapter, the ribose solution was limited to a concentration of 400 mM in de-ionized water, a solution of approximately 400 mOsm. The photosensitizer CASPc was solubilized in the ribose solution to 15 mM and the tissue was treated as before. The 320-grit sandpaper was used to investigate the effects of physical debridement of the tissue surface over enzymatic modification.

The set of protocols run at 37°C is given in Table 10. As before, controls were collected for enzymatic treatments with no photosensitizer or irradiation, and for the photosensitizer with only ambient light. A sample size of eight per group (n=8) was collected except for those cases where no bonding occurred. In those cases, a sample size of 4 or 6 was again deemed sufficient. The Traut's Reagent was incorporated into one group by immersing both cartilage samples in 1.5 mg/ml of the reagent solubilized in PBS for ten minutes after enzymatic modification (CH15), but prior to treatment of one tissue slice with photosensitizer (7.5 mM CASPc). All other treatment of this group was as described.

All other procedures were conducted as for the room temperature experiments with one notable difference. In one protocol, pressure was reduced to 330 kPa, one third of that imposed by the clamped slides, to ensure that firm contact and not excessive pressure was the determining requirement for bonding. This was accomplished by placing two 200-gram weights on top of the slides, one to either side.

Table 10: Bonding Experiments Conducted at 37°C

Treatment Designation	Tissue	Enzyme Treatment /Other	CASPc	W/cm^2, J/cm^2
CH15-PT	CAC	CH15	15 mM	1.7, 1022
CH15-PT	CAC	CH15, 330 kPa bond pressure	15 mM	1.7, 1022
CH15-PSH-PT	CAC	CH15	7.5 mM	1.7, 1022
CH15-PSQ-PT	CAC	CH15	3.25 mM	1.7, 1022
CH15-IR15-PT	CAC	CH15	15 mM	1.7, 1533
CH15-IR5-PT	CAC	CH15	15 mM	1.7, 511
CH15-IR15P2/3-PT	CAC	CH15	15 mM	1.1, 1022
CH15-IR10P1/2-PT	CAC	CH15	15 mM	0.9, 511
CH15-PSH-TR-RT	CAC	CH15, Traut's Reagent	7.5 mM	1.7, 1022
CH15-RIB-PT	CAC	CH15	15 mM in ribose/DI-H_2O	1.7, 1022
CH15-ZNPc-PT	CAC	CH15	15 mM ZNPc	1.7, 1022
Debride-PT	CAC	Debride with 320-grit sandpaper	15 mM	1.7, 1022

Notes: CAC= condylar articular cartilage, PT=physiologic temperature (37°C), ZNPc refers to the hydrophobic phthalocyanine described in Chapter VII

Experimental Comparison with the Non-Supported Lap Configuration

Tests were conducted using the CH15 baseline treatment at 37ºC with the standard single-lap configuration, without any supports across the bond area. For these tests, grips were machined to be identical except that the outside of the grip was limited to 5 mm in height, the same height as the steel file gripping surface shown in Figure 29. Tests using the standard, unsupported single-lap configuration used the CH15-PT protocol and 15.5 mM CASPc as described.

Since a compressive preload was induced on some of the single-lap specimens as the file grips were tightened, seen as residual load on the force output plots given the load cell tare once the specimens were positioned, experiments were run in the support-free configuration taking care to eliminate the compressive preload. This was easier to accomplish in this configuration since the specimen was already constrained across the bond in the supported lap case. Any movement or adjustment of those specimens could have sheared the bond prior to test. Therefore, the lack of a sample preload was evaluated in the support-free case to ensure no variation in results due to the preload caused by tightening the steel grips.

Dermabond Testing

Tests were also performed using Dermabond, a medical-grade adhesive, as a comparatory benchmark in the support-free configuration. The effect of test rate on the measured strength was also evaluated using Dermabond as the adhesive. Tests were

conducted at axial displacement rates of 0.5 mm/min (as for all other groups), 2 mm/min, and 4 mm/min. Laps were placed in apposition as before, and 0.2 μL of Dermabond was applied using a 2 μL pipette. The same moistened tissue paper sandwich construction was used as for the photochemical experiments, but the tissue was not clamped. After the Dermabond was allowed to set for ten minutes, analogous to the irradiation time in the photosensitized experiments, the bonded samples were hydrated for ten minutes in PBS prior to mechanical testing as described previously. The bond overlap length was 3 mm.

Statistical Analyses

Comparison of multiple levels of a given factor were performed using one-factor, unbalanced analysis of variance (ANOVA), followed by Tukey's test for pairwise comparisons. Comparisons of two factors with multiple levels were performed using the analogous two-factor, unbalanced ANOVA, also followed by Tukey's test for pairwise comparisons. Of the groups collected for the purpose of point comparison with the baseline case, two-tailed, unpaired t-tests for independent samples were performed.

Results

Photosensitizer and Traut's Reagent Viability Evaluation

The viability of cartilage tissue exposed to photosensitizers and to Traut's Reagent was assessed immediately after harvest as described. Plates showing representative viability results are shown in Figure 30, with red and green signifying dead and live cells respectively. All images represent 921 μm by 921 μm areas that include the sample edge.

None of the treatments (controls, CASPc, T4MPyP-tt, Traut's Reagent) resulted in excessive cell death. Control specimens typically exhibited a necrosis zone near the cut surface ranging from 30-40 μm, with the smallest at 30 μm and the worst case at 240 μm. Similar results were seen with the CASPc. Necrosis zones with this photosensitizer ranged from 20-300 μm (best to worst), but were typically from 30-70 μm in depth.

Cell death in tissue incubated with the T4MPyP-tt, was much more difficult to see due to the red fluorescence exhibited by the photosensitizer that overwhelmed that of the dead cell stain (ETH-HD-1). Necrosis zones, distinguished by a lack of green-fluorescence, ranged from 30-200 μm and were typically on the order of 40-50 μm in depth. Figure 31 shows two samples treated with T4MPyP-tt: one stained using the live/dead assay kit, and one with no live/dead stain. (The red intensity in the images has been adjusted for better visibility.) Dead cells appear as dark spots in the T4MPyP-tt

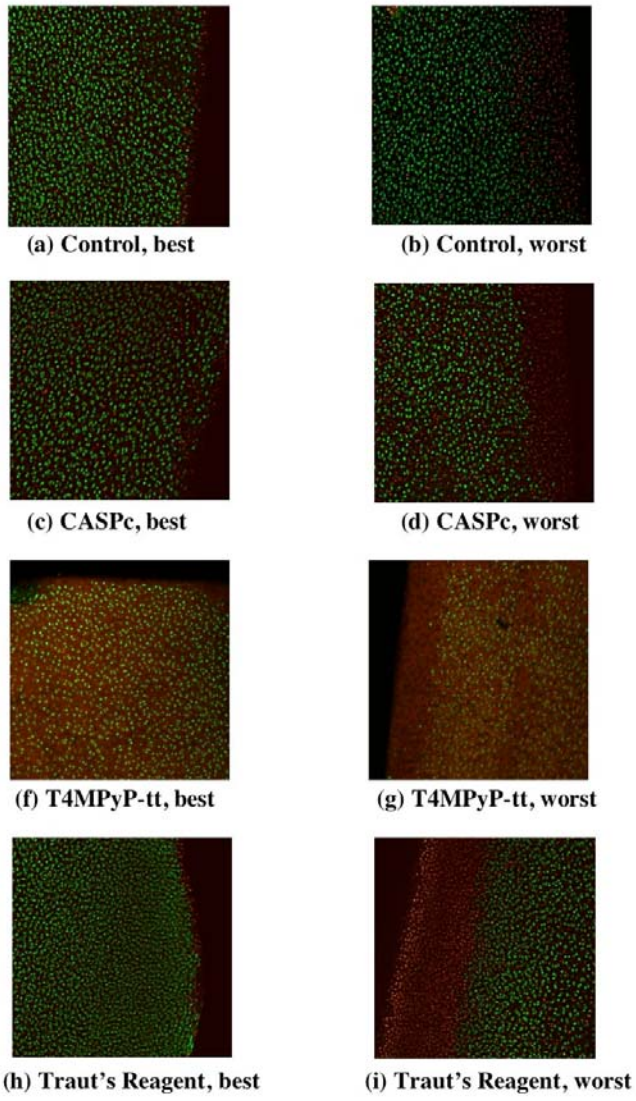

Figure 30: Viability results for controls, CASPc, TMPyP-tt, and Traut's Reagent treated cartilage specimens

matrix that is fluorescing red. This is expected since T4MPyP-tt is a hydrophilic photosensitizer and should not penetrate the cell membranes. Being cationic, however, it is expected to permeate and bind to the polyanionic matrix of cartilage, which apparently it does.

Traut's Reagent, however, induced a bit more cell death than the photosensitizers. Zones showing cell death with this reagent were typically on the order of 50-100 μm, with extremes of 30 μm and 320 μm. More cell death was also seen dispersed throughout the tissue center with Traut's Reagent, as shown in Figure 32.

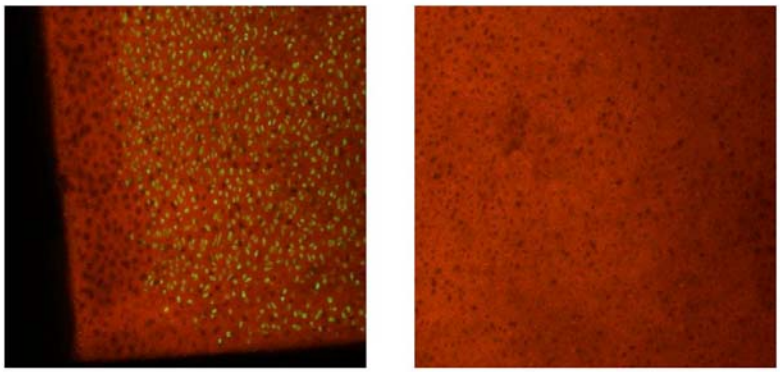

(a) With live/dead stain (b) Without live/dead stain

Figure 31: Selected confocal images of TMPyP-tt treated cartilage (a) with live/dead staining, and (b) without live/dead staining

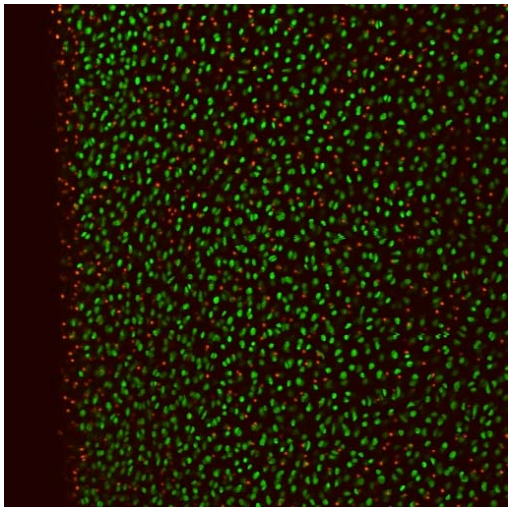

Figure 32: Selected confocal image showing increased internal cell death for a Traut's Reagent treated cartilage specimen

Optical Penetration

All of the strength results reported here are from treatment protocols using CASPc as the photosensitizer in conjunction with the 667 nm system. None are reported using T4MPyP-tt and the 420 nm system because no bonding of tissue was achieved using that photosensitizer and optical system. After several unsuccessful boding attempts using T4MPyP-tt and 420 nm irradiation, the irradiances incident on the detector with various materials placed in the optical path were investigated. The results are presented in Figure 33.

The 4 mm diameter spot of light emanating from the 667 nm diode system was able to penetrate a microscope slide layered with a 0.5 mm thick cartilage to a 53-67% of the power incident on the detector face without the slide and tissue section in the beam path. The 420 nm system, however, produced a much lower power and was not a collimated beam. This system could only penetrate the slide and tissue to 7% of the incident irradiance, a 93% loss. Since the original power density was limited, this means that only 0.01 W/cm^2 penetrated a single slice of tissue with no photosensitizer treatment using the 420 nm system. Practically speaking, with respect to the experimental set-up used to bond the single-lap specimens, this is the amount of light that would reach the bond interface. The cartilage subjected to 420 nm irradiation was also observed to exhibit a moderate red fluorescence. This likely emanated from remnant porphyrin compounds dispersed throughout the tissue matrix and concentrated near vascular microchannels still present due to the young age of the animal. Recall that most porphyrin compounds, including hematoporphyrin in the blood and the T4MPyP-tt photosensitizer from this study, absorb heavily between 400-420 nm and fluoresce red.

Similarly, negligible irradiance reached the detector with the 667 nm system when the cartilage slice had been treated with the photosensitizer CASPc. This was the reason behind treating only the bottom slice of tissue with the photosensitizer prior to irradiation for bonding; treating both surfaces would prevent adequate power from reaching the bond interface.

A Coherent Lasercheck handheld power meter was used for these measurements. This device can measure power for 0.5 μW to 1 W within ±5% calibrated accuracy from 400-1064 nm.

(a) Average Irradiance (mW/cm2) through to the Bond Interface for the 667 nm Diode System

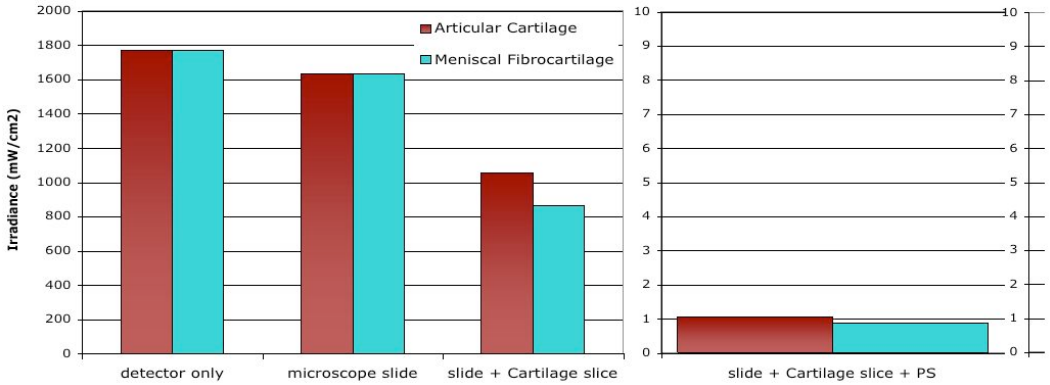

(b) Average Irradiance (mW/cm2) through to the Bond Interface for the 420 nm Diode System

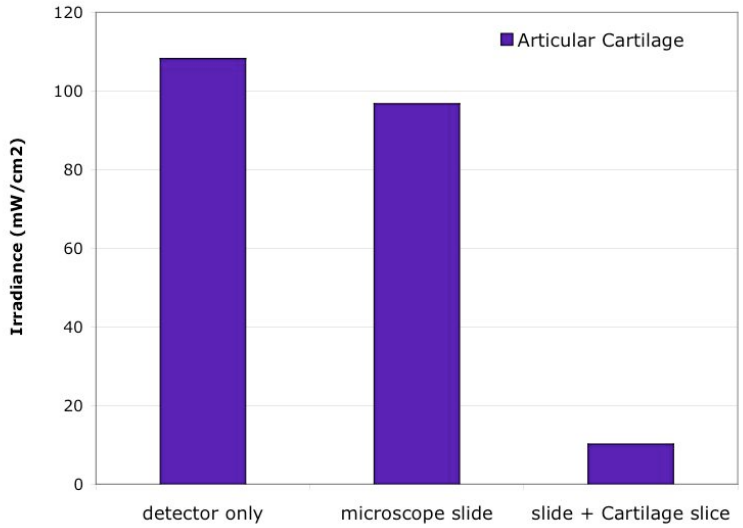

Figure 33: Optical penetration of the (a) 667 nm and (b) 420 nm diode systems representing an average of n=2 for each series

Experimental Comparison of the Supported and Non-Supported Lap Configurations

Comparison with the non-supported lap configuration used in previous integrative cartilage repair studies showed a mean nominal shear strength of 30.3±1.9 kPa (mean ± SEM) for the non-supported case. This non-supported configuration value is directly in line with the 30-34 kPa values cited for the integrative repair non-supported single-lap models after two to three weeks in culture. There was no difference in the means for the cases where a small compressive preload occurred when compared to the samples where care was taken to avoid such a preload (n=8 and a mean force of 0.32±0.02 N for each, with a standard deviation of 0.07 N for the group exhibiting a small preload and 0.09 N for the group exhibiting no preload). Therefore, it is not believed that this preload, being compressive in nature, had any effect on the final measured tensile strength of the bond.

Compared to the same enzymatic and photosensitizer treatment tested in the supported lap configuration (CH15-PT at 37ºC, to be reported in detail in the "*Cartilage Bonding at 37ºC: Comparison of Parameters against a Baseline Procedure"* section that follows), the non-supported test specimens failed at a lower measured peak force. The calculated mean nominal shear strength was reduced from 45.9±3.6 kPa for the supported case (n=13) to 30.3±1.9 kPa for the non-supported case. Statistical analysis using a t-test for point-wise comparison between the two groups found the difference significant to p=0.0004. Figure 34 depicts the force curves comparing these two test configurations.

Considering the ABAQUS model results in the previous chapter, it was expected that specimens tested in the non-supported configuration would fail at a lower measured force value than when tested in the supported configuration due to the reduction of the

peak stresses occurring at the bond edges with the addition of the supports. The model demonstrated that the addition of supports along the bond area reduced these edge shear stresses to approximately 48% and 24% of the non-supported lap values for shear and peel respectively. It would be expected that this reduction in peak edge stresses would in turn translate into a higher measured failure load. The test specimen would still fail due to peel-initiated forces, but the environment for these forces would be less severe and thus the test specimen could sustain a higher load prior to failure. Experimentally, this concept was validated for the cartilage single-lap specimens. The addition of supports was found to increase the measured failure load, and therefore the calculated nominal shear strength, to 151% of the strength obtained with the non-supported configuration.

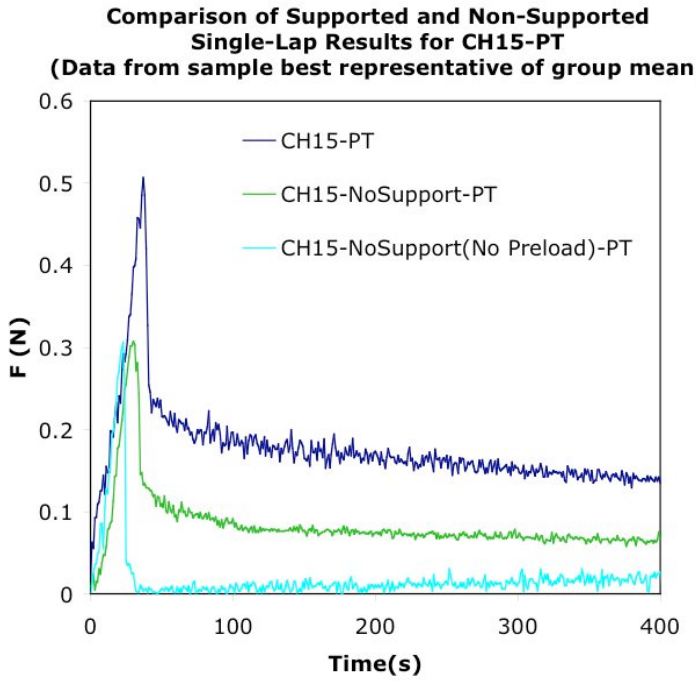

Figure 34: Comparison of supported and non-supported configuration test results

Dermabond Comparison Tests

Dermabond, a medical grade cyanoacrylate, was used as the adhesive benchmark system for the cartilage single-lap tests. The purpose was simply to apply a well-characterized adhesive to the specific specimen geometry, test rate, and test configuration used in this study in order to provide a direct basis for comparison. Test rates of 0.5 mm/min, 2 mm/min, and 4 mm/min were investigated. The first rate offered a direct comparison to the cartilage photochemical bonding results, while the latter two rates allowed investigation of the effect of test rate on the measured bond strength.

Even at the minute amount of Dermabond used for adhesion here, the bond was sufficiently strong that loading induced significant tissue deformation prior to failure. All samples tested in the supported lap configuration either pulled out of the tissue grips or suffered tissue failure. Tests were therefore completed with Dermabond using the non-supported lap configuration, and thus bonds finally failed due to high peel stresses at the ends of the bonds as the lap deformation due to the bending moment became visibly obvious at these high failure strengths.

Some of the tissue samples still failed prior to the bond in the non-supported lap configuration, and all samples were observed to fail between the bond and the top of the steel file grip face. Tissue from animals this young still maintains some degree of vascularity as discussed earlier. These vascular channels are sometimes visible as translucent, meandering lines in 0.5 mm thick cartilage slices washed in PBS. As such, these channels produce tissue inhomogeneities that could be responsible for some of the tissue failure seen here. When tissue failure occurred, it usually did so between 6-8 N,

corresponding to a failure stress of approximately 4.6 MPa for the tissue specimens, calculated as the load at failure divided by the cross-sectional area of the individual tissue specimen (0.5 mm by 3 mm).

Recall that the photosensitized bond in the non-supported lap configuration failed at a mean nominal stress of 30.3±1.9 kPa. Tissue adhered with Dermabond in the same configuration and tested at the same rate failed at 644.8±37.4 kPa, an order of magnitude greater. The bond strength increased to 702.6±32.4 kPa and 974.5±40.4 kPa when tested at the 2 and 4 mm/min displacement rates respectively. This was an expected result in agreement with the well-known stiffening behavior of viscoelastic materials when subjected to higher loading rates. These values are in line with the previous bond strengths for cyanoacrylates and tissues as referenced in Table 1 (1000 kPa), although no rate, bond area, or adhesive quantity information was given for that value. Results for the Dermabond tests are shown in Figure 35.

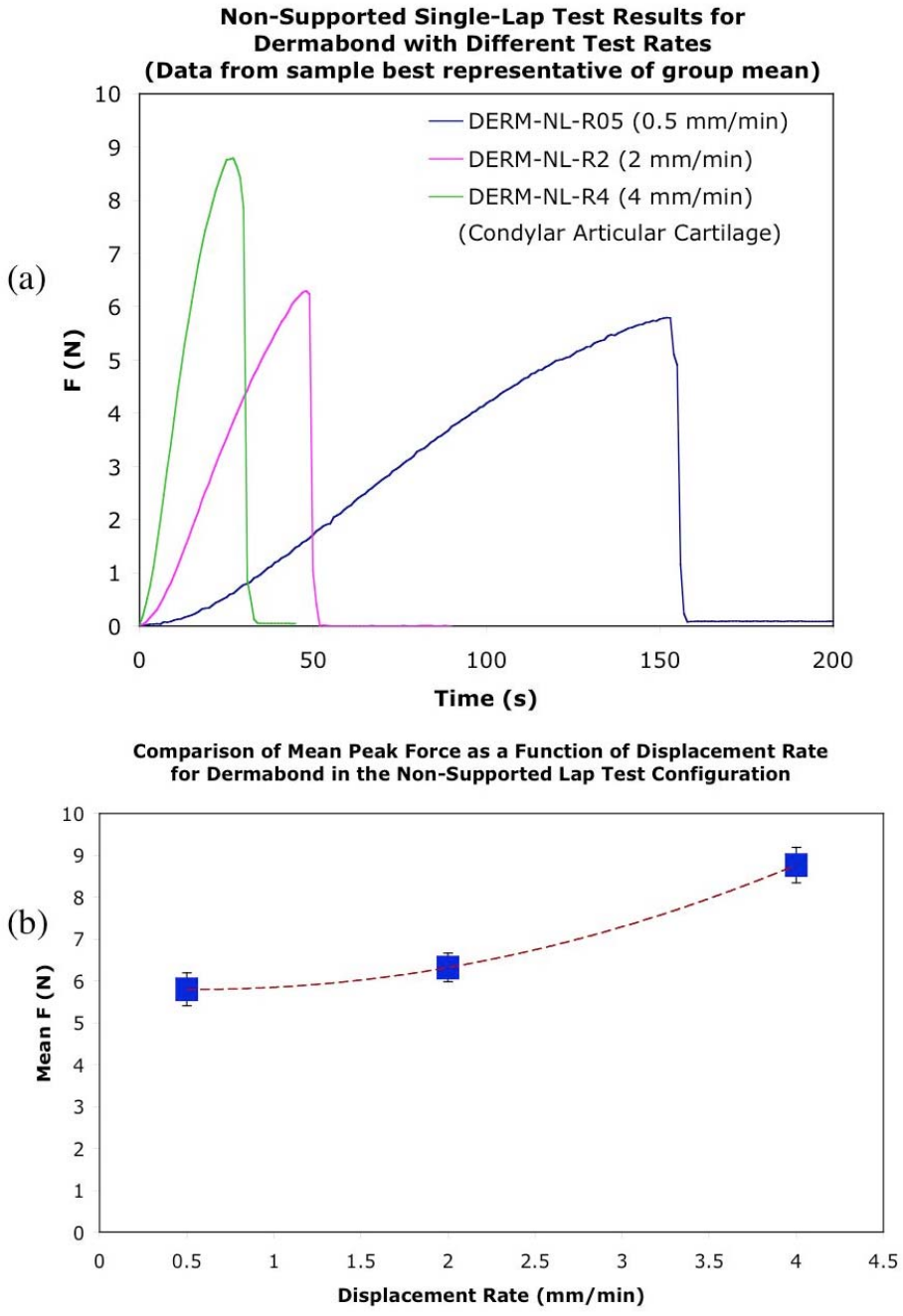

Figure 35: Comparative strength results for Dermabond at different displacement rates

Cartilage Bonding at Room Temperature: Comparison of Enzymes and Tissues

Photochemical bonding tests were conducted at room temperature to determine which method or methods would be effective for which tissue (femoral condylar articular cartilage (CAC), patellofemoral groove articular cartilage (FG), and meniscal fibrocartilage (MFC)). All tests used CASPc at 15 mM in PBS as the photosensitizing solution and were irradiated for ten minutes at 1.7 W/cm^2 (giving 1022 J/cm^2). A Coherent Fieldmaster-GS power meter with an LM3 Smartsensor thermal sensor head (LM-3 HTD, 10 mW – 3 W, ±2% accuracy from 250-10,600 nm) was used to validate power every few samples to validate consistency.

Only meniscal tissue exhibited any bonding when treated with photosensitizer and irradiation alone. Articular cartilage from either anatomical site harvested would not bond with this treatment. All articular cartilage samples fell apart during hydration, prior to mechanical testing. Control samples were either irradiated only (MFC and CAC), or treated with photosensitizer and ambient light (MFC). None of the control samples were still together in apposition following hydration.

Various enzymatic treatments were then examined in an effort to remove the proteoglycans from the immediate tissue surface and expose the collagen fibrils. Protocols followed were similar to those already well-characterized in the literature. Treatment with collagenase (type 2) or hyaluronidase, followed by photosensitizer treatment and irradiation, produced no bonding of articular cartilage specimens. However, treatment with chondroitinase-ABC at 1 U/ml for 15 or 20 minutes produced bonding for all tissue groups with photosensitizer treatment and irradiation. Similarly,

the protocols that combined chondroitinase-ABC and hyaluronidase either sequentially (CHHY) or in combination (CHYBRID) also produced bonding for all tissue groups.

Statistical comparisons were performed using one-factor ANOVA testing for a given tissue group to compare treatments and a two-factor ANOVA to test for the treatment differences with different tissues. These results are summarized in Table 11. In general, treatment of cartilage with chondroitinase-ABC for twenty minutes prior to photosensitizer and irradiation exposure produced stronger bonds than the group similarly treated for only fifteen minutes. Sequential enzymatic modification using the CHHY protocol resulted in the highest bond strengths. In contrast, the combined CHYBRID enzymatic solution did not produce any measurable strength gains over chondroitinase alone for comparable enzymatic exposure times. None of the control samples (enzymatic treatment/ photosensitizer/ ambient light, or enzymatic treatment/ ambient light) maintained structural integrity during hydration.

Table 11: Statistical Summary for Room Temperature Treatments

Test For:	**Group p-value**	**Pairwise Comparisons on the Means**
Treatment differences with MFC tissue	0.4410	No Sig Diff
Treatment differences with CAC tissue	<0.0001	PS<CH15, CH20, CHHY to p<0.01 CH15<CH20, CHHY to p<0.01 CH20, CHHY – No Sig Diff
Treatment difference (CH20 & CHHY only), and tissue difference (CAC, FG, MFC)	Treatment: p=1 Tissue: p=0.0005	CAC>FG to p<0.05 CAC>MFC to p<0.01 MFC, FG – No Sig Diff

Two observations were readily apparent from these results: that meniscal and articular cartilage behaved differently, and that condylar articular cartilage produced the strongest bonds upon enzymatic modification. Recalling that meniscal fibrocartilage would bond with only photosensitizer and irradiation while articular cartilage tissue samples would not, Figure 36 (a) shows strength results for the MFC tissue treated with photosensitizer and irradiation only. The force curves represent the maximum, minimum, and that data curve best representative of the group mean. To compare all tissue types, Figure 36 (b) gives strength results for all tissues (CAC, FG, MFC) with the CH20 treatment, with force curves best representative of the group mean. The meniscal tissue presents a considerably different force curve than the comparatively stiffer articular cartilage samples. The architecture and composition of the two tissues is quite different, and so when trimmed down to a 0.5 mm thickness as was done in this study, the articular cartilage tissue was still rigid enough to maintain its shape. The meniscal tissue, however, behaved more like a fabric at this thickness. The force curves for meniscal samples most likely reflect straightening of the tissue (the immediate force increase) and then straightening of the collagen fibers within the tissue matrix.

The second observation is that with chondroitinase-ABC treatment condylar articular cartilage shows greater bond strength than either femoral groove cartilage or meniscal fibrocartilage. There was no significant difference found for meniscal tissue groups with no enzymatic treatment or across the groups with differing enzymatic treatment. For the condylar articular cartilage (CAC), however, there were definitive treatment differences. Nominal shear strength results are presented in Figure 37.

(a)

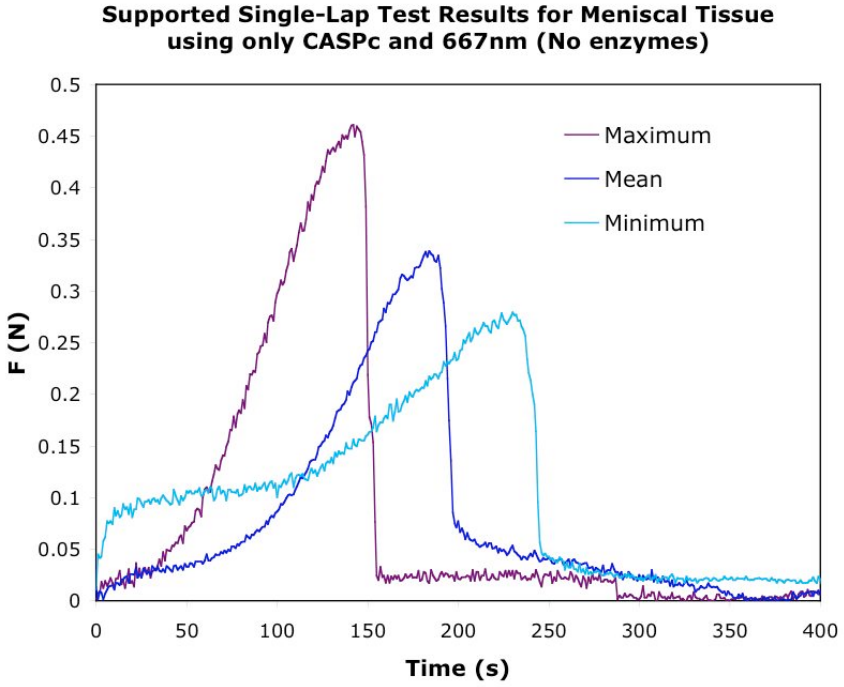

(b)

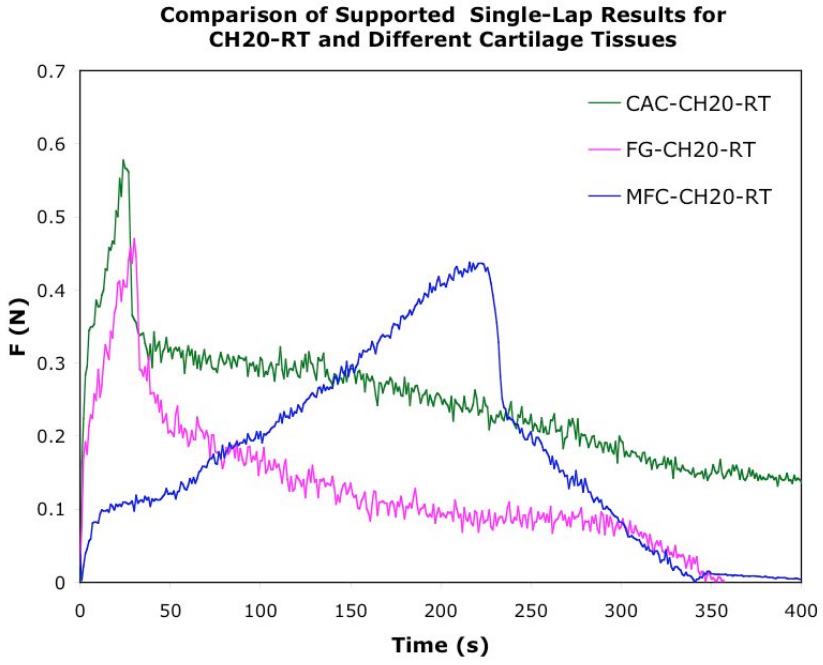

Figure 36: Supported single-lap results from room temperature treatments for (a) meniscal fibrocartilage treated with CASPc and irradiation only (max, mean, and min values), and (b) different behavior of meniscal and articular cartilage samples with the CH20 protocol (data represent samples approximating the mean for each tissue group)

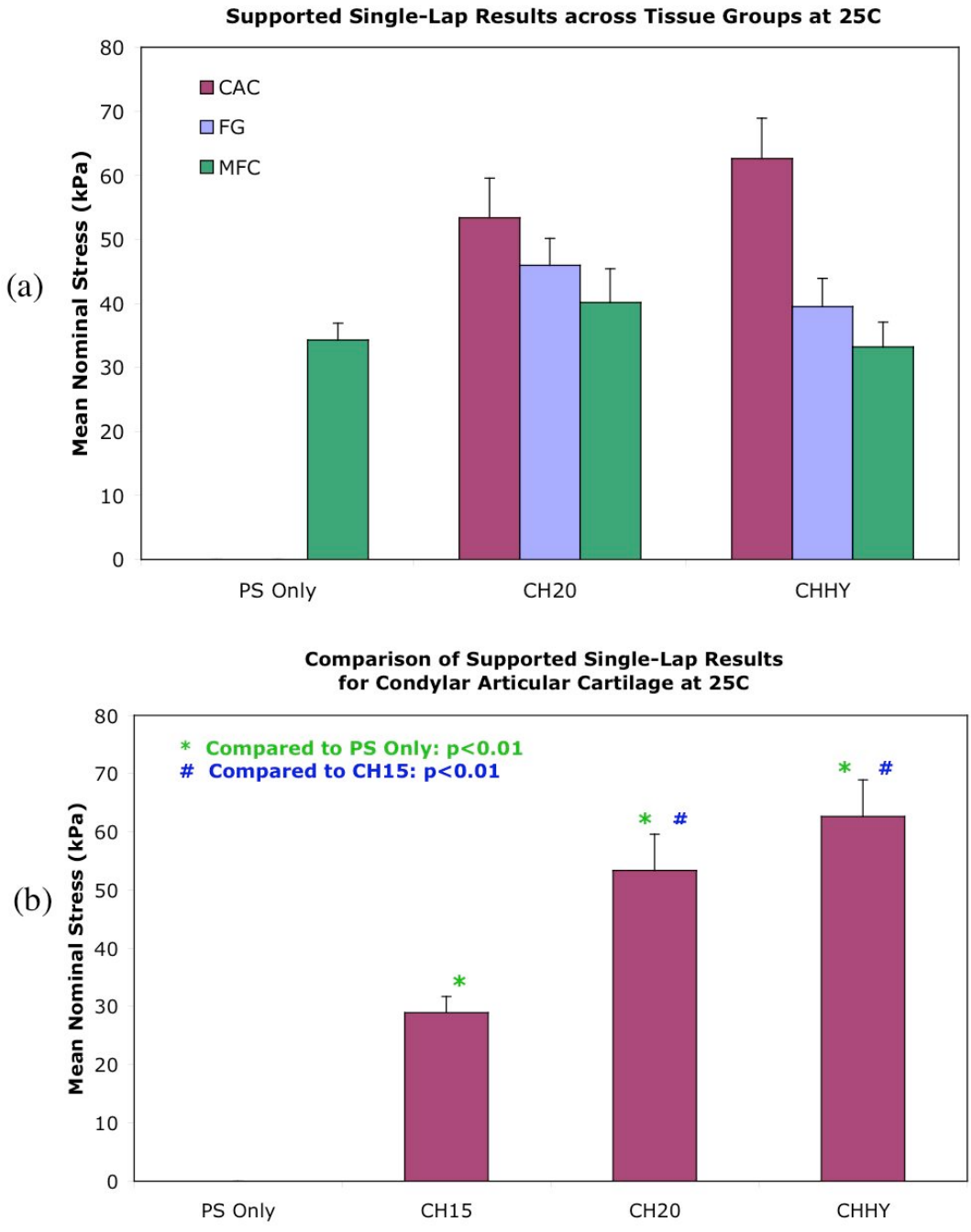

Figure 37: Nominal shear strengths across (a) treatments and tissues, and (b) condylar articular cartilage at room temperature (Error bars correspond to SEM)

Meniscal fibrocartilage and articular cartilage samples were harvested to analyze the relative compositional percentages of glycosaminoglycan and collagen concentration. Data reported here represents that portion of the specimens where FG and CAC tissue samples were preserved from the same stifle (n=3). The assays determined percentages based on sample dry weight and found 26.0±0.9 % sGAG and 46.3±5.4 % collagen for CAC, and 28.1±3.1 % sGAG and 46.7±2.8 % collagen for FG samples. (All data reported as mean±SEM.) Meniscal tissue, as expected, contained much higher collagen (90.0±5.7 %) and lower sGAG (1.7±0.7 %) contents respectively. Water content was approximately similar for the FG and CAC samples, but slightly lower for the MFC samples by comparison. Remember that meniscal tissue contains predominantly collagen type-I while articular cartilage contains principally type-II collagen. Since condylar articular cartilage was the tissue most tested, and the tissue used exclusively in the experiments conducted at 37°C, there were few samples of femoral groove articular cartilage or meniscal fibrocartilage collected. Results for sGAG, percent collagen as determined by hydroxyproline, and water content (% water) are therefore given in Table 12 for comparatory purposes but without statistical analysis.

Table 12: sGAG and Collagen (via Hydroxyproline) Assay Results for Cartilage Samples in the Room Temperature Tests

	FG Samples			***CAC Samples***			***MFC Samples***		
	% sGAG	**% collagen**	**% water**	**% sGAG**	**% collagen**	**% water**	**% sGAG**	**% collagen**	**% water**
	27.6	50.8	82.3	27.6	56.9	76.1			
	23.0	41.4	83.1	24.4	38.9	79.6	2.3	84.3	70.1
	33.8	47.9	80.9	26.1	43.2	78.2	1.0	95.8	72.8
MEAN	*28.1*	*46.7*	*82.1*	*26.0*	*46.3*	*78.0*	*1.7*	*90.0*	*71.5*
n	*3*	*3*	*3*	*3*	*3*	*3*	*2*	*2*	*2*
Std Deviation	*5.43*	*4.84*	*1.11*	*1.60*	*9.37*	*1.76*	*0.94*	*8.11*	*1.91*
SEM	*3.1*	*2.8*	*0.6*	*0.9*	*5.4*	*1.0*	*0.7*	*5.7*	*1.4*

From the room temperature tests, the CH15 protocol (1 U/ml of chondroitinase-ABC for fifteen minutes) using articular cartilage harvested from the femoral condyles was subject to the least experimental error, without using multiple solutions or multiple solution transfers, and exhibited the smallest standard deviation among the articular cartilage tissues. This tissue and protocol combination was therefore selected for the baseline case in the 37°C experiments.

Complete summaries for the experiments at room temperature are included in Appendix A5.

Cartilage Bonding at 37°C: Comparison of Parameters against a Baseline Procedure

Strength Results

All test groups conducted at 37°C used articular cartilage harvested from the femoral condyles and the enzymatic modification protocol CH15 (1 U/ml chondroitinase-ABC for fifteen minutes) as the baseline for comparison. Many groups were point comparisons against different treatments such as Traut's Reagent or the hydrophobic photosensitizer ZNPc. Other groups were run for the purpose of evaluating photosensitizer concentration or irradiance/exposure parameters. Refer back to Table 10 for a complete listing of the treatment parameters investigated in the 37°C experiments. All groups consisted of eight samples (n=8) except for CH15 (n=13) and those groups exhibiting no bonding (n=4).

Complete peak force and corresponding mean nominal shear stress values for all groups are given in Appendix A5. Point-wise comparisons varying one parameter were

analyzed against the baseline case of CH15 (1.7 W/cm^2, 1022 J/cm^2) using two-tailed, unpaired t-tests for independent samples. Groups that reflected three variations of the same treatment parameter were analyzed using a one-factor, unbalanced ANOVA. Complete statistical results are given in Table 13.

At 37°C where the chondroitinase enzyme was more active, the CH15 procedure produced a mean nominal shear stress of 45.9±3.6 kPa (mean±SEM) as compared to 28.9±2.8 kPa produced with room temperature enzymatic treatment. Mean nominal shear values are given for the complete array of treatments in Figure 38. Absent from this figure are values for the control specimens because, as for the room temperature tests, they produced no measurable bond or fell apart during hydration. The control groups evaluated for the 37°C tests were:

- CH15 protocol with photosensitizer and ambient light,
- CH15 protocol with ambient light only, and
- CH15 with 667 nm irradiation and no photosensitizer.

As described, the ZNPc group used an analogous hydrophobic phthalocyanine compound solubilized in PBS that became highly aggregated and did not completely go into solution. It was expected that the severe aggregation would adversely affect the photochemical efficiency and thus result in decreased bond strength. The significantly lowered bond strength using ZNPc compared to CASPc suggests this was indeed the case. For the other treatment variations, the CASPc/400 mM ribose solution produced no significant difference in nominal shear strength when compared to the baseline case, and debridement with 320-grit sandpaper produced no measurable bond strength.

Table 13: Statistical Results for 37°C Test Groups

t-Tests for Point-wise Comparison Against Baseline Case (All groups: 1.7 W/cm^2 and 1022 J/cm^2)			
Baseline Treatment/ Nom. Shear (kPa) ***[mean±SEM]***	**Challenging Treatment**	**p-value**	**Nominal Shear (kPa)** ***[mean±SEM]***
CH15 45.9±3.6	CH15-P1/3 (330 kPa pressure)	0.8881	45.1±4.3
	CH15-Ribose (CASPc in 400 mM ribose solution)	0.0732	36.4±2.4
	CH15-ZNPc (hydrophobic sensitizer)	0.0038	28.9±2.9
	CH15-PSH-TR (7.5 mM CASPc and Traut's Reagent)	< 0.0001	92.1±9.3
	Debride-PT (No enzyme; 320 grit sandpaper debridement)	< 0.0001	1.6±1.6
t-Tests for Point-wise Comparison Against Baseline Case: Irradiance/Exposure Variations			
CH15 – 1.7 W/cm^2, 1022 J/cm^2	CH15-IR15-P2/3 – 1.1 W/cm^2, 1022 J/cm^2	0.0004	
CH15-IR5 – 1.7 W/cm^2, 511 J/cm^2	CH15-IR10-P1/2 – 0.9 W/cm^2, 511 J/cm^2	0.0040	

One-Factor ANOVA Analyses / Tukey's Pairwise Comparison of the Means		
Test For:	**Group p-value**	**Pairwise Comparisons on the Means**
Differences with CASPc concentration (CH15 – 15mM; CH15-PSH – 7.5mM, and CH15-PSQ – 3.25 mM)	0.2312	No Sig Diff
Differences with exposure, All groups 15mM CASPc, 1.7 W/cm^2: (CH15-IR15 – 15 min, 1533 J/cm^2; CH15 – 10 min, 1022 J/cm^2; CH15-IR5 – 10 min, 511 J/cm^2)	0.0116	CH15, CH15-IR15 – No Sig Diff CH15-IR5, CH15-IR15 – No Sig Diff CH15-IR5<CH15 to p<0.01

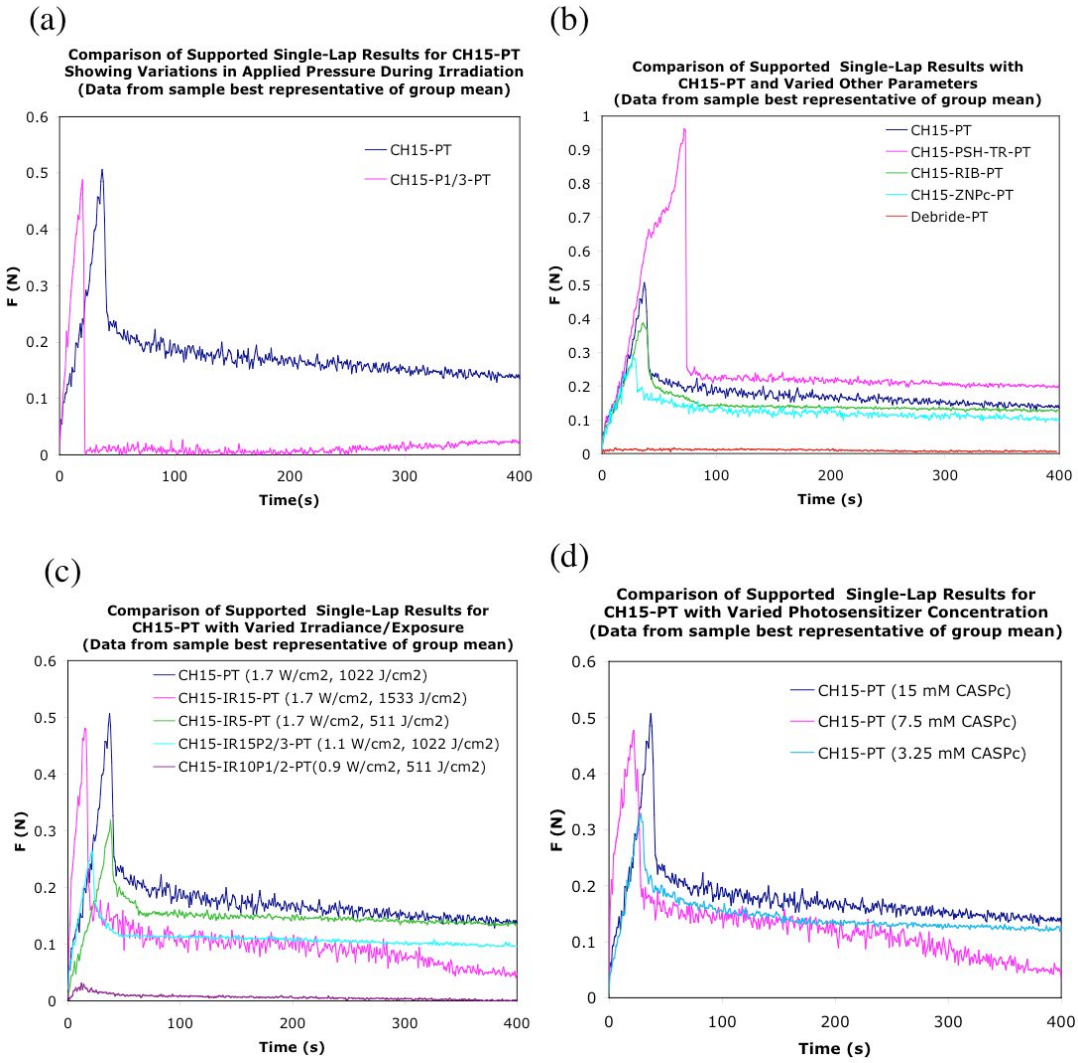

Figure 38: Comparison of treatment variations at 37°C to the baseline case using enzyme protocol CH15 and condylar articular cartilage

Traut's Reagent was used as described in order to investigate the potential of functionalizing the tissue matrix with oxidatively reactive groups as a means of increasing the bond strength. This protocol had the effect of nearly doubling the bond strength over the baseline case to 92.1±9.3. Reducing the interfacial contact pressure to 330 kPa, one-third of the clamp value (using two 200-gram weights to replace the clamps as described in the Methods section), produced no statistically significant difference compared to the baseline case, suggesting that the intimate contact between the bond faces and not pressure was the critical parameter within this range.

No significant differences to $p<0.05$ were observed across the three levels of photosensitizer or among the pairwise comparisons of the levels. Mean nominal shear stress values were 45.9±3.6, 43.5±4.8, and 36.6±2.2 kPa for the 15 mM, 7.5 mM, and 3.25 mM CASPc concentrations respectively. In contrast, varying power and exposure had a significant effect. Holding the exposure constant at 1022 J/cm^2 and reducing the irradiance from 1.7 W/cm^2 to 1.1 W/cm^2, resulted in a significant reduction in the nominal shear strength from 45.9±3.6 to 23.8±2.9 kPa ($p<0.001$). Similarly, holding the exposure constant at 511 J/cm^2 and reducing the irradiance from 1.7 W/cm^2 to 0.9 W/cm^2 resulted in a significant reduction in the nominal shear strength from 27.8±4.5 to 3.3±1.9 kPa ($p<0.01$). Holding the irradiance constant at 1.7 W/cm^2 and varying exposure from 1533 J/cm^2 to 1022 J/cm^2 to 511 J/cm^2, gave a general difference between groups of $p=0.012$. Mean nominal shear strength values were 41.7±4.0, 45.9±3.6, and 27.8±4.5 kPa respectively, yet Tukey pairwise comparisons only found the 1022 J/cm^2 and 511 J/cm^2 groups to be statistically different ($p<0.01$).

Mean nominal shear strength results for all treatments are shown in Figure 39.

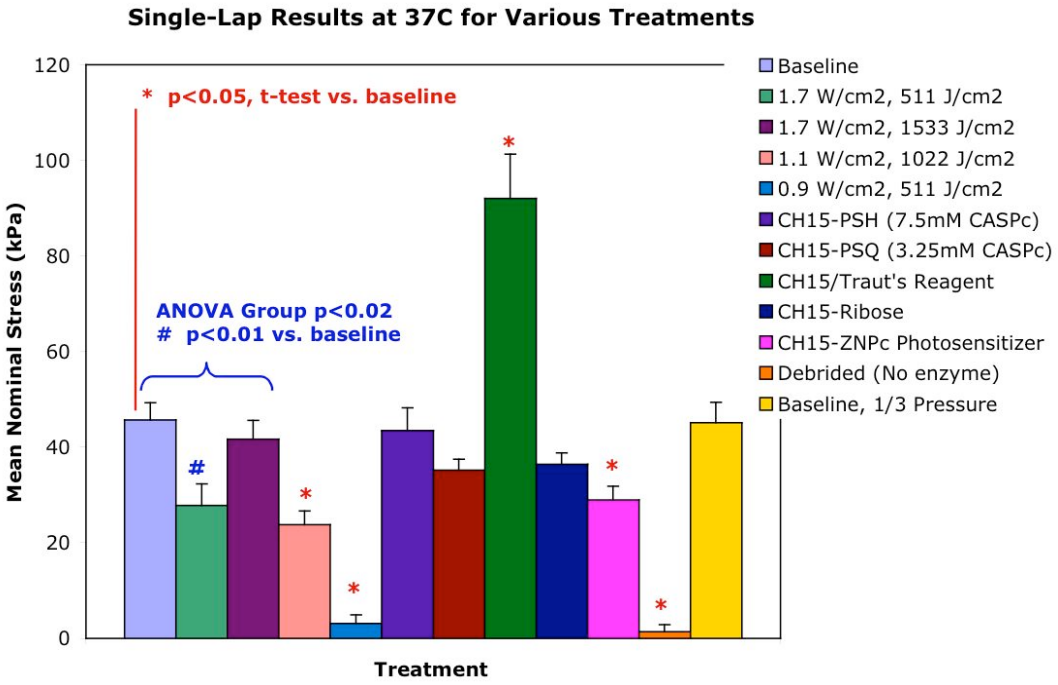

Figure 39: Nominal shear strength of treatments investigated for condylar articular cartilage at 37°C (Baseline case represents CH15: 1U/ml chondroitinase-ABC for 15 minutes, 1.7 W/cm^2, 1022 J/cm^2, and 15 mM CASPc)

Discussion

Results from the mechanical testing section provided some experimental verification of some theoretical ideas and mathematical modeling. First, the measured peak force at failure is greater for an adhesive system using a supported lap configuration than for the classical, non-supported case. This is expected from the ABAQUS results in Chapter XIII that showed the peak force at the bond edges decreasing with the addition of supports across the bond area. Also, the nominal strength results for the non-supported

lap were directly comparable to the previous studies on integrative cartilage repair that also used a non-supported lap configuration. The rates of these tests were identical and the specimen geometry was similar, yet the process and time required to achieve the bond – minutes versus weeks – were considerably different.

The tremendous differences in apparent strength seen as the rate was increased with the Dermabond adhesive really serve to highlight the importance of displacement rate when comparing tensile failure of adhesives in biopolymer systems. Obviously, until a limiting case is reached, increasing the test rate will increase the measured failure strength. What strength is a most "accurate" assessment will depend on both the tissue and the application. In practice, this means that comparisons of different tissue adhesive systems must be investigated at rates that are the same or only marginally different.

Finally, the concept of enhancing the photochemical bond by functionalizing the collagen surface with groups more readily susceptible to the photo-oxidation process was experimentally found to work to a significant degree. The nominal shear strengths using Traut's Reagent treatment in conjunction with the photosensitizer were double those with photosensitizer alone. This does not, however, answer the questions pertaining to long-term stability of the bond or viability of the cells, and thus a culture test is needed.

The most apparent critical factor presenting itself in these experiments is the need for enzymatic surface modification prior to achieving a photochemical bond for articular cartilage tissues. Meniscal tissue, with its significantly lower proteoglycan content, required no such modification. Whether or not the difference in collagen type is also contributory could not be ascertained here. The type of enzyme was also found to be

critical over the treatment durations used in these experiments, which may be explained by considering how these different enzymes affect the cartilage proteoglycans.

The primary proteoglycan aggregate in cartilage is comprised of core proteins bound to a hyaluronic acid (HA) backbone. Off of these core proteins, the glycosaminoglycan chondroitin sulfate and keratan sulfate chains protrude like bristles, with the keratin sulfate chains closer to the link protein[3,13] as depicted in Figure 40.

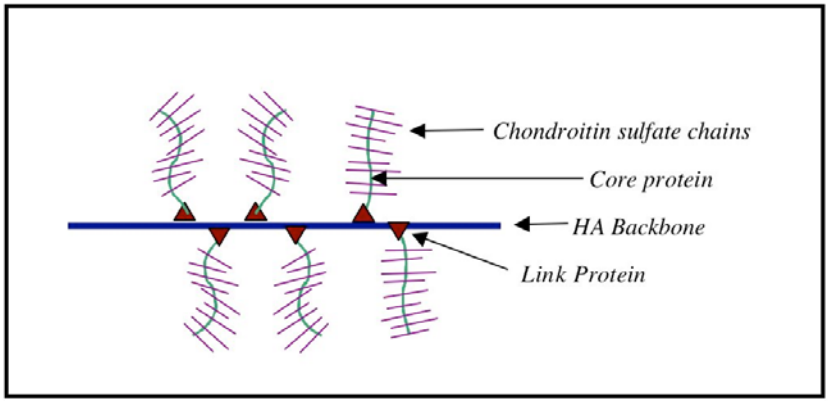

Figure 40: Representation of cartilage proteoglycan aggregate

The enzymes used in these experiments for proteoglycan modification affected different sites on this aggregate macromolecule. . For example, chondroitinase-ABC acts on chondroitin-6-sulfate, chondroitin-4-sulfate, dermatan sulfate, and only more slowly on hyaluronic acid. Hyaluronidase is more widely active, hydrolyzing linkages in the hyaluronic acid, but acting more slowly on chondroitin, chondroitin-6 and chondroitin-4 sulfates.[168] Collagenase, as the name suggests, acts on collagen, cleaving the molecule

into fragments. However, there are findings in the literature that collagenase must be used after prior treatment with a hyaluronidase in order to free up the collagen molecules for enzymatic attack.[169]

The enzymatic effect on bond strength may therefore be either a consequence of the enzyme site specificity or of the ability of the enzyme to penetrate to its targeted site in the amount of time allowed due to the locations of sites on which it is most active. Another possible target for the chondroitinase enzyme that may affect the availability of collagen amino residues for photochemical bonding is its effect on decorin. Decorin is a small proteoglycan that binds directly to the collagen fibrils in articular cartilage and contains one chondroitin sulfate and one dermatan sulfate chain.[170]

An interesting side possibility with respect to the removal of proteoglycans allowing photochemical bonding of the collagen fibrils may be an intrinsic functionality. Aside from the opening up of active amino site, proteoglycans and glycosaminoglycans have been found to act as antioxidants.[171,172] With a crosslinking method that relies on oxidation of select amino acid residues, the presence of an anti-oxidative molecule would tend to inhibit the photosensitizing affect.

Other findings to note here are the short-term effect on chondrocyte viability with photosensitizer and Traut's Reagent exposure and the outcomes of the mechanical testing. With respect to the viability, there was no significant cell death by observation as compared to the control samples. However, short-term effects do not necessarily translate into longer-term effects, especially when irradiation and subsequent photo-oxidation are included. The effect on chondrocyte viability post-irradiation will need to be assessed in a more clinically relevant model.

CHAPTER X.

DEFECT MODEL AND CULTURE TEST

Introduction

While the single-lap experiments demonstrated the potential of the photochemical technique to bond cartilage tissues, questions pertaining to the stability of the bonds and the effect on cell viability over a longer time period remained unaddressed. Although the single-lap model provided a solid comparison to the integrative repair studies cited previously, it was also not a model that could be readily translated into a clinical situation. Most defect models performed in animals center around a chondral or osteochondral cylindrical defect on the femoral condyle.[165,173,174] This is partly due to analogous clinical solutions in humans: auto or allograft transfers, or even the Carticel technique, are applied by creating a cylindrical defect that removes the damaged tissue.[86] Consequently, one in vitro method to study tissue viability and effects during culture is to construct a disc/annulus assembly analogous to the defect model used in animal studies.[32,148]

In this model, a cylindrical disc is inserted into an annulus having an inside diameter similar to the disc. A schematic of this configuration is shown in Figure 41. Push-out tests as described in Chapter VIII have been used to assess the strength of the disc/annulus interface, and previous investigations have used rates of 0.5 mm/min[32] and

0.5 mm/sec.[148] The advantage of the 0.5 mm/sec rate is that bond failure occurs prior to most tissue deformation. In contrast, a much slower rate could result in significant tissue deformation occurring as the result of indentation prior to bond failure, thus complicating the interpretation of failure strength for this model. The 0.5 mm/sec test rate will therefore be used in this study.

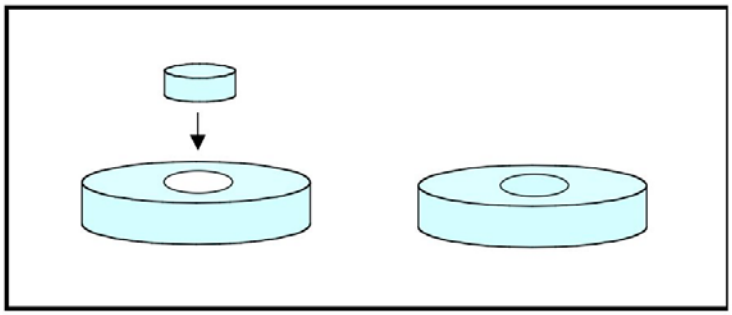

Figure 41: Schematic of the disc/annulus defect model

The purpose of this portion of the study was to perform photochemical bonding on articular cartilage explant disc/annulus assemblies and compare the viability and bond strength over seven days in culture. This allowed analysis to determine whether the bonds would be relatively stable or if they would hydrolyze over time in culture. In addition, culturing these constructs provided a means to assess whether or not the full photochemical process would induce cell death that could increase with time in culture when compared to controls. The set of protocols for the culture study was: 1 U/ml of chondroitinase-ABC for fifteen minutes with no CASPc or irradiation, 1 U/ml of

chondroitinase-ABC for fifteen minutes with CASPC and irradiation (CH15), and additional treatment with Traut's Reagent (CH15-PSH-TR) described in Chapter IX.

Methods

Disc/Annulus Assembly

General harvesting and culture procedures were as described in Chapter IV. Cylindrical cores 8 mm and 4 mm in diameter were harvested from the femoral condyles and the patellofemoral groove of stifles from two different immature calves and trimmed to a thickness of 2 mm that excluded the superficial and calcified zones. Both punches used for the core harvesting were from Miltex, with internal/external diameters for the 4 mm punch measured with digital calipers to be 3.93 mm and 4.35 mm respectively. Samples were stored in the serum-free wash solution overnight in an incubator.

To create annuli, cores were removed from the 8 mm diameter discs using a Fray 3.5 mm biopsy punch having internal and external diameters measured to be 3.53 mm and 3.99 mm respectively. During previous investigations, it was found that none of the 4 mm diameter discs would remain in the 3.5 mm annulus hole unless both the plug and the annulus had undergone enzymatic surface modification. Therefore, the control group for these tests was subjected to the CH15 enzyme protocol but not treated with photosensitizer or irradiation. The mismatch in diameters was selected such that each disc

would be press-fit into an annulus, thus ensuring intimate contact between apposing surfaces despite enzymatic degradation.

Treatment Procedures, Subsequent Assembly, and Irradiations

The chondroitinase enzyme solution was prepared as previously described and brought to 37°C in a water bath. Two annuli and two discs were placed in 0.6 ml of the enzyme solution per well of a 48-well plate and placed in an incubator for fifteen minutes without agitation. All samples were then removed, one disc and one annulus were placed into one well containing 0.6ml PBS, and the specimens were returned to the incubator for ten minutes to soak. No more than four plugs and annuli were enzymatically treated at any given time such that construct assembly for each could be completed without much time passing between the completion of the first and the last constructs in a given treatment set. Aseptic technique was used for all procedures and assembly was performed under a sterile culture hood. No attempt was made to match tissue (femoral groove of condylar cartilage) or animal source. All discs and annuli were selected randomly for assembly.

For the control samples, the annulus was blotted dry using sterile pads, and the inside surface of the annulus was dried with a sterile cotton-tipped applicator. The disc was similarly blotted dry and then inserted while holding both disc and annulus with the sterile pad. The samples were then immersed in PBS for approximately 25 minutes. Samples that were to be mechanically evaluated for the day zero time point were taken for push-out testing after their immersion in PBS. The samples to be cultured were

placed in a DMEM/antibiotic/antimycotic wash solution as described in Chapter IV and returned to the incubator.

Photosensitizer-treated samples were treated similarly to the controls, except that after an annulus was lightly blotted dry with a sterile pad, it was immersed in 15 mM CASPc for approximately 20 seconds. The annulus was then removed, dried, and assembled with the disc in the same manner as the control samples. The discs were not treated with photosensitizer solution. The assembly was then seated on a sterile cotton ball soaked with a PBS/AB/AM solution (described in Chapter IV) in a small petrie dish, covered with a piece of cover glass to prevent air dehydration, and irradiated for ten minutes. After irradiation, the photosensitized sample was immersed in PBS for 25 minutes and then either mechanically tested or placed in the DMEM/AB/AM wash solution and returned to the incubator.

The protocol using Traut's Reagent was also analogous to that used in Chapter IX. This procedure was identical to that used for photosensitized samples except that both plugs and annuli were soaked in 1.5 mg/ml of Traut's Reagent for ten minutes prior to photosensitizer treatment with 7.5 mM CASPc. Again, only the annulus was treated with photosensitizer solution.

For these experiments, the spot of the 667 nm diode system was expanded to 5 mm in diameter (from the 4 mm used earlier). By irradiating normal to the plug surface with a 5 mm diameter spot, the interface was encompassed in the irradiation. No attempt was made to angle the construct or otherwise flip over or move the sample. Instead, irradiation was only incident on one surface. The intent was that since biological tissue, and especially cartilage, is highly forward scattering in the visible range, enough light

could be scattered out to the interface throughout the depth of the plug to achieve bonding. An illustration of this irradiation set up is shown in Figure 42. This procedure with the 5 mm spot gave an irradiance and exposure of 1.1 W/cm^2 and 667 J/cm^2.

For the samples in culture, the wash solution was replaced with feed media containing serum on day one. Media were changed on day three and day five of culture.

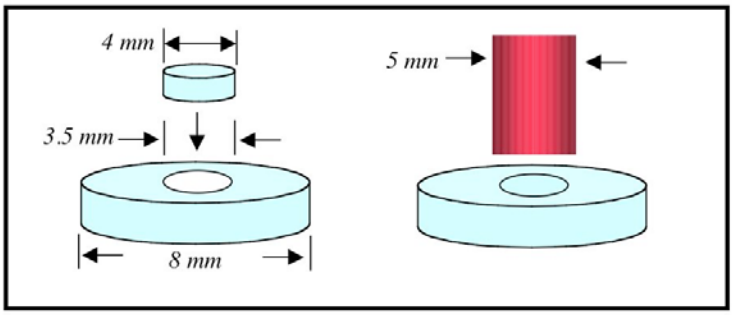

Figure 42: Construct dimensions and irradiation setup

Mechanical Testing: Push-Out Tests

Push-out tests were conducted on an Enduratec ELF 3200 test machine using the same load cell as for the single-lap tests. A custom sample holder was constructed such that a 3.45 mm diameter plunger pushed the central disc out through the annulus at a rate of 0.5 mm/s and down through a 4.9 mm diameter hole, as shown in Figure 43. The final diameter of the discs inside the annuli were estimated using digital calipers to average 3.75 mm. The peak force sustained by the assembly divided by the lateral area of the

deformed core (height times circumference at a diameter of 3.75 mm) was taken as the failure stress. Strength assessments were performed for day zero, day three, and day seven of culture.

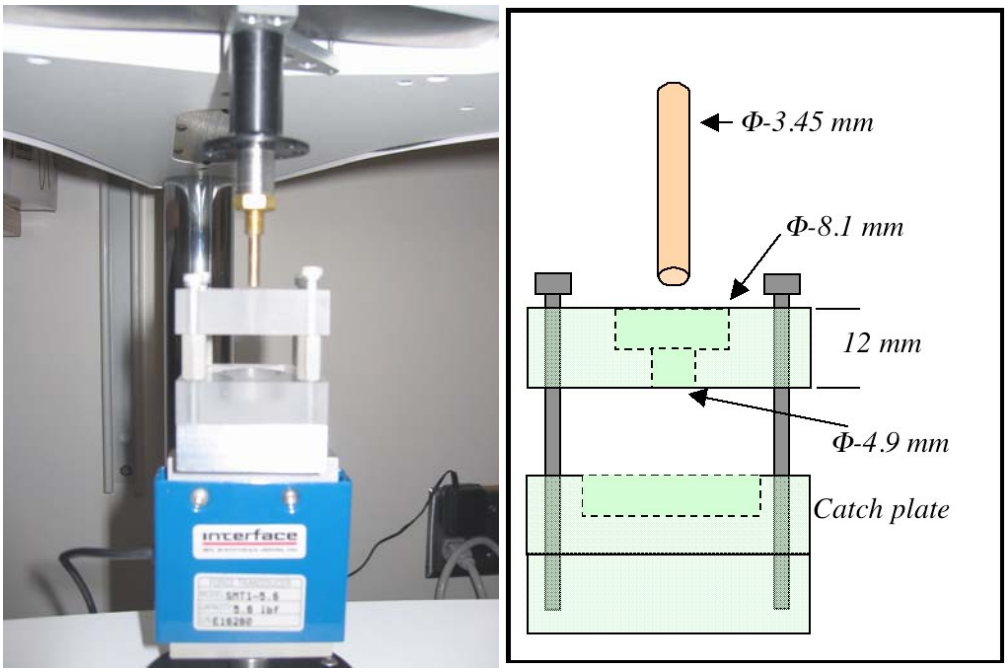

Figure 43: Push-out test configuration

Viability Evaluation

Separated discs and annuli were immediately returned to culture media after testing and the standard procedures described for completing the live/dead assay were followed. Viability assessments were performed at day three and day seven of culture.

Statistical Analysis

The data were first analyzed using a two-factor, unbalanced ANOVA. Data sets with and without the apparent outlier data point for the PSTR-DAY 7 were considered. There was a significant difference with respect to treatment group but not for days in culture. The pairwise comparisons using Tukey's test showed that both the CTL and PS group means were statistically less than the PSTR group to the p=0.01 level, but no significant difference existed between the CTL and PS groups. A follow-up one-factor ANOVA was performed grouping the data by treatment only and found similar results.

Given the small sample sizes and the unequal variances, however, the data set was checked for normality. MATLAB was used to plot the probability distribution of the data, where deviation from a linear fit represented the degree of non-normality of the data. It was found that the data set was non-normal, indicating a non-homogeneity of variances, and thus the results from the ANOVA on the untransformed data might not sufficiently or accurately detect group differences.

When this occurs, one technique to stabilize the variances and produce a more nearly normal distribution of data is to non-linearly transform the data.[175,176] The basis for this procedure assumes that variance is a function of the mean for the data in question. That is:

$$\sigma_i = c\ \mu_i^p$$

where:

σ_i is the standard deviation of the i^{th} group,

c is a proportionality constant,

μ_i represents the mean of the i^{th} group, and

p is a power representing the distribution characteristics.

When the variances are a function of the mean as described in this equation, the data may be transformed using the relation $X_{ij} \rightarrow X_{ij}^{(1-p)}$. If the particular relationship between the variance and mean for a given data set is unknown, it is possible to empirically estimate p by taking the log of $\sigma_i = c\ \mu_i^p$ and replacing the unknown distribution parameters σ_i and μ_i with their sample values S_i and $X_{i\bullet}$:

$$\ln (S_i) = \ln(c) + p \ln(X_{i\bullet})$$

The value for p can now be estimated from the slope of the line fitted to a plot of ln (S_i) as a function of ln($X_{i\bullet}$), and the data transformed accordingly. The data transformation procedure is well established[175,176,177,178] as a means to handle non-normally distributed data sets, and the transformed data are then able to be analyzed using parametric statistical methods.

Results

Viability Evaluation

None of the treatment groups resulted in cell death to the extent of the osmotic sugar solution immersion. There was no more cell death seen after the irradiations than had occurred for the photosensitizer live/dead evaluations performed in the previous chapter. On day three, the controls and photosensitized samples showed roughly the same amount of cell death around the periphery of the plugs and the inside of the annulus from 60-160 μm. The only apparent difference seen was that the photosensitized samples showed a small but consistent necrosis zone around the outside of the annulus of approximately 60-75 μm while the controls samples ranged from 20-60 μm in cell death at this location. Traut's Reagent treated samples showed only slightly more necrosis from the edges of the constructs than the photosensitized only samples. There was, however, a greater percentage of cell death randomly distributed throughout the more central portions of the tissue.

Day seven results were very similar. Controls and photosensitized samples showed from 20-120 μm of cell death, with the plugs and inside surfaces of the annuli tending to average around 70 μm and the outside of the annuli around 40 μm in depth. The Traut's Reagent treated samples again showed increased cell death over the other two treatments, with necrosis zones ranging from 75-180 μm in depth on the plugs and inside annuli surfaces and approximately 75 μm on the outside annuli surfaces.

Approximately half of all samples showed edge effects in the form of zones of increased necrosis protruding in from the corners of a plug or the inside surface of an annulus. Confocal images depicting these results are included in Appendix A6.

Mechanical Testing

A data summary describing the mean, standard deviation, and standard error of the mean for all treatment groups is given in Table 14. Actual force data for the controls (CTL), photosensitizer/irradiation (PS), and photosensitizer/Traut's Reagent/irradiation (PSTR) are given in Figures 44, 45, and 46 respectively. There were four samples for each treatment on each time point except for the PS treatment on day seven, for which there were three samples.

In summary, both the PS and PSTR treatments demonstrated greater strength than the controls. The PSTR groups sustained a much higher stress on day zero before decreasing to approximately one-third of its initial value by day three. The PSTR data on day seven would give a strength of 161±25.6 kPa without including the outlier data point, bringing it in line with the strength shown for day three. In Figure 47, the nominal shear strength for PSTR with and without this point are shown for comparison. The strength of the PS group appeared to initially slightly increase in value and then hold relatively constant between days three and seven, and the control group appeared to maintain a fairly constant strength across the time points.

Table 14: Data Summary for Push-Out Tests with Respect to Treatment Group and Days in Culture

Treatment	Days in Culture 0		3		7		
	1.50	60.53	1.27	51.43	1.66	67.20	MEAN
CTL	0.60	24.17	0.67	27.19	1.46	59.06	ST DEV
	0.30	12.09	0.34	13.60	0.73	29.53	SEM
	1.97	79.73	3.01	121.67	2.82	113.85	MEAN
PS	0.88	35.71	1.59	64.11	1.47	59.50	ST DEV
	0.44	17.85	0.79	32.06	0.85	34.36	SEM
	10.77	435.12	3.45	139.25	6.51	263.14	MEAN
PSTR	2.98	120.61	1.48	59.88	5.14	207.70	ST DEV
	1.49	60.30	0.74	29.94	2.57	103.85	SEM
	Force (N)	Stress (kPa)	Force (N)	Stress (kPa)	Force (N)	Stress (kPa)	

(CTL=controls, PS=photosensitizer and irradiation, PSTR= photosensitizer, Traut's Reagent and irradiation)

At the time the data were collected, an apparent internal software error overwrote the data acquisition rate with the rate from the parent file used for the single-lap tests. This was discovered and corrected for the day seven tests. Analyzing the low speed data against the high speed data for the control samples, which maintained a constant mean at all time points, there were no significant differences between the data sets. Therefore, the slower data acquisition rate was sufficient to capture the data for this set of experiments.

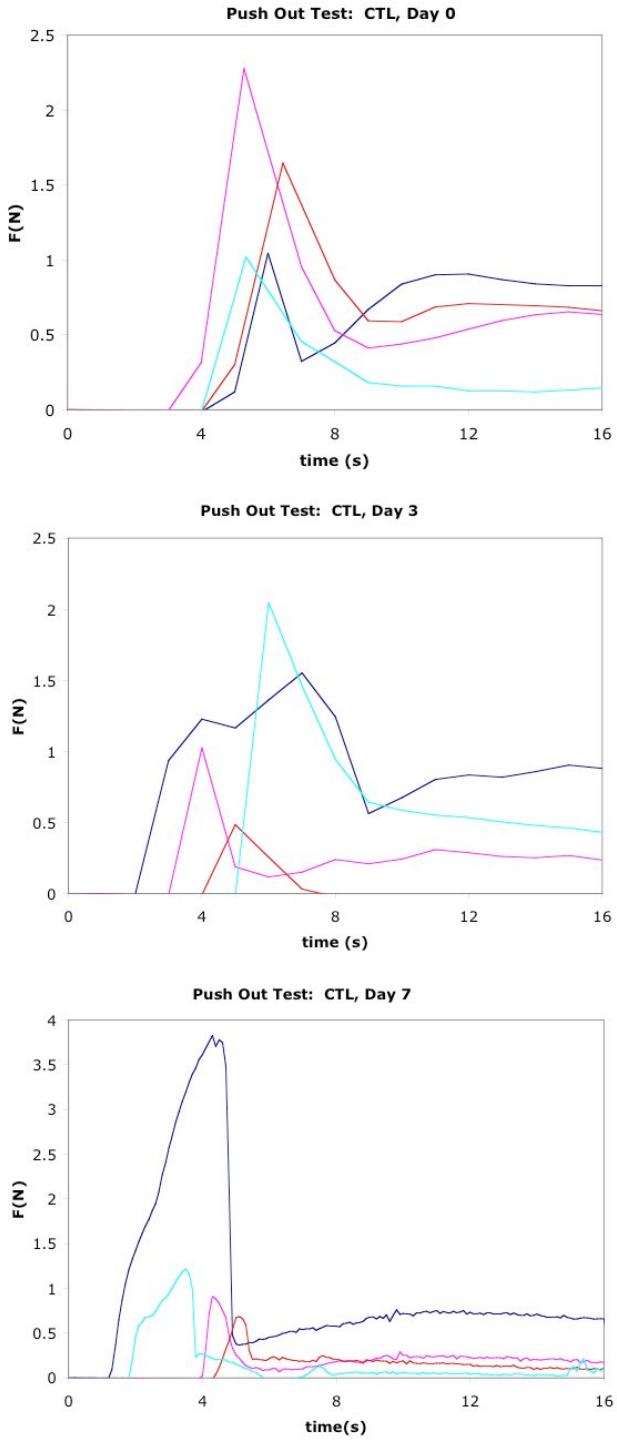

Figure 44: Strength results for push-out tests on the control (CTL) samples. Each force curve represents a different sample.

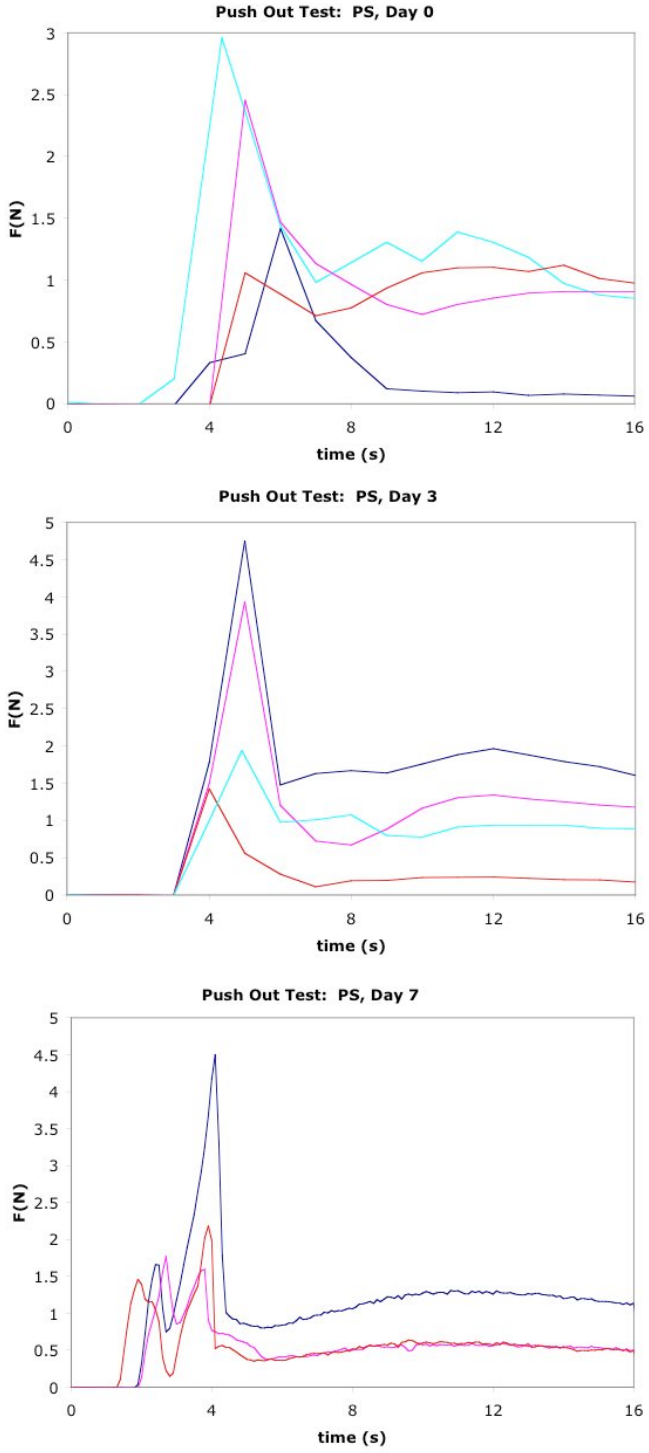

Figure 45: Strength results for push-out tests on the photosensitizer/irradiation (PS) samples. Each force curve represents a different sample.

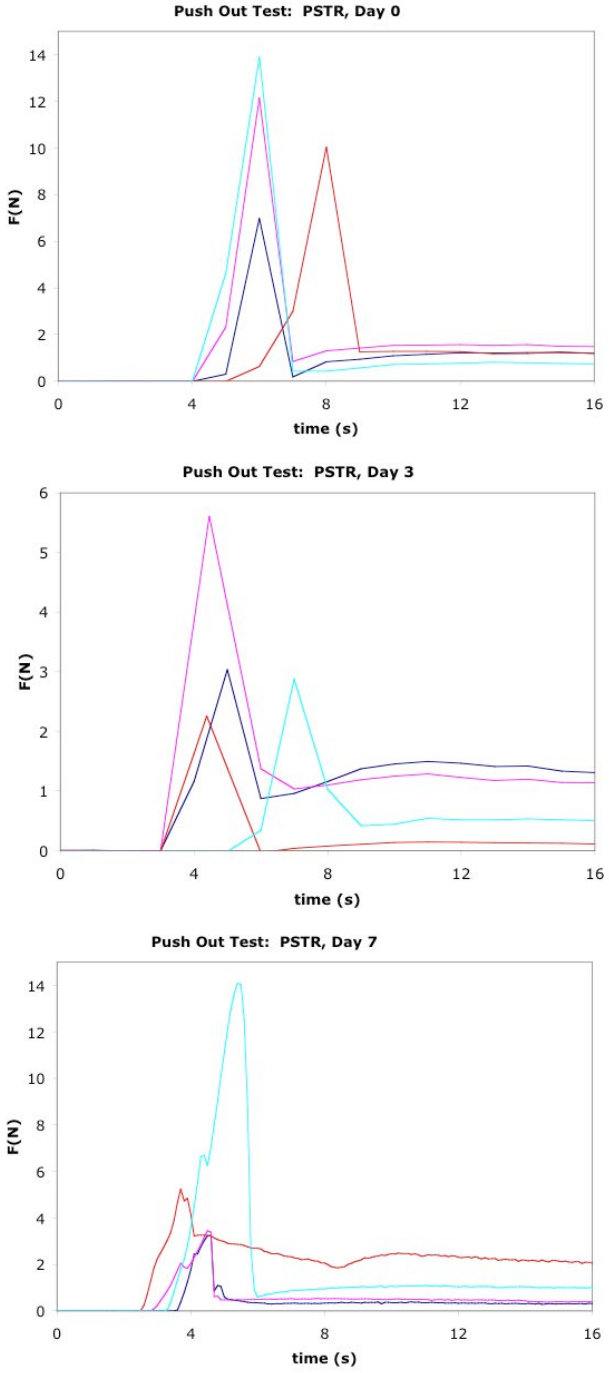

Figure 46: Strength results for push-out tests on the photosensitizer/Traut's Reagent/irradiation (PSTR) samples. Each force curve represents a different sample.

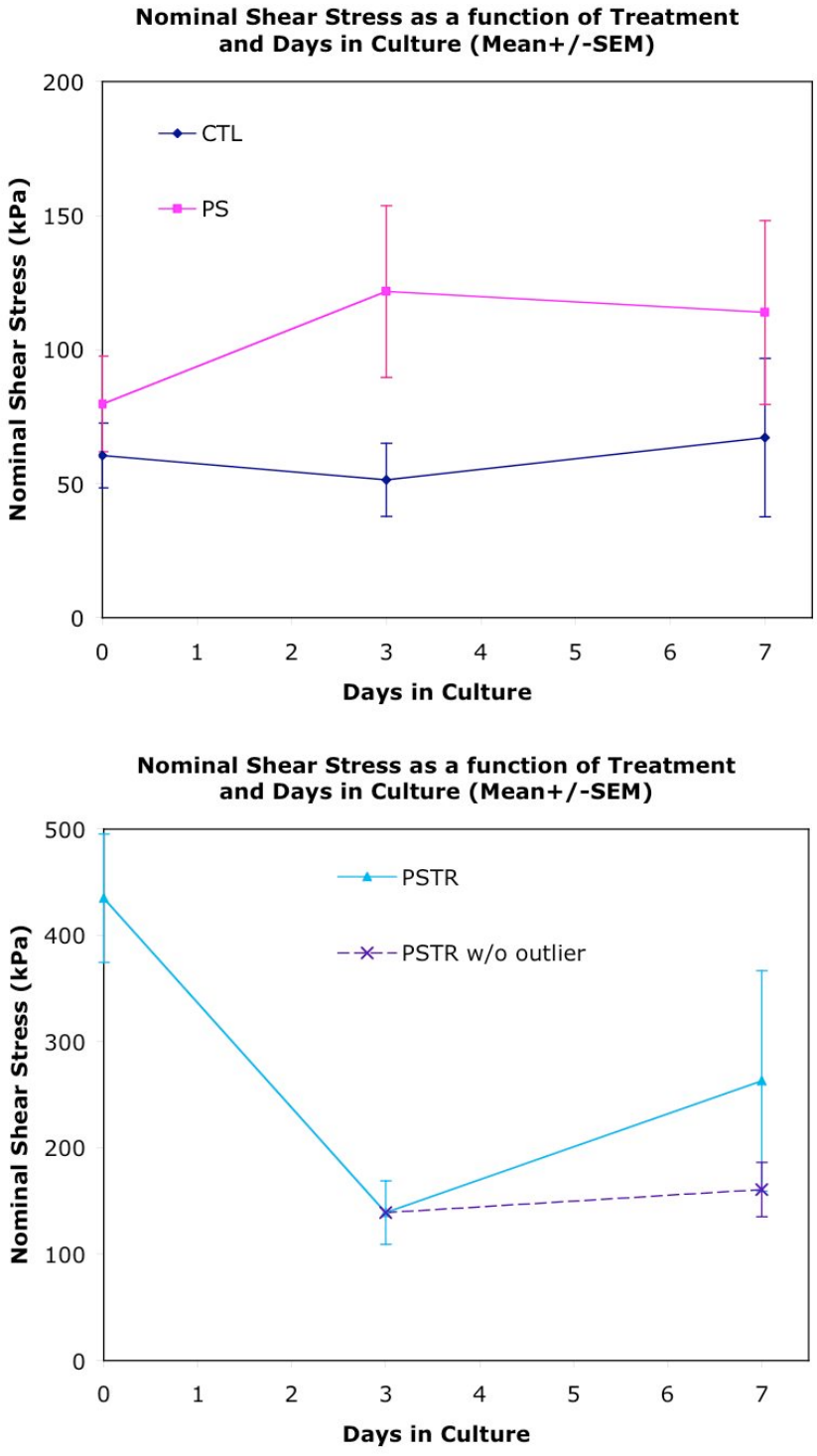

Figure 47: Mean nominal shear stress for all treatments with day in culture (mean±SEM)

Comparison to the Supported Single-Lap Test

The results from the single-lap tests clearly demonstrated an effect of test rate on the measured strength of the tissue bond. Therefore, to provide some measure of comparison to those results, the supported single-lap test was repeated using protocol CH15 with photosensitizer and irradiation as described for the baseline group at 37°C in Chapter IX. Figure 48 presents those results. Recall that the supported single-lap experiments using this protocol and a 0.5 mm/min displacement rate produced a mean nominal shear strength of 45.9±3.6 kPa. At the 0.5 mm/s rate, the mean peak force for the supported single-lap test was 1.7 N, corresponding to a mean nominal shear strength of 162±23.6 kPa. This is in comparison to a mean nominal shear strength of 104±15.7 kPa for the corresponding treatment group (enzyme/photosensitizer/irradiation – group PS) in the push-out tests across all time points.

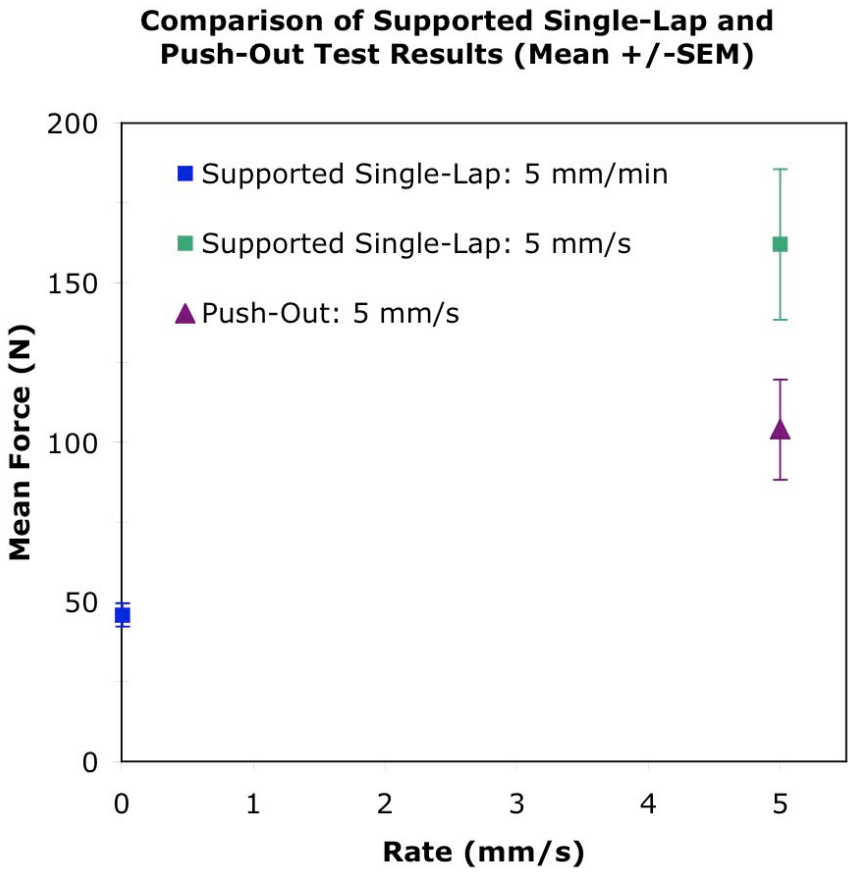

Figure 48: Strength results using the supported single-lap test using the baseline case (CH15) and the analogous protocol from the push-out tests (PS) at displacement rates of 5 mm/min and 5 mm/s

Statistical Analysis

As detailed in the *Methods* section of this chapter, the data were analyzed for normality using MATLAB to plot the probability distribution of the data. As seen by data deviations from the straight line in Figure 49, the data set was clearly not normally distributed. The data were thus transformed using the procedure described by empirically determining the data transformation directly from the characteristics of the data set. For the push-out data, the log plot of the sample variances as a function of the sample means to determine the power best describing the distribution characteristics (from $\sigma_i = c\ \mu_i^p$) is illustrated in Figure 50.

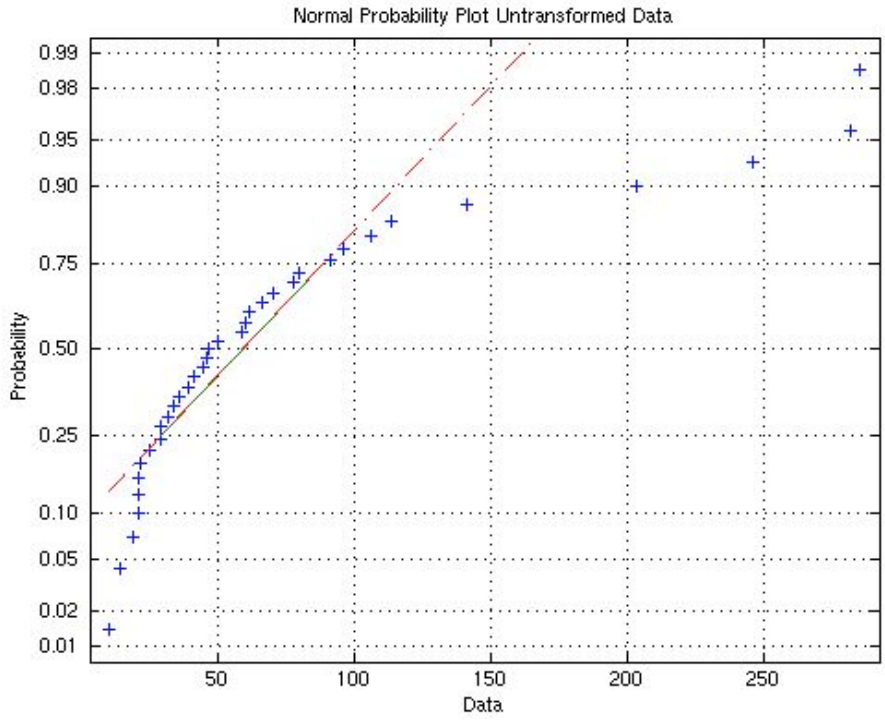

Figure 49: Probability distribution plot of untransformed push-out data

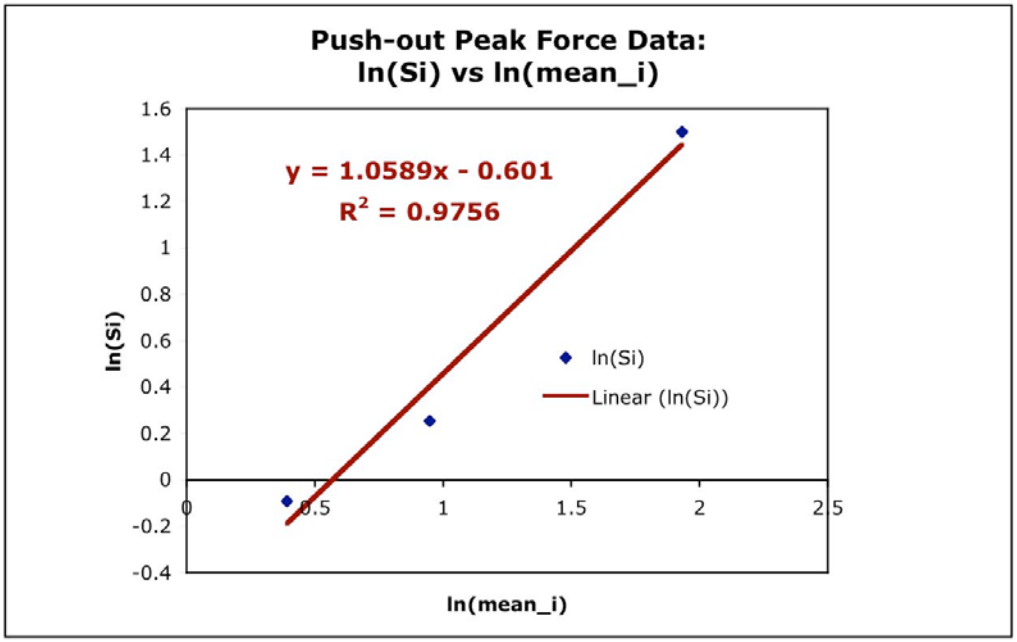

Figure 50: Plot of ln (S_i) as a function of ln(X_i.) for the push-out data

Taking p=1.0589, the data was transformed according to:

$$X_{ij} \rightarrow X_{ij}^{(1-1.059)}$$

So, using the transformation:

$$X_{ij} \rightarrow 100 * X_{ij}^{(-0.059)},$$

the data was re-evaluated for normality. (The factor of 100 was simply a scale and has no effect on the statistical outcome.) A probability distribution plot of the transformed data is shown in Figure 51, and is significantly more nearly normal than for the untransformed case.

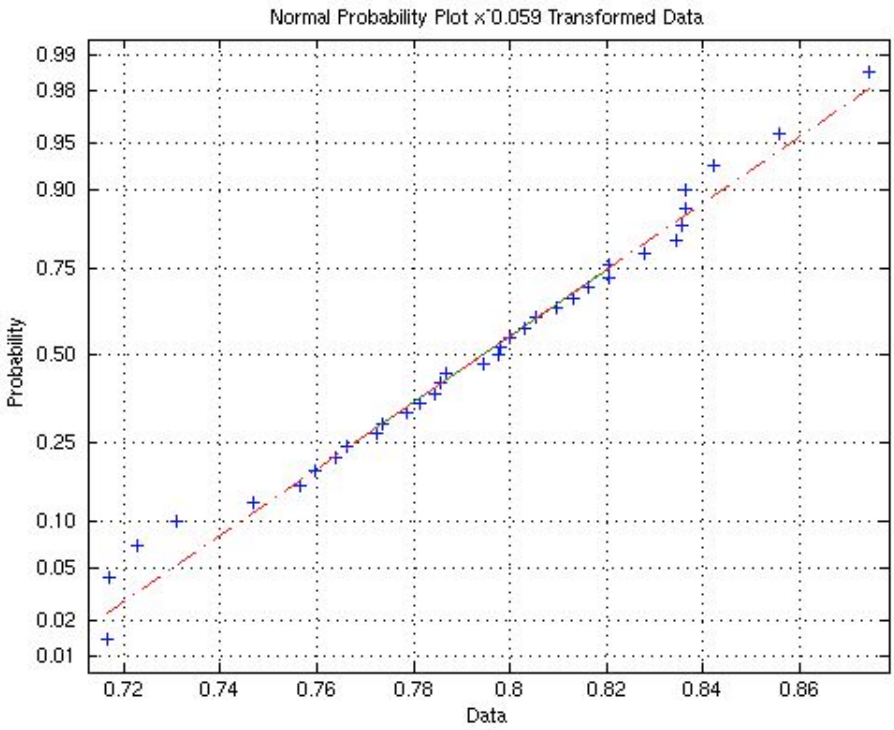

Figure 51: Probability distribution plot of untransformed push-out data

The transformed data were then analyzed using parametric methods, and the ANOVA results on the transformed data are given in Table 15. The results for the transformed data, which resolved the non-normality issue associated with the raw data, gave significant differences between treatment groups but not between days in culture or the interaction thereof. There was a greater degree of statistical difference between the CTL and PS groups with respect to the PSTR group (0.01 level) than between the CTL and the PS groups (0.05 level).

Table 15: Statistical Results for Push-Out Tests using Transformed Data

Statistical Results for Push-Out Tests: Transformed Data

Case	Test	ANOVA p-values	Tukey's Pairwise Comparisons
With PSTR outlier	2-factor: treatment, day	Treatment: p=0.345 Day: p<0.001 Treatment*Day: p=0.126	CTL, PS – No Sig Diff CTL, PS < PSTR, p<0.01
Without PSTR outlier	2-factor: treatment, day	Treatment: p=0.263 Day: p<0.001 Treatment*Day: p=0.065	CTL, PS – No Sig Diff CTL, PS < PSTR, p<0.01
With PSTR outlier	1-factor: treatment	Treatment: p<0.0001	CTL < PS, p<0.05 CTL, PS < PSTR, p<0.01
Without PSTR outlier	1-factor: treatment	Treatment: p<0.0001	CTL < PS, p<0.05 CTL, PS < PSTR, p<0.01

Discussion

The in vitro defect model used for the push-out test provided first-round answers to the outstanding questions remaining after completion of the single-lap tests. Namely:

- Would the bonds remain stable with time in culture?
- Would the photocrosslinking procedure induce immediate or delayed cell death?
- Was the photocrosslinking process capable of being performed in a clinically relevant model?

With respect to the viability results, it is already well known in the field that cell death occurs near to a cut surface in cartilage tissues, and the photosensitized group did not appear to elicit a substantially greater degree of cell death than that seen with the controls. The diffusion ranges of singlet oxygen or other radicals generated by the photoexcitation are estimated to be no more than 45 nm in cellular media[179] due to the high reactivity of the species, and thus were not expected to cause excessive cell death over what would occur in response to the trauma of a cut surface.

Cell death near the cut edge could also be due to the pressure of the press-fit of the plug in the annulus. Previous work has estimated the press-fit interfacial pressure to be on the order of 75 kPa for cartilage with similar properties and dimensions. The press-fit model assumed linear elasticity and orthotropic isotropy and solved the two-dimensional (cylindrical coordinates) coupled boundary value problem describing the stress strain relationship for 7 mm plug press fit into a 6 mm inside diameter of an annulus. The percent reduction in cross-sectional diameter and area were determined to be 10% and 20% respectively.[180] Using values from the defect model used here, the percent reduction in diameter and area were approximately similar (6% and 12%, respectively). Therefore, it is reasonable to assume that the press-fit stress in the defect model employed in these studies would be on the same order of magnitude as that found previously given the same assumptions.

As seen by the strength results, the bonds did stay remarkably stable in culture. The photosensitized group (PS) and controls (CTL) averaged 104±15.7 kPa and 60±10.6 kPa, respectively, across all time points. Only the Traut's Reagent suffered an appreciable decrease in strength from Day 0 to Days 3 and 7 (435±60.3, 139±30.0, and

236±104 kPa respectively). Recall that Traut's Reagent is used to thiolate amine residues that then become highly susceptible to oxidation and subsequent formation of disulfide crosslinks. In many cases, however, the creation of disulfide crosslinks by direct oxidation is reversible or difficult to control.[45] This was demonstrated here to some degree as the bond strength of the PSTR group decreased before holding relatively steady, although the strength of this group did stay significantly above the PS and CTL groups. The incorporation of Traut's Reagent in the procedure was not to propose this specific agent for enhancing cartilage bonding, but rather to investigate the potential of functionalizing the cartilage collagen as a means of strengthening the photodynamic method. Toward this end, it was successful.

Obviously, more samples and more time in culture would be beneficial toward establishing the long-term effects of the photocrosslinking technique. The many biochemical interactions that could take place or be evaluated to better establish the nature of and limitations of these bonds and how they affect the long-term integration mechanisms of cartilage, should be investigated in future studies with expanded parameters and data points. However, the goals for this initial in vitro culture study were solidly met: the photochemical bonds were relatively stable for up to seven days in culture, the cell death induced by the photochemical technique itself was not substantially increased over controls, and the procedure was successfully demonstrated in a clinically relevant model.

CHAPTER XI.

DISCUSSION AND RECCOMENDATIONS

Integrative repair of cartilage damage due to disease or injury is one of the critical issues facing long-term success of tissue engineered constructs or even autograft and allograft transplantation. The many modes of cartilage injury ranging from tears, to fissures, cracking, or fibrillation do not typically heal spontaneously and often lead to more advanced degeneration and possibly presentation of an osteoarthritic condition.[29,86] It has further been found that spontaneously generated repair tissue fails to integrate adequately with the native surrounding tissue, likely due to the failure of the collagenous networks of the repair tissue and the native tissue to intermingle.[86] This integration of the collagen fibrillar architecture has been postulated to be the deciding factor for successful tissue repair in the case of cartilage injuries.[28]

The tissue models used in this study, both the single-lap and disc/annulus defect model, are representative of lateral bonding of an implant to host tissue within a chondral defect or to repair of vertical fissures. A lack of such lateral support and integration has been found to be the critical factor leading to failure of osteochondral autograft transfers in sheep. [181] Similarly, clinical use of chondral grafts has not been widely investigated because of the inherent difficulty in securing such grafts to native tissue[86], and periosteal/perichondral grafts have presented complications resulting from poor integration and a lack of structural bonding with immediately adjacent tissue.[182] Thus repair of any chondral defect, whether partial thickness or full thickness, will require

lateral integration providing some degree of matrix continuity in order to resolve associated functional and nutritional deficiencies.

The aim of the present study was to investigate a means of linking the collagen fibrils in adjacent cartilage tissues in a clinically relevant procedural time span in order to provide an immediate structural link. Without extensive cell death above that already caused by the cut surface and with stability of the bond formed, it is hoped that the initial fixation will lead to enhanced integration and thus repair. Results demonstrated the potential of combining enzymatic surface modification with photodynamic techniques to directly bond cartilage tissues. Of particular note, the bond strength achieved with a ten-minute irradiation was on the order of that previously achieved through several weeks of culture, and bond strength was maintained for one week in culture without evidence of increased cell death.

Previous push-out testing of disc/annulus defect models, using similar dimensions to those used here, involving native explants (as opposed to harvested fetal tissue grafts, tissue engineered construct, or devitalized tissue) produced strengths of 28.5±8.7 or 33.3±7.0 kPa at twenty days and forty days respectively.[148] Although the defects involved inserting the cored disc back into the defect that it came from (the inside of its parent annulus), there was no press-fit maintaining an interfacial pressure as there was in this study. In another explant-to-explant disc/annulus study, the interfacial push-out strength at 56 days was found to be approximately 155 kPa for both untreated explant assemblies and for explant assemblies treated with 1% trypsin for 10 to 20 minutes (corresponding to treatment times of disc and annulus respectively).[32] By comparison, push-out strength results from the present study produced a mean nominal strength of

104±16 kPa for the photosensitized samples across all time points. Similarly, previous single-lap tests on integrative cartilage repair have produced strengths on the order of 30-35 kPa after 14-21 days in culture in a non-supported single lap configuration, while those in this study were approximately equal at 30.3±1.9 kPa for the same test rate and configuration.

While further studies are required to assess whether photoactivated crosslinking of collagen molecules across this tissue interface results in enhanced integrative repair over longer culture periods and *in vivo*, these initial studies indicate that this approach may have clinical utility for fixation of cartilage transplants or fixation of engineered tissues. Due to the difficulty of predicting the behavior of such a method *in vivo* due to the vastly increased biochemical signals and an altered loading environment that cannot be reproduced in vitro, however, an animal model will be required prior to any consideration of use in humans.

To date, the most common, and consequently well-defined, animal models for cartilage repair are mice, rabbits, and canines,[173,183] with more recent studies employing larger animals such as goats[184], sheep[174], and mini-pigs[185,186,187,188]. Each model has its respective advantages or disadvantages depending on the goals of the study. For example, mice produce articular cartilage only three to five cell layers thick and do not reach full skeletal maturity. Rabbits are larger, reach skeletal maturity faster, and are thus the most widely used and accepted cartilage model. By comparison, the size of the larger animals manifests increased depth of cartilage in comparison to rats or rabbits. These differences in cartilage thicknesses available for different animal models highlight one of the most serious issues facing proper selection and use of an animal model, none

of which are completely representative of humans, which is the scale compared to the human joint. Quite simply, the depth of a chondral defect in a human translates to an osteochondral defect in a rabbit or even a goat. Considering rabbits, for example, it may not be possible to scale down the defect size to present an analogous chondrally limited defect in the animal model. Scaling the defect size down may or may not present a system with adequate biochemical and/or biomechanical relevance to the human condition.[86]

That being said, however, the rabbit appears to be the best characterized and most widely used animal model for initial cartilage integration studies. Rabbits also allow ease of researching on mature tissue, more clinically relevant to human injury and disease, since many species, particularly the New Zealand white rabbit, reach skeletal maturity by four to six months of age. Initial studies involving implant/native tissue integration may not require a representative loading environment to elucidate adhesion and soft tissue remodeling mechanisms, and thus the rabbit model would suffice. Yet there are still issues associated with differing biochemical signals, aging, potential for chondrogenesis or lack thereof within six to twelve months of age, and the near necessity to work with a full-thickness defect.[173,183,189,190]

Working with a full-thickness defect alters the repair response from that seen in chondrally limited models by involving spontaneous repair mechanisms introduced by exposing the underlying subchondral bone.[86] Such considerations must be taken into account when interpreting data from an animal, usually with healthy tissue, and extrapolating to the clinical situation with different tissue volumes and likely altered biochemical expression due to injury or disease of the surrounding cartilage. When the

stage of the research reaches a level of maturity necessitating use of a larger animal, the mini-pig or goat appear to be the preferred models. With mini-pigs and goats, partial thickness chondral defects can be created and, in the case of the mini-pig, some degree of biochemical similarity maintained.

Prior to investigation in an in vivo environment though, a greater number of in vitro defect model experiments are necessary to more accurately characterize the nature of the bond and its effects. A culture of several weeks instead of one, followed with imaging or other microscopy of the interfacial area may provide insight to the mechanics and repair response involved, as well as to the functional modification of the enzymatically exposed collagenous matrix such as was performed in this study using Traut's Reagent. There also exists the potential for the formation of larger constructs by sequential bonding of additional annuli. Investigations using tissue explants of different ages as was done for many of the integrative cartilage repair studies might also offer insights to enhance the process or what the limiting factors might be. Yet toward the goal of cartilage repair, it remains to be seen if the critical issue facing adhesion and subsequent integration of chondral implants is to regain a functional integration that promotes structural integrity and nutrition or if the native structural and biochemical integrative mechanisms need to be restored. Perhaps a method such as that designed in this study, which promotes a bond of collagen fibrils across the defect interface, can assist in answering that question.

While there are many potential avenues of expansion for the current study, one possibility would be to build directly on the findings here. The hydrophilic phthalocyanine used in this study is hardly the most efficient photosensitizer

available[191,192,193] though it suited the purposes of this study. Longer-wavelength, more efficient photosensitizers, are continuously being developed. For example, a bacteriochlorin with an absorbance peak around 780 nm[135] could provide distinct advantages. Results here showed that bond strength was still increasing with irradiance up to the maximum power available from the current diode system, and there are systems centering in the 780-800 nm range that offer more power. This wavelength range would also offer more penetration, estimating depth to be approximately 1.5-3.1 mm compared to the 0.7-1.9 mm at 667 nm, as mathematically estimated from the cartilage studies in Chapter V. There are also many functional modification strategies, both with respect to tissue and to polymeric substrates typically used as cell carriers in tissue engineering, that could be investigated to enhance the photochemical bond.

Another possible direction could be to tailor the photodynamic effect to create an injury/disease model. Specifically, reactive oxygen species are thought to be involved in rheumatoid arthritis. It is known that over time excessive reactive oxygen production by phagocytes degrades the cartilage extra-cellular matrix and initiates expression of damaging cytokines and leukocytic cell adhesion molecules.[172] It is conceivable that photosensitizer supplemented media and intermittent irradiation could be used to simulate the damage mechanisms of certain disease or injury characteristics, thereby creating a model system for future in vitro study.

Taking the photosensitized effect to a lesser degree, it may be possible to use low levels of photosensitizer-induced oxidation to enhance chondrocytic metabolism in vitro, and perhaps increase the production of extra-cellular matrix production in tissue-engineered constructs. Long-duration photo-oxidation has been known to strengthen and

stabilize the mechanical properties of proteinous, acellular materials prior to implantation in vivo,[174,194] and unrelated studies have shown that mild photodynamic treatment actually exhibits chondroprotective effects on cartilage tissue and can activate the latent growth factor TGF-b.[195] It is therefore possible that mild photo-oxidation during culture might serve to enhance the cellular proliferative abilities and further strengthen the extra-cellular matrix of tissue-engineered constructs.

APPENDICES

A.1 Materials and Sources

Materials and Sources	
Acetic acid	Sigma
Albumin, bovine	Sigma
Antibiotic/Antimycotic	Gibco
Ascorbate (L-ascorbic acid)	Sigma
Chloramine-T OR	Mallinckrodt
Dulbecco's modified Eagle Medium (High Glucose)	Gibco
Dulbecco's phosphate buffered saline (without calcium or magnesium)	Gibco
Fetal bovine serum	Hyclone
Gentamicin	Gibco
HEPES buffer solution	Gibco
Hydroxyproline	Sigma
Kanamycin	Sigma
MEM Non-essential amino acids	Gibco
p-(dimethylamino)benzalaldehyde	JT Baker
Proteinase-K	VWR
Chondroitinase-ABC	Sigma
Collagenase (type 2)	Worthington Biochemcials
Hyaluronidase	Sigma
Chloro-aluminum phthalocyanine tetrasulfonic acid	Frontier Scientific
Zinc phthalocyanine tetrasulfonic acid	Frontier Scientific
meso-tetra(N-methyl-4-pyridyl)porphine tetra tosylate	Frontier Scientific
Traut's Reagent	Pierce
Riboflavin-5-phosphate	MP Biomedical
Calf stifles	Research 87
Collagen type I (acid soluble)	MP Biomedical
Collagen type I (insoluble)	MP Biomedical
Collagen type II (acid soluble)	MP Biomedical
Gelatin, type A	MP Biomedical
Dermabond	School Health
Live/Dead Assay Kit , L3224	Molecular Probes

A.2 420 nm Diode System Electronic Diagrams

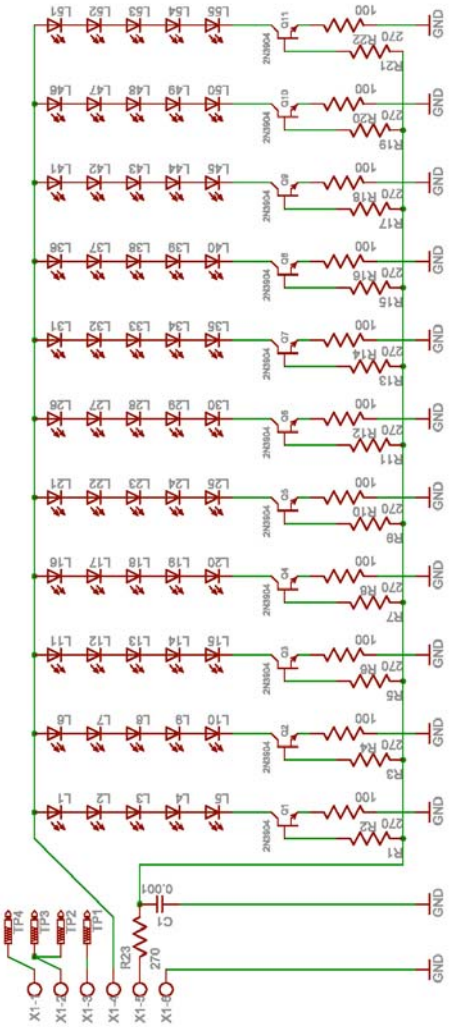

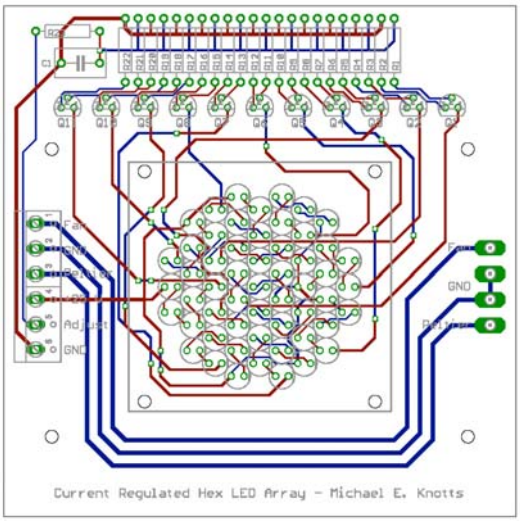

(Contributed by Michael Knotts, Georgia Tech Research Institute)

LED Circuit Diagram

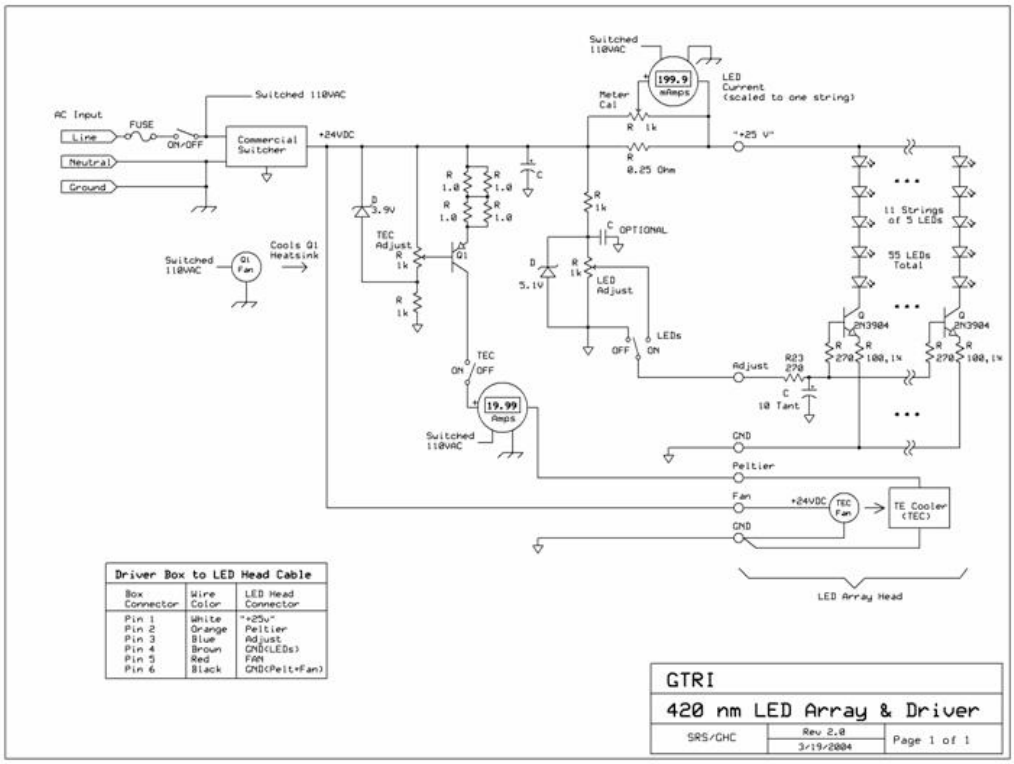

(Contributed by Glenn Champion and Steve Sharpe, Georgia Tech Research Institute)

420 nm LED System Power and Control Electronics

A.3 Optical Scattering Viability Results

In the following images, red and green signify dead and live cells respectively. All images represent an area of 912 μm by 912 μm. The terms "best", "worst", and "typical" refer to the best case, worst case, or typical result for a given set of data.

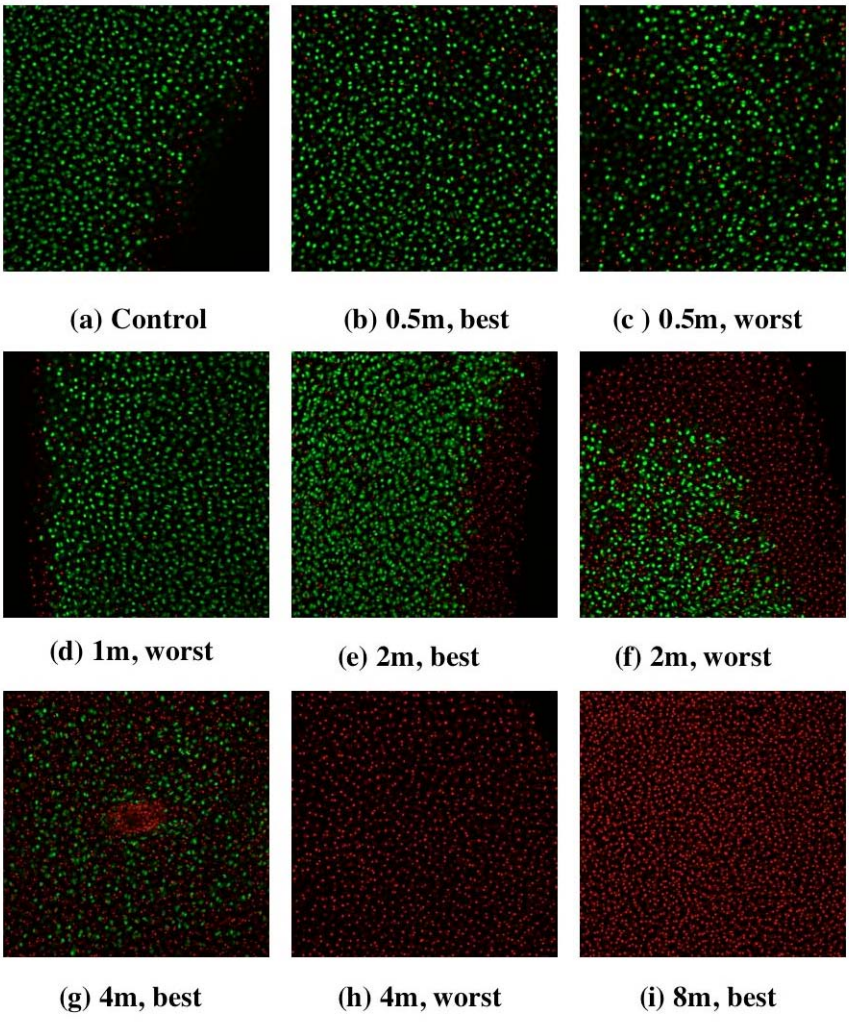

Viability Results after Shock Immersion in Fructose Solutions and 48 hours of Culture

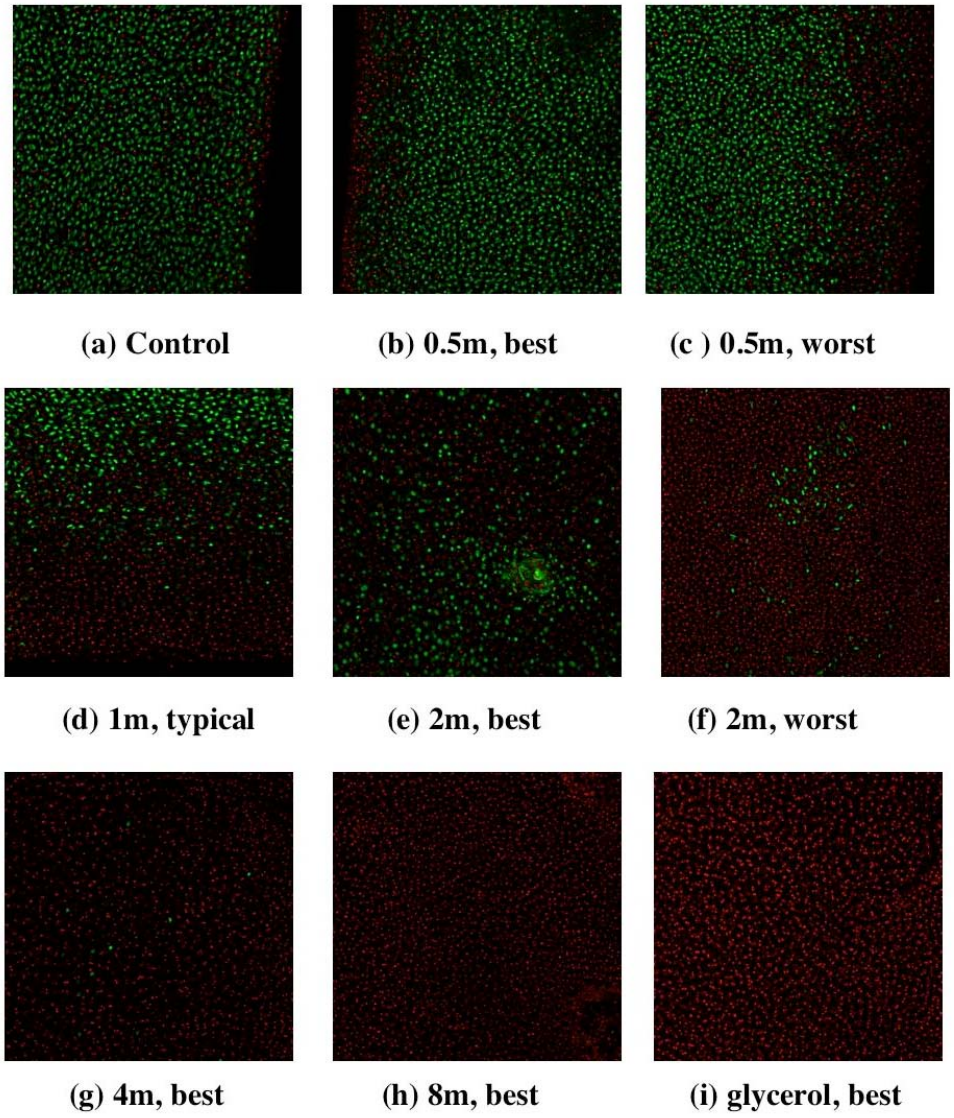

(a) Control (b) 0.5m, best (c) 0.5m, worst

(d) 1m, typical (e) 2m, best (f) 2m, worst

(g) 4m, best (h) 8m, best (i) glycerol, best

Viability Results after Shock Immersion in Ribose Solutions Immediately after Immersion

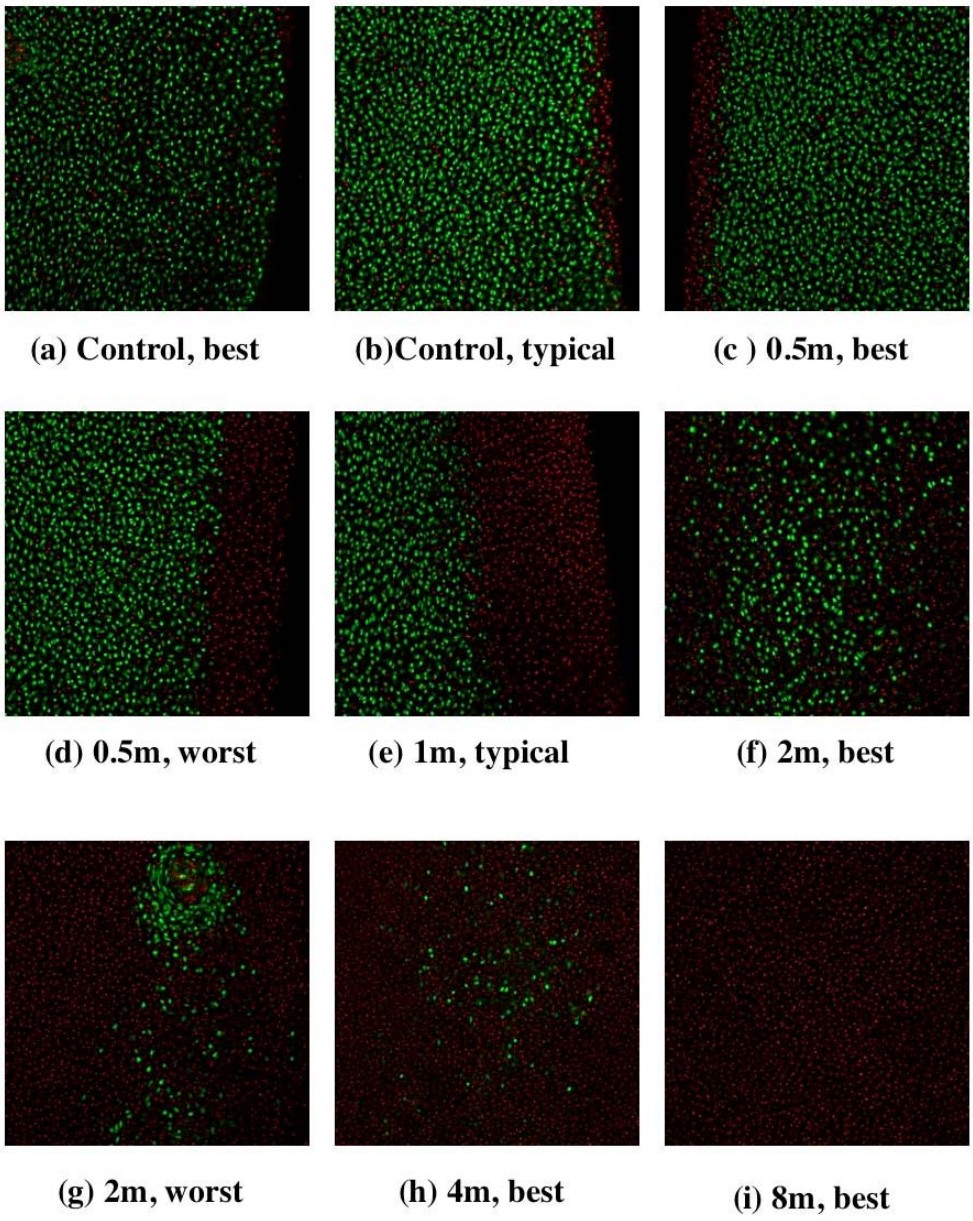

Viability Results after Shock Immersion in Ribose Solutions and 48 hours of Culture

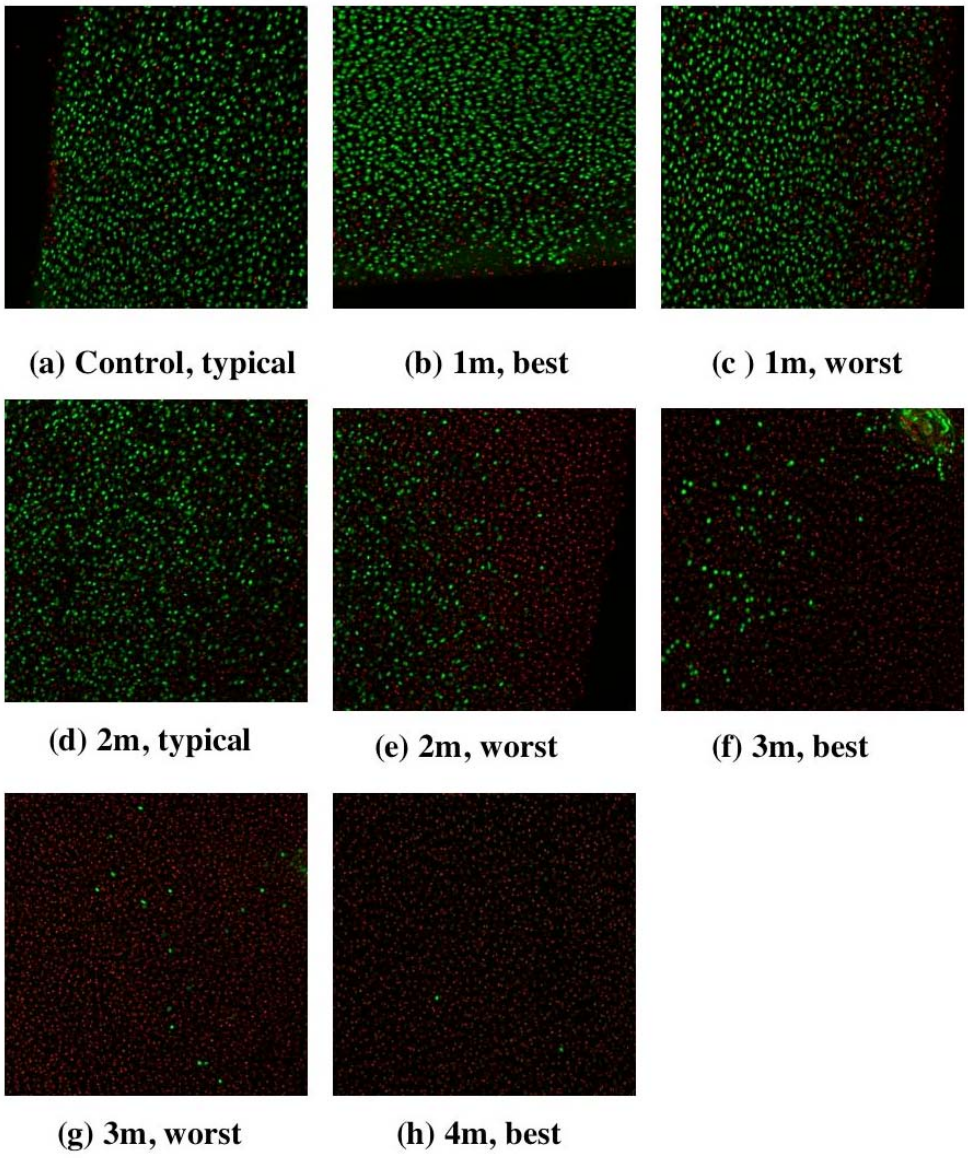

(a) Control, typical (b) 1m, best (c) 1m, worst

(d) 2m, typical (e) 2m, worst (f) 3m, best

(g) 3m, worst (h) 4m, best

Viability Results after Step-Wise Immersion in Ribose Solutions Immediately after Treatments

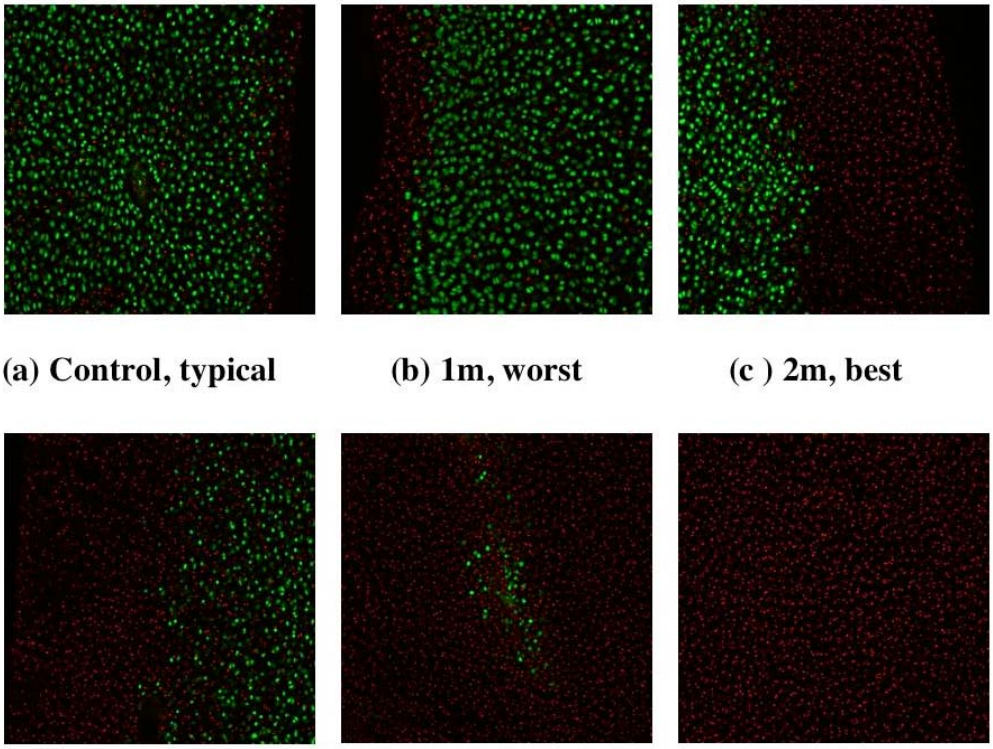

(a) Control, typical (b) 1m, worst (c) 2m, best

(d) 2m, worst (e) 3m, best (f) 4m, best

Viability Results after Step-Wise Immersion in Ribose Solutions and 48 hours of Culture

A.4 FTIR Peak Amide Band Ratios

	Peak Center (cm-1)			FTIR absorbance value: Collagen-II with T4MPyP-tt						
		control	control	irrad-10m	irrad-10m	irrad-10m	irrad-10m	irrad-10m	irrad-20m	irrad-20m
X	**1410**	9.04	9.24	3.65	6.36	5.94	4.88	5.94	2.05	2.01
Amide II	**1558**	10.06	11.1	7.71	10.7	10.8	6.41	9.74	10	8.69
Amide I	**1653**	3.22	3.71	6.29	7.34	8.09	4.23	7.24	9.24	7.87
	AII/AI	**3.124**	**2.992**	**1.226**	**1.458**	**1.335**	**1.515**	**1.345**	**1.082**	**1.104**
	X/AI	**2.807**	**2.491**	**0.580**	**0.866**	**0.734**	**1.154**	**0.820**	**0.222**	**0.255**
	X/AII	0.899	0.832	0.473	0.594	0.550	0.761	0.610	0.205	0.231
	X*AII/AI	28.243	27.645	4.474	9.271	7.930	7.395	7.991	2.219	2.219
	X*AI/AII	2.894	3.088	2.978	4.363	4.450	3.220	4.415	1.894	1.820
	AI*AII/X	3.583	4.457	13.287	12.349	14.709	5.556	11.872	45.073	34.025

	Peak Center (cm-1)			FTIR absorbance value: Collagen-II witlCASPc						
		control	control	irrad-10m	irrad-10m	irrad-10m	irrad-10m	irrad-10m	irrad-10m	irrad-10m
X	**1410**	4.38	6.46	7.11	6.31	4.37	5.94	4.99	5.89	2.7
Amide II	**1558**	5.66	8.25	9.58	9.27	6.17	8.74	6.71	7.55	3.74
Amide I	**1653**	2.88	3.9	7.66	7.54	6.39	6.07	5.32	4.96	3.48
	AII/AI	**1.965**	**2.115**	**1.251**	**1.229**	**0.966**	**1.440**	**1.261**	**1.522**	**1.075**
	X/AI	**1.521**	**1.656**	**0.928**	**0.837**	**0.684**	**0.979**	**0.938**	**1.188**	**0.776**
	X/AII	0.774	0.783	0.742	0.681	0.708	0.680	0.744	0.780	0.722
	X*AII/AI	8.608	13.665	8.892	7.758	4.220	8.553	6.294	8.966	2.902
	X*AI/AII	2.229	3.054	5.685	5.132	4.526	4.125	3.956	3.869	2.512
	AI*AII/X	3.722	4.981	10.321	11.077	9.022	8.931	7.154	6.358	4.820

A.5 Supported Single-Lap Test Experimental Data

Supported Single-Lap Tests at 25C

MAX(i)	MFC-NoEnz	CAC-NoEnz	FG-NoEnz	MFC-IRonly	MFC-PSamb	CAC-IRonly
1	0.46	0.00	0.00	0.04	0	0
2	0.34	0.00	0.00	0.05	0	0
3	0.28	0.00	0.00	0.00	0	0
4	0.46	0.00	0.00	0.00	0	0
5	0.30	0.00	0.00			
6	0.33	0.00	0.00			
7	0.28					
8	0.43					
MEAN (N)	0.36	0.00	0.00	0.02	0.00	0.00
Nominal Shear (kPa)	34.3	0.0	0.0	2.3	0.0	0.0
n	**8**	**6**	**6**	**4**	**4**	**4**
MEAN	**0.36**	**0.00**	**0.00**	**0.02**	**0.00**	**0.00**
STDEV	**0.08**	**0.00**	**0.00**	**0.03**	**0.00**	**0.00**
SEM	**0.03**	**0.00**	**0.00**	**0.01**	**0.00**	**0.00**

MAX(i)	CAC-CH15-RT	FG-Chybrid-RT	CAC-HY15-RT	CAC-COLT2-RT
1	0.36	0.59	0.00	0
2	0.40	0.30	0.00	0
3	0.33	0.38	0.00	0
4	0.23	0.32	0.00	0
5	0.16	0.32		
6	0.24	0.49		
7	0.37	0.27		
8	0.34	0.49		
MEAN (N)	0.30	0.39	0.00	0.00
Nominal Shear (kPa)	28.9	37.6	0.0	0.0
n	**8**	**8**	**4**	**4**
MEAN	**0.30**	**0.39**	**0.00**	**0.00**
STDEV	**0.08**	**0.12**	**0.00**	**0.00**
SEM	**0.03**	**0.04**	**0.00**	**0.00**

Supported Single-Lap Tests at 25C

MAX(I)	CAC-CH20-RT	FG-CH20-RT	MFC-CH20-RT	CAC-CH20-Psamb	CAC-CH20-NoPS/IR	MFC-CH20-Psamb	MFC-CH20-NoPS/IR
1	0.61	0.61	0.53	0	0	0.04	0
2	0.58	0.34	0.44	0	0	0.00	0
3	0.41	0.47	0.50	0	0	0.00	0
4	0.33	0.36	0.75	0	0	0.00	0
5	0.72	0.59	0.22				
6	0.58	0.57	0.23				
7	0.39	0.33	0.44				
8	0.47	0.61	0.35				
9	0.97		0.34				
MEAN (N)	0.56	0.48	0.42	0.00	0.00	0.01	0.00
Nominal Shear (kPa)	53.4	46.1	40.1	0.0	0.0	0.9	0.0
n	**9**	**8**	**9**	**4**	**4**	**4**	
MEAN	**0.56**	**0.48**	**0.42**	**0.00**	**0.00**	**0.01**	
STDEV	**0.20**	**0.12**	**0.17**	**0.00**	**0.00**	**0.02**	
SEM	**0.07**	**0.04**	**0.06**	**0.00**	**0.00**	**0.01**	

MAX(I)	CAC-CHHY-RT	FG-CHHY-RT	MFC-CHHY-RT	FG-CHHY-RT-PSamb	FG-CHHY-RT-NoPS/IR
1	0.81	0.18	0.39	0	0
2	0.79	0.44	0.40	0	0
3	0.68	0.52	0.17	0	0
4	0.93	0.37	0.46	0	0
5	0.40	0.30	0.35		
6	0.70	0.65	0.46		
7	0.76	0.31	0.18		
8	0.35	0.47	0.38		
9	0.50	0.49			
MEAN (N)	0.66	0.41	0.35	0.00	0.00
Nominal Shear (kPa)	62.6	39.5	33.1	0.0	0.0
n	**9**	**9**	**8**	**4**	**4**
MEAN	**0.66**	**0.41**	**0.35**	**0.00**	**0.00**
STDEV	**0.20**	**0.14**	**0.11**	**0.00**	**0.00**
SEM	**0.07**	**0.05**	**0.04**	**0.00**	**0.00**

Supported Single-Lap Tests at 37C					
MAX(i)	CAC-CH15-PT	CAC-CH15-PT-P1/3	CAC-Ch15-PT-PSamb	CAC-CH15-PT-NoPS/IR	CAC-CH15-PT-NoPS
1	0.34	0.64	0.00	0.00	0.00
2	0.47	0.59	0.00	0.00	0.00
3	0.71	0.42	0.00	0.00	0.00
4	0.39	0.35	0.00	0.00	0.00
5	0.42	0.49			
6	0.74	0.60			
7	0.49	0.29			
8	0.45	0.41			
9	0.33				
10	0.42				
11	0.35				
12	0.51				
13	0.65				
MEAN (N)	0.48	0.47	0.00	0.00	0.00
Nominal Shear (kPa)	45.9	45.1	0.0	0.0	0.0
n	**13**	**8**	**4**	**4**	**4**
MEAN	**0.48**	**0.47**	**0.00**	**0.00**	**0.00**
STDEV	**0.14**	**0.13**	**0.00**	**0.00**	**0.00**
SEM	**0.04**	**0.04**	**0.00**	**0.00**	**0.00**
MAX(i)	CAC-CH15-PT-PSq	CAC-CH15-PT-PSh		CAC-CH15-PT-PushOutRate	
1	0.33	0.33		2.04	
2	0.42	0.48		2.17	
3	0.42	0.31		1.44	
4	0.36	0.58		1.12	
5	0.49	0.41			
6	0.41	0.29			
7	0.28	0.58			
8	0.37	0.67			
MEAN (N)	0.38	0.46		1.70	
Nominal Shear (kPa)	36.6	43.5		161.5	
n	**8**	**8**		**4**	
MEAN	**0.38**	**0.46**		**1.70**	
STDEV	**0.06**	**0.14**		**0.50**	
SEM	**0.02**	**0.05**		**0.25**	

Supported Single-Lap Tests at 37C				
MAX(i)	CAC-CH15-PT-IR15	CAC-CH15-PT-IR5	CAC-CH15-PT-IR15P2/3	CAC-CH15-PT-IR10P1/2
1	0.40	0.16	0.38	0.07
2	0.64	0.33	0.23	0.06
3	0.30	0.46	0.35	0.00
4	0.57	0.42	0.27	0.00
5	0.48	0.39	0.16	
6	0.36	0.14	0.26	
7	0.37	0.12	0.13	
8	0.38	0.32	0.22	
MEAN (N)	0.44	0.29	0.25	0.03
Nominal Shear (kPa)	41.7	27.8	23.8	3.3
n	**8**	**8**	**8**	**4**
MEAN	**0.44**	**0.29**	**0.25**	**0.03**
STDEV	**0.12**	**0.13**	**0.09**	**0.04**
SEM	**0.04**	**0.05**	**0.03**	**0.02**
MAX(i)	CAC-CH15-PT-TRPSh	CAC-CH15-PT-Rib	CAC-CH15-PT-ZNPC	CAC-Debride-320G
1	1.27	0.39	0.20	0.07
2	1.43	0.51	0.29	0.00
3	0.78	0.32	0.23	0.00
4	0.96	0.32	0.42	0.00
5	0.77	0.35	0.33	
6	1.10	0.31	0.21	
7	0.67	0.42	0.35	
8	0.75	0.44	0.40	
MEAN (N)	0.97	0.38	0.30	0.02
Nominal Shear (kPa)	92.1	36.4	28.9	1.6
n	**8**	**8**	**8**	**4**
MEAN	**0.97**	**0.38**	**0.30**	**0.02**
STDEV	**0.28**	**0.07**	**0.09**	**0.03**
SEM	**0.10**	**0.03**	**0.03**	**0.02**

DERMABOND TESTS			
MAX(i)	DERM-NL-RSL	DERM-NL-R2	DERM-NL-R4
1	5.25	6.01	9.87
2	4.58	6.30	7.81
3	6.84	5.70	8.61
4	6.57	7.28	8.79
5	7.49		
6	4.29		
7	5.80		
8	5.62		
MEAN (N)	5.80	6.32	8.77
Nominal Shear (kPa)	644.8	702.6	974.5
n	**8**	**4**	**4**
MEAN	**5.80**	**6.32**	**8.77**
STDEV	**1.11**	**0.68**	**0.85**
SEM	**0.39**	**0.34**	**0.42**

Non-Supported Single-Lap Tests at 37C				
MAX(i)	CAC-CH15-PT-NoLap	Preload (N)	CAC-CH15-PT-NoLap/Pre	Preload (N)
1	0.34	0.14	0.41	0.02
2	0.27	0.11	0.20	0.01
3	0.31	0.06	0.41	0.01
4	0.43	0.05	0.31	0.02
5	0.21	0.06	0.35	0.02
6	0.37	0.03	0.17	0.02
7	0.36	0.05	0.30	0.01
8	0.28	0.07	0.39	0.02
MEAN (N)	0.32	0.07	0.32	0.02
Nominal Shear (kPa)	30.6	6.9	30.1	1.5
n	**8**	**8**	**8**	**8**
MEAN	**0.32**	**0.07**	**0.32**	**0.02**
STDEV	**0.07**	**0.04**	**0.09**	**0.01**
SEM	**0.02**	**0.013**	**0.03**	**0.002**

A.6 Defect Culture Model Viability Result

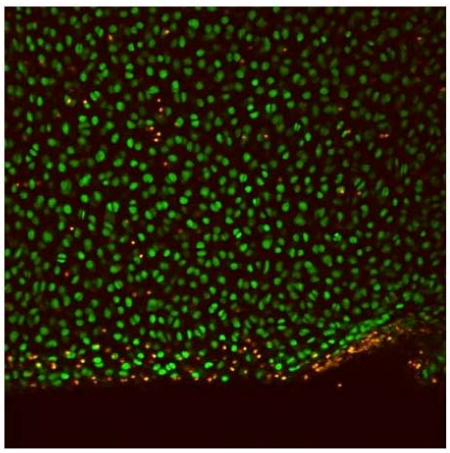

CTL: Plug, Day 3

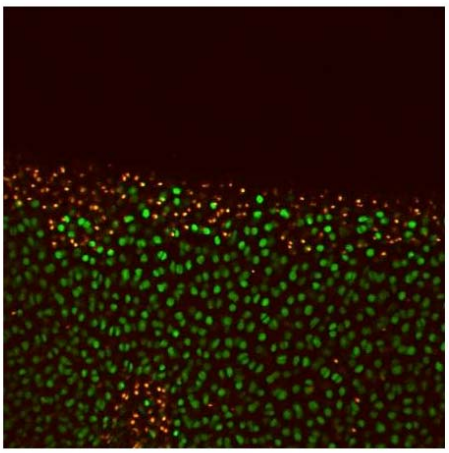

CTL: Plug, Day 3

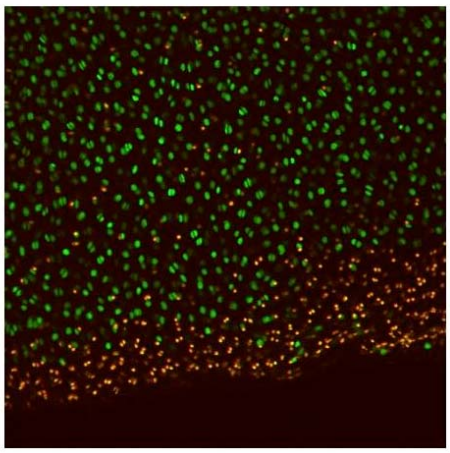

CTL: Annulus Inside, Day 3

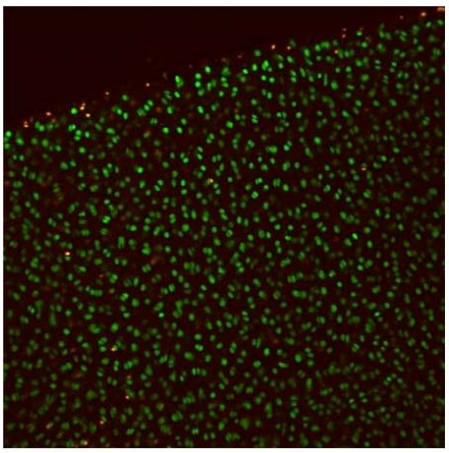

CTL: Annulus Outside, Day 3

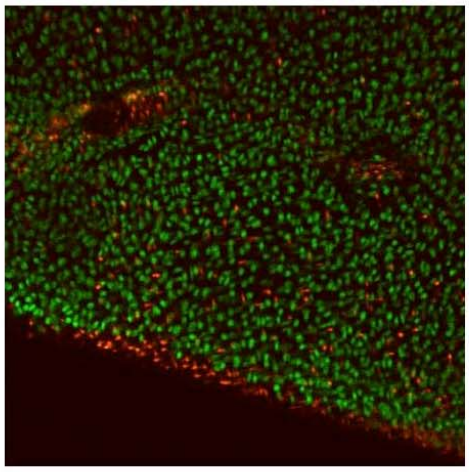

CTL: Plug, Day 7

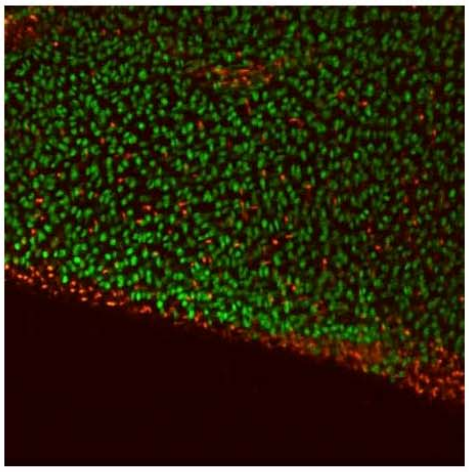

CTL: Plug, Day 7

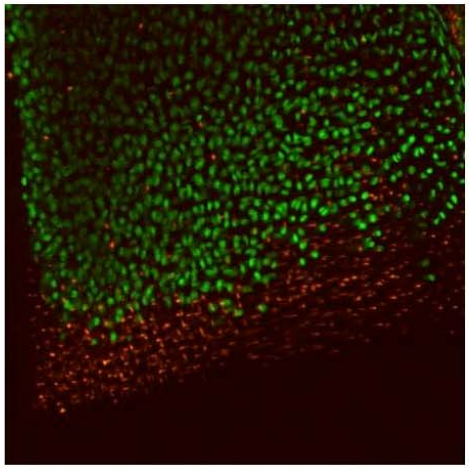

CTL: Annulus Inside, Day 7

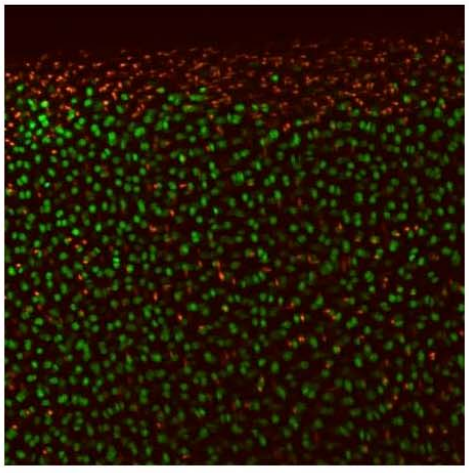

CTL: Annulus Inside, Day 7

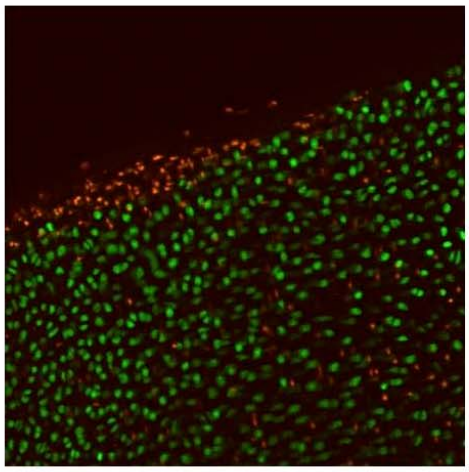

CTL: Annulus Outside, Day 7

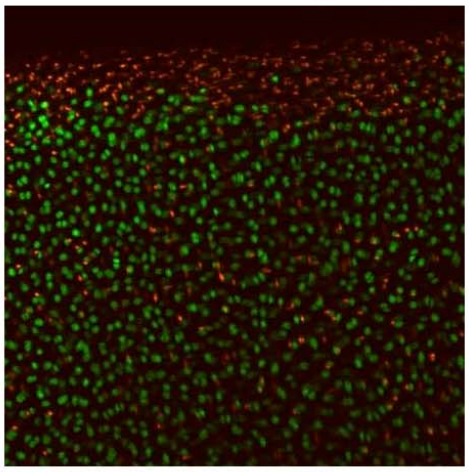

CTL: Annulus Outside, Day 7

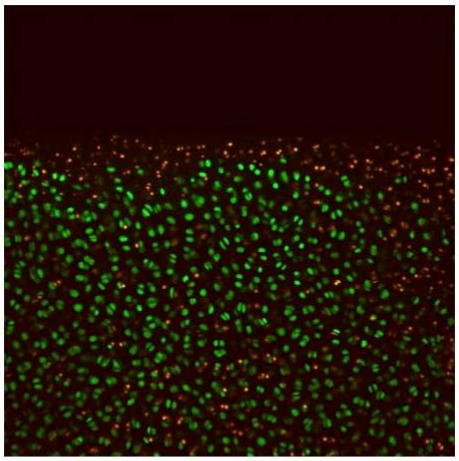

PS: Plug, Day 3

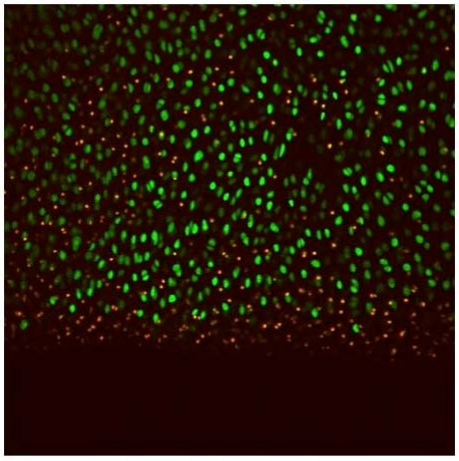

PS: Annulus Inside, Day 3

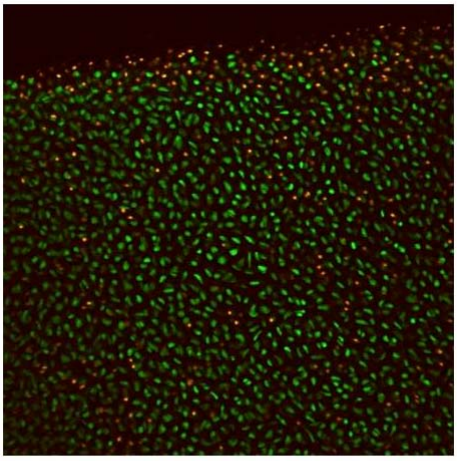

PS: Annulus Outside, Day 3

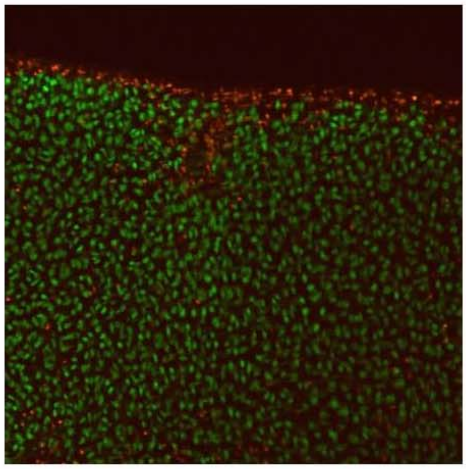

PS: Plug, Day 7

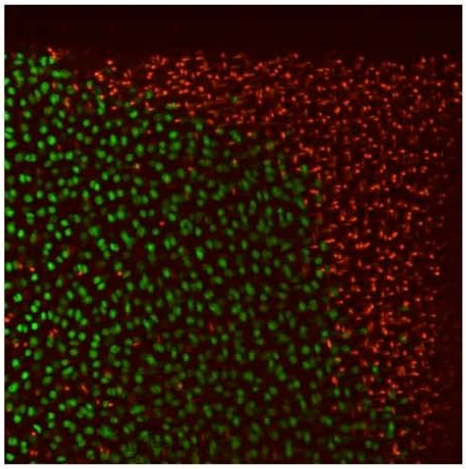

PS: Plug, Day 7

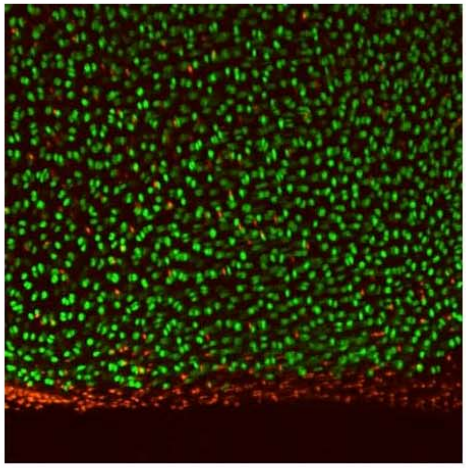

PS: Annulus Inside, Day 7

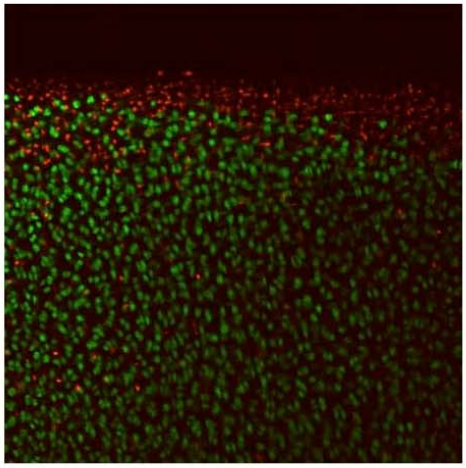

PS: Annulus Inside, Day 7

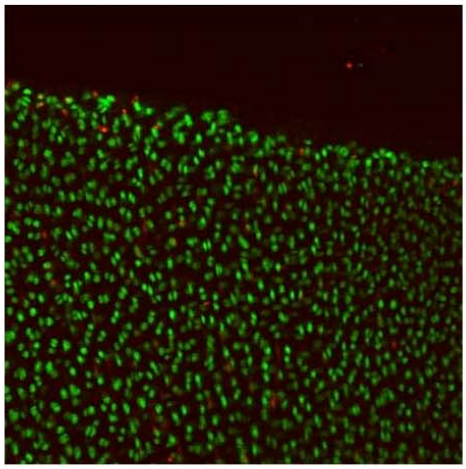

PS: Annulus Outside, Day 7

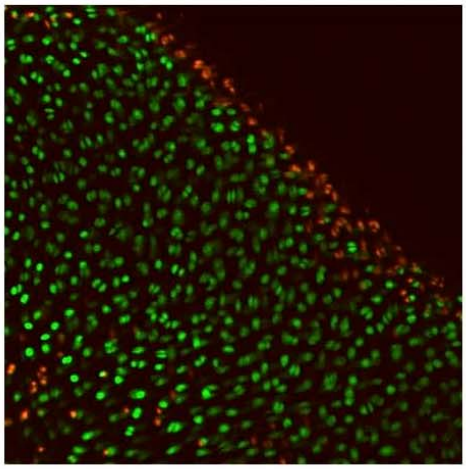

PS: Annulus Outside, Day 7

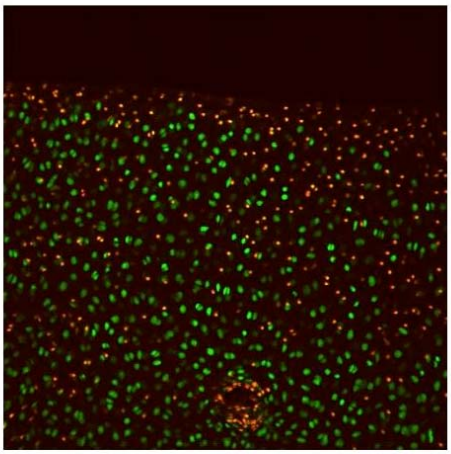

PSTR: Plug, Day 3

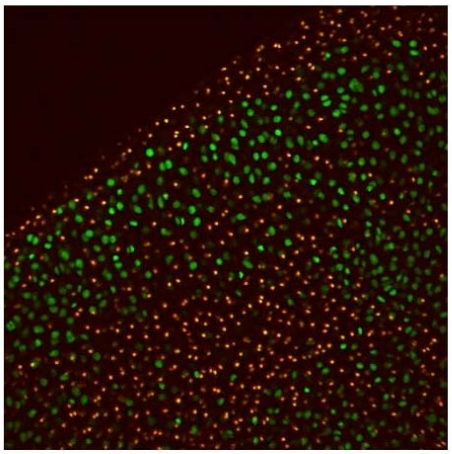

PSTR: Plug, Day 3

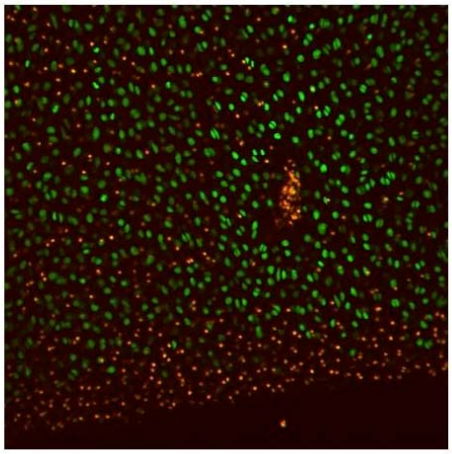

PSTR: Annulus Inside, Day 3

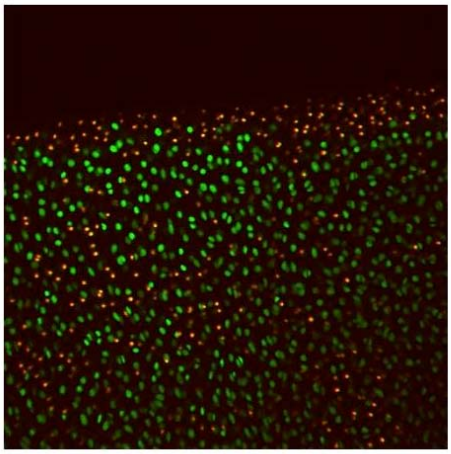

PSTR: Annulus Outside, Day 3

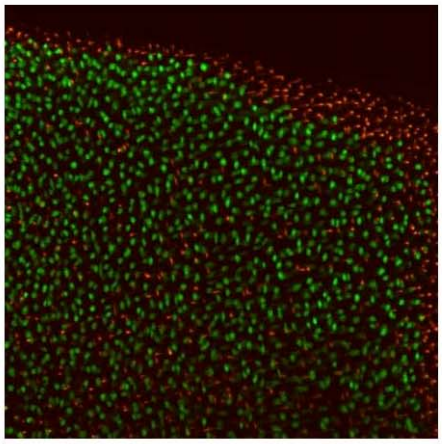

PSTR: Plug, Day 7

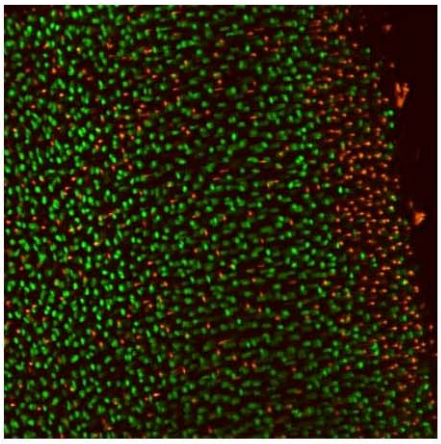

PSTR: Plug, Day 7

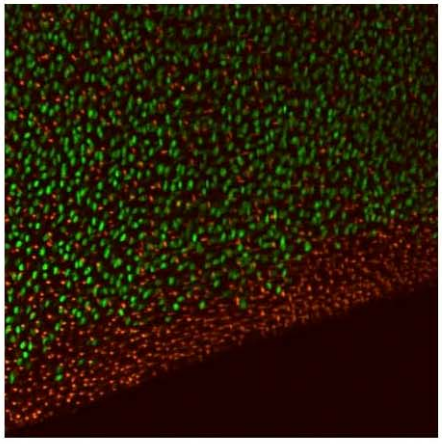

PSTR: Annulus Inside, Day 7

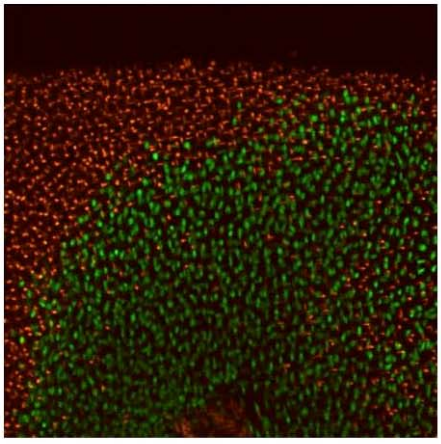

PSTR: Annulus Inside, Day 7

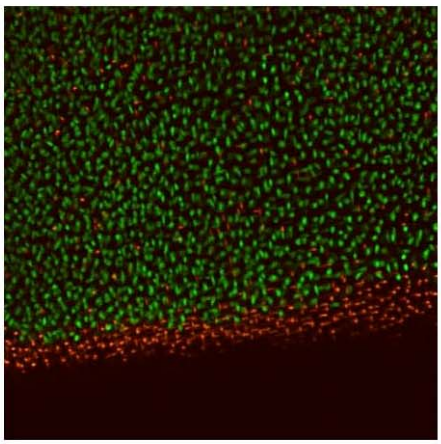

PSTR: Annulus Outside, Day 7

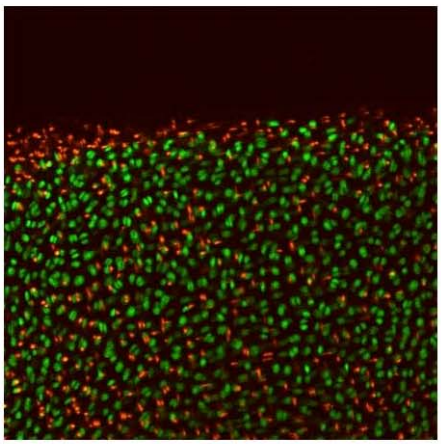

PSTR: Annulus Outside, Day 7

REFERENCES

1. National Arthritis Action Plan: Public Health Strategy (1999). Arthritis Foundation.

2. Sitterle, V. and D. Roberts (2003). Photoactivated Methods for Enabling Cartilage-to-Cartilage Tissue Fixation. Lasers in Surgery: Advanced Characterization, Therapeutics, and Systems XIII, San Jose, CA, SPIE **4949**: 162-172.

3. Voet, D., J. G. Voet and C. W. Pratt (1999). Fundamentals of Biochemistry. New York, John Wiley & Sons, Inc.

4. Eyre, D. (1987). "Collagen Crosslinking Amino Acids." Methods in Enzymology **144**: 115-139.

5. Gelse, G., E. Poschl and T. Aigner (2003). "Collagens - Structure, Functions, and Biosynthesis." Advanced Drug Delivery Reviews **55**: 1531-1546.

6. Smith-Mungo, L. I. and H. M. Kagan (1998). "Lysyl Oxidase: Properties, Regulation, and Multiple Functions in Biology." Matrix Biology **16**(7): 387-398.

7. Riesle, J., A. P. Hollander, R. Langer, L. E. Freed and G. Vunjak-Novakovic (1998). "Collagen in Tissue-Engineered Cartilage: Types, Structure, and Crosslinks." Journal of Cellular Biochemistry **71**: 313-327.

8. Aigner, T. and J. Stove (2003). "Collagens - Major Component of the Physiological Cartilage Matrix, Major Target of Cartilage Degneration, Major Tool in Cartilage Repair." Advanced Srug Delivery Reviews **55**: 1569-1593.

9. Jackson, D. W., M. J. Scheer and T. M. Simon (2001). "Cartilage Substitutes: Overview of Basic Science and Treatment Options." The Journal of the American Academy of Orthopaedic Surgeons **9**(1): 37-52.

10. LeBaron, R. G. and K. A. Athanasiou (2000). "Ex Vivo Synthesis of Articular Cartilage." Biomaterials **21**(24): 2575-2587.

11. Mow, V. C. and A. F. Mak (1987). Lubrication of Diarthrodial Joints. Handbook of Bioengineering. R. Salak and S. Chien, McGraw-Hill**:** 5.1-5.34.

12. Shrive, N. G. and C. B. Frank (1999). Biomaterials: Articular Cartilage. Biomechanics of the Musculo-Skeletal System. B. M. Nigg and W. Herzog, John Wiley & Sons**:** 79-105.

13. Mow, V. C. and A. Ratcliffe (1997). Structure and Function of Articular Cartialge and Meniscus. Basic Orthopedic Biomechanics. Van C Mow and W. C. Hayes. Philadelphia, Lippencott-Raven Publishers**:** 113-177.

14. Swiegert, M. A., A. C. Aufderheide and K. A. Athanasiou (2003). Fibrochondrocyes and Their Use in Tissue Engineering of the Meniscus. Topics in Tissue Engineering. N Ashammakhi and P. Ferretti.

15. Boyd, K. T. and P. T. Myers (2003). "Meniscus Preservation: Rationale, Repair Techniques, and Results." The Knee **10**(1): 1-11.

16. Bobic, V. (May 29, 1999). Treatment of Full-Thickness Injuries in Articular Cartilage. International Society of Arthroscopy, Knee Surgery, and Orthopaedic Sports Medicine, Medscape Report on ISAKOS Conference.

17. Bobic, V. (May 30, 1999). Articular Cartilage Transplantation. International Society of Arthroscopy, Knee Surgery, and Orthopaedic Sports Medicine, Medscape Report on ISAKOS Conference.

18. Genzyme Tissue Repair Licenses Technology from Sentron (April 18, 2000). Pharmalicensing**:** http://atlas.pharmalicensing.com (Bridgehead International).

19. "The Long and the Short of It." (April 23, 1999). Techvest **1 (5)**(5).

20. Behrens (November 2000). "Matrix-Induced Autologous Chondrocyte Implantation (M.A.C.I. ®) for Cartilage Repair." Knee Surgery, Sports Traumatology, Arthroscopy: 297.

21. Meisner, U., E. Ehlers, P. Muller, A. Idouraine, M. Russlies and P. Behrens (2001). Comparison of Three Different Fibrin Tissue Adhesives and Their Effect on Human Articular Chondrocytes. 47th Annual Meeting, Orthopaedic Research Society, February 25 - 28, San Francisco, California **26**: Paper 0618.

22. Marcacci, M., S. Zaffagnini, E. Kon, A. Visani, F. Iacono and I. Loreti (2002). "Arthroscopic Autologous Chondrocyte Transplantation: Technical Note." Knee Surgery, Sports Traumatology, Arthroscopy **10**(3): 154-159.

23. Orr, T. E., A. M. Patel, B. Wong, G. P. Hatzigiannis, T. Minas and M. Spector (1999). "Attachment of Periosteal Grafts to Articular Cartilage with Fibrin Sealant." Journal of Biomedical Materials Research **44**(3): 308-313.

24. Jurgensen, K., D. Aeschlimann, V. Cavin, M. Genge and E. B. Hunziker (1997). "A New Biological Glue for Cartilage-Cartilage Interfaces: Tissue Transglutaminase." The Journal of Bone and Joint Surgery. American Volume **79**(2): 185-193.

25. Brittberg, M., E. Sjogren-Jansson, A. Lindahl and L. Peterson (1997). "Influence of Fibrin Sealant (Tisseel(R)) on Osteochondral Defect Repair in the Rabbit Knee." Biomaterials **18**(3): 235-242.

26. Chivers, R. A. and R. G. Wolowacz (1997). "The Strength of Adhesive-Bonded Tissue Joints." International Journal of Adhesion and Adhesives **17**(2): 127-132.

27. Silverman, R. P., L. Bonasser, D. Passaretti, M. A. Randolph and M. J. Yaremchuk (2000). "Adhesion of Tissue-Engineered Cartilage to Native Cartilage." Plastic and Reconstructive Surgery **105**(4): 1393-1398.

28. DiMicco, M. A. and R. L. Sah (2001). "Integrative Cartilage Repair: Adhesive Strength Is Correlated with Collagen Deposition." Journal of Orthopaedic Research **19**(6): 1105-1112.

29. Ahsan, T. and R. L. Sah (1999). "Biomechanics of Integrative Cartilage Repair." Osteoarthritis and Cartilage **7**(1): 29-40.

30. Reindel, E. S., A. M. Ayroso, A. C. Chen, D. M. Chun, R. M. Schinagl and R. L. Sah (1995). "Integrative Repair of Articular Cartilage in Vitro: Adhesive Strength of the Interface Region." Journal of Orthopaedic Research **13**(5): 751-760.

31. Giuera, A., M. A. DiMicco, W. H. Akeson and R. L. Sah (2002). "Development Associated Differences in Integrative Cartilage Repair: Roles of Biosynthesis and Matrix." Journal of Orthopaedic Research **20**: 1274-1281.

32. Obradovic, B., I. Martin, R. F. Padera, S. Treppo, L. E. Freed and G. Vunjak-Novakovic (2001). "Integration of Engineered Cartilage." Journal of Orthopaedic Research **19**(6): 1089-1097.

33. Kafkalidis, M. S. and M. D. Thouless (2002). "The Effects of Geometry and Material Properties on the Fracture of Single Lap-Shear Joints." International Journal of Solids and Structures **39**(17): 4367-4383.

34. Yannas, I. V. (1996). Classes of Materials Used in Medicine: Natural Materials. Biomaterials Science. B. D. Ratner, A. S. Hoffman, F. J. Schoen and J. E. Lemons. San Diego, Academic Press**:** 84-94.

35. Weadock, K. S., E. J. Miller, l. D. Bellincampi, J. P. Zawadsky and M. G. Dunn (1995). "Physical Crosslinking of Collagen Fibers; Comparison of Ultraviolet

Irradiation and Dehydrothermal Treatment." Journal of Biomedical Materials Research **29**(11): 1373-1379.

36. Lee, C. R., A. J. Grodzinsky and M. Spector (2001). "The Effects of Cross-Linking of Collagen-Glycosaminoglycan Scaffolds on Compressive Stiffness, Chondrocyte-Mediated Contraction, Proliferation and Biosynthesis." Biomaterials **22**(23): 3145-3154.

37. Sionkowska, A. and T. Wess (2004). "Mechanical Properties of UV Irradiated Rat Tail Tendon Collagen." International Journal of Biological Macromolecules **34**(1-2): 9-12.

38. Sionkowska, A. (2000). "Modification of Collagen Films by Ultraviolet Irradiation." Polymer Degradation and Stability **68**(2): 147-151.

39. Bailey, A. J. (2001). "Molecular Mechanisms of Ageing in Connective Tissues." Mechanisms of Ageing and Development **122**(7): 735-755.

40. Mentink, C., M. Hendriks, A. Levels and B. Wolffenbuttel (2002). "Glucose-Mediated Crosslinking of Collagen in Rat Tendon and Skin." Clinica Chimica Acta **321**: 69-76.

41. Brownlee, M. (2001). "Biochemistry and Molecular Cell Biology of Diabetic Complications." Nature **414**: 813-820.

42. DeGroot, J., N. Verzijl, K. M. G. Jacobs, M. Budde, R. A. Bank, J. W. J. Bijlsma, T. J. M and F. P. J. G. Lafeber (2001). "Accumulation of Advanced Glycation Endproducts Reduces Chondrocyte-Mediated Extracellular Matrix Turnover in Human Articular Cartialge." Osteoarthritis and Cartilage **9**: 720-726.

43. Litchfield, J., S. Thorpe and J. Baynes (1999). "Oxygen Is Not Required for the Browning and Crosslinking of Protein by Pentoses: Relevance to Maillard Reactions in Vivo." The International Journal of Biochemistry & Cell Biology **31**: 1297-1305.

44. Sajithlal, G., P. Chithra and G. Chandrakasan (1998). "Advanced Glycation End Products Induce Crosslinking of Collagen in Vitro." Biochimica et Biophysica Acta **1407**: 215-224.

45. Hermanson, G. T. (1996). Bioconjugate Techniques. San Diego, Academic Press for Elsevier Science**:** 3-286.

46. Sung, H.-W., W.-H. Chang, C.-Y. Ma and M.-H. Lee (2003). "Crosslinking of Biological Tissues Using Genipin and/or Carbodiimide." Journal of Biomedical Materials Research **64A**(3): 427-438.

47. Schmidt, C. E. and J. M. Baier (2000). "Acellular Vascular Tissues: Natural Biomaterials for Tissue Repair and Tissue Engineering." Biomaterials **21**: 2215-2231.

48. Charulatha, V. and A. Rajaram (2003). "Influence of Different Crosslinking Treatments on the Physical Properties of Collagen Membranes." Biomaterials **24**(5): 759-767.

49. Sung, H.-W., C.-N. Chen, R.-N. Huang, J.-C. Hsu and W.-H. Chang (2000). "In Vitro Surface Characterization of a Biological Patch Fixed with a Naturally Occurring Crosslinking Agent." Biomaterials **21**: 1353-1362.

50. Calero, P., E. Jorge-Herrero, J. Turnay, N. Olmo, I. Lopez de Silanes, M. A. Lizarbe, M. MArtin Maestro, B. Arenaz and J. L. Castillo-Olivares (2002). "Gelatinases in Soft Tissue Biomaterials. Analysis of Different Crosslinking Agents." Biomaterials **23**: 3473-3478.

51. Osborne, C. S., W. H. Reid and M. H. Grant (1999). "Investigation into the Biological Stability of Collagen/Chondroitin-6-Sulfate Gels and Their Contraction by Fibroblasts and Keratinocytes: The Effect of Crosslinking Agents and Diamines." Biomaterials **20**: 283-290.

52. Pieper, J. S., T. Hafmans, J. H. Veerkamp and T. H. van Kuppevelt (2000). "Development of Tailor-Made Collagen-Glycosaminoglycan Matrices: EDC/NHS Crosslinking, and Ultrastructural Aspects." Biomaterials **21**: 581-593.

53. Pieper, J. S., P. M. van der Kraan, T. Hafmans, J. Kamp, P. Buma, J. L. C. van Susante, W. B. van der Berg, J. H. Veerkamp and T. H. van Kuppevelt (2002). "Crosslinked Type-II Collagen Matrices: Preparation, Characterization, and Potential for Cartilage Tissue Engineering." Biomaterials **23**: 3183-3192.

54. van Susante, J. L. C., J. S. Pieper, P. Buma, T. H. van Kuppevelt, H. van Beuningen, P. M. van der Kraan, J. H. Veerkamp, W. B. van der Berg and R. P. H. Veth (2002). "Linkage of Chondroitin-Sulfate to Type I Collagen Scaffolds Stimulates the Bioactivity of Seeded Chondrocytes in Vitro." Biomaterials **22**: 2359-2369.

55. Chang, C. H., H. C. Liu, C. C. Lin and C. H. Chou (2003). "Gelatin-Chondroitin-Hyaluron Tri-Copolymer Scaffold for Cartilage Tissue Engineering." Biomaterials **24**: 4853-4858.

56. Rabek, J. F. (1987). Mechanisms of Photophysical Processess and Photochemical Reactions in Polymers : Theory and Applications. New York, Wiley**:** 1-69.

57. Fisher, J. P., D. Dean, P. S. Engel and A. G. Mikos (2001). "Photoinitiated Polymerization of Biomaterials." Annual Review of Materials Research **37**: 171-181.

58. Small, W., 4th, N. J. Heredia, D. J. Maitland, L. B. Da Silva and D. L. Matthews (1997). "Dye-Enhanced Protein Solders and Patches in Laser-Assisted Tissue Welding." Journal of Clinical Laser Medicine & Surgery **15**(5): 205-208.

59. McNally, K. M., B. S. Sorg, N. C. Bhavaraju, M. G. Ducros, A. J. Welch and J. M. Dawes (1999). "Optical and Thermal Characterization of Albumin Protein Solders." Applied Optics **38**(31): 6661-6672.

60. Grasso, M. and R. Caruso (2002 (January 4)). "Lasers in Urology." eMedicine Journal **3**(1).

61. Cooper, C. S., I. P. Schwartz, D. Suh and A. J. Kirsch (2001). "Optimal Solder and Power Density for Diode Laser Tissue Soldering." Lasers in Surgery and Medicine **29**(1): 53-61.

62. Birch, J. F., D. J. Mandley, S. L. Williams, D. R. Worrall, P. J. Trotter, F. Wilkinson and P. R. Bell (2000). "Methylene Blue Based Protein Solder for Vascular Anastomoses: An in Vitro Burst Pressure Study." Lasers in Surgery and Medicine **26**(3): 323-329.

63. Mandley, D. J., J. F. Birch, S. L. Williams, P. J. Trotter, F. Wilkinson and G. A. Davies (2000). "Photon Activated Biological Adhesives in Surgery." International Journal of Adhesion and Adhesives **20**(2): 97-102.

64. Sorg, B. S. and A. J. Welch (2001). "Laser-Tissue Soldering with Biodegradable Polymer Films in Vitro: Film Surface Morphology and Hydration Effects." Lasers in Surgery and Medicine **28**(4): 297-306.

65. Bleustein, C. B., C. N. Walker, D. Felsen and D. P. Poppas (2000). "Semi-Solid Albumin Solder Improved Mechanical Properties for Laser Tissue Welding." Lasers in Surgery and Medicine **27**(2): 140-146.

66. Stewart, R. B., C. B. Bleustein, P. B. Petratos, K. C. Chin, D. P. Poppas and R. T. Kung (2001). "Concentrated Autologous Plasma Protein: A Biochemically Neutral Solder for Tissue Welding." Lasers in Surgery and Medicine **29**(4): 336-342.

67. Ebert, D., C. Roberts, S. Farrar, W. Johnston, A. Litsky and A. Bertone (1998). "Articular Cartilage Optical Properties in the Spectral Range 300-850nm." Journal of Biomedical Optics **3**(3): 326-333.

68. Youn, J.-I., A. Telenkov, E. Kim, N. Bhavaraju, B. Wong, J. Valvano and T. Milner (2000). "Optical and Thermal Properties of Nasal Septal Cartilage." Lasers in Surgery and Medicine **27**: 119-128.

69. Shangguan, H., S. A. Prahl, S. L. Jaques, L. W. Casperson and K. W. Gregory (1998). Pressue Effects on Soft Tissues Monitored by Changes in Tissue Optical Properties. Laser Tissue Interaction IX, Proc. SPIE 3254 **3524**: 366-371.

70. Chan, E. K., Q. Lu, B. Bell, M. Motamedi, C. Frederickson, D. T. Brown, I. S. Kovach and A. J. Welch (1998). "Laser Assisted Soldering: Microdroplet Accumulation with a Microjet Device." Lasers in Surgery and Medicine **23**(4): 213-220.

71. Lauto, A., R. Stewart, M. Ohebshalom, N. D. Nikkoi, D. Felsen and D. P. Poppas (2001). "Impact of Solubility on Laser Tissue-Welding with Albumin Solid Solders." Lasers in Surgery and Medicine **28**(1): 44-49.

72. Zuger, B. J., B. Ott, P. Mainil-Varlet, T. Schaffner, J. F. Clemence, H. P. Weber and M. Frenz (2001). "Laser Solder Welding of Articular Cartilage: Tensile Strength and Chondrocyte Viability." Lasers in Surgery and Medicine **28**(5): 427-434.

73. Kovach, I., E. K. Chan, M. Frenz, A. Welch and K. Athanasiou (1997). Laser Tissue Welding of Articular Cartilage Using a Protein-Based Solder. Proceedings of the 43rd Annual Meeting of the Orthopaedic Research Society, San Francisco, CA **22**: 343.

74. Chivers, R. A. (2000). "In Vitor Tissue Welding Using Albumin Solder: Bond Strengths and Bonding Temperatures." International journal of Adhesion & Adhesives **20**: 179-187.

75. Chan, E. K., D. T. Brown, I. S. Kovach and A. J. Welch (1998). "Laser Assisted Soldering: Effects of Hydration on Solder-Tissue Adhesion." Journal of Biomedical Optics **3**(4): 456-461.

76. Rivlin, R. (1975). Riboflavin. New York, Plenum Press.

77. Spoerl, E., M. Huhle and T. Seiler (1998). "Induction of Crosslinks in Corneal Tissue." Experimental Eye Research **66**: 97-103.

78. Spoerl, E. and T. Seiler (1999). "Techniques for Stiffening the Cornea." Journal of Refractive Surgery **15**: 711-713.

79. Merguerian, P. A., J. L. Pugach and L. Lilge (1999). Non-Thermal Ureteral Tissue Bonding: Comparison of Photochemcial Collagen Crosslinking with Thermal Laser Bonding. SPIE Proceedings: Lasers in Surgery: Advanced

Characterization, Theraputics, and Systems IX, San Jose, CA, SPIE **3590**: 194-202.

80. Khadem, J., T. Truong and J. T. Ernest (1994). "Photodynamic Biologic Tissue Glue." Cornea **13**(5): 406-410.

81. Mulroy, L., J. Kim, I. Wu, P. Scharper, S. Melki, D. Azar, R. Redmond and I. Kochevar (2000). "Photochemical Keratodesmos for Repair of Lamellar Corneal Incisions." Investigative Ophthalmology and Visual Science **41**(11): 3335-3340.

82. Chan, B. P., I. E. Kochevar and R. W. Redmond (2002). "Enhancement of Porcine Skin Graft Adherence Using a Light-Activated Process." Journal of Surgical Research **108**: 77-84.

83. Judy, M. M., H. Nosir, R. W. Jackson, J. L. Mathews, D. E. Lewis, R. E. Utecht and D. Yuan (1996). Bonding of Human Meniscal and Articular Cartilage with Photoactive 1-8 Naphthalimide Dyes. Proceedings of lasers in surgery : advanced characterization, therapeutics, and systems VI, SPIE **2671**: 251-255.

84. Judy, M. M., H. Nosir, R. W. Jackson, J. L. Mathews, D. E. Lewis, R. E. Utecht and D. Yuan (1996). Repair of Articular Cartilage and Meniscal Tears by Photoactive Dyes: In Vivo Study. Proceedings of laser applications in medicine and dentistry, Vienna, Austria, SPIE **2922**: 436-440.

85. Judy, M. M., H. Nosir, R. W. Jackson, J. L. Mathews, D. E. Lewis, R. E. Utecht and D. Yuan (1997). Healing Results in Meniscus and Articular Cartilage Photochemically Welded with 1,8-Naphthalimide Dyes. Proceedings of lasers in surgery : advanced characterization, therapeutics, and systems VII, San Jose, CA, SPIE **2970**: 257-260.

86. Hunziker, E. B. (2002). "Articular Cartilage Repair: Basic Science and Clinical Progress. A Review of the Current Status and Prospects." Osteoarthritis and Cartilage **10**(6): 432-463.

87. Prahl, S. A., T. Denison and E. LaJoie (2001). Laser Repair of Liver. Lasers in Surgery: Advanced Characterization, Therapeutics, and Systems, SPIE **4244**: 215-219.

88. Nehrer, S., H. A. Breinan, A. Ramappa, H.-P. Hsu, T. Minas, S. Shortkroff, C. B. Sledge, I. V. Yannas and M. Spector (1998). "Chondrocyte-Seeded Collagen Matrices Implanted in a Chondral Defect in a Canine Model." Biomaterials **19**(24): 2313-2328.

89. Farndale, R. W., D. J. Buttle and B. A. J (1986). "Improved Quantitationand Discrimination of Sulfated Glycosaminoglycans by Use of Dimethylmethylene Blue." Biochimica et Biophysica Acta **883**(2): 173-177.

90. Woessner, J. F. J. (1961). "The Determination of Hydroxyproline in Tissue and Protein Samples Containing Small Proportions of This Imino Acid." Archives of Biochemistry and Biophysics **93**: 440-447.

91. Reddy, G. K. and C. Enwemeka (1996). "A Simplified Method for the Analysis of Hydroxyproline in Biological Tissue." Clinical Biochemistry **29**(3): 225-229.

92. Welch, A. J., M. J. C. van Gemert, W. M. Star and B. C. Wilson (1995). Definitions and Overview of Tissue Optics. Optical-Thermal Response of Irradiated Tissue. A. J. Welch and M. J. C. van Gemert. New York, Plenum Press**:** 15-46.

93. Welch, A. J. and M. J. C. Van Gemert, Eds. (1995). Optical and Thermal Response of Laser-Irradiated Tissue. Lasers, Photonics, and Electro-Optics. New York, Plenum Press.

94. Cheong, W., S. Prahl and A. Welch (1999). A Review of the Optical Properties of Biological Tissues. Selected Papers on Tissue Optics: Applications in Medical Diagnostics and Therapy. V. Tuchin. Bellingham, WA, SPIE. **MS102:** 129-148.

95. Welch, A. J. and M. J. C. van Gemert (1995). Introduction to Medical Applications. Optical-Thermal Response of Irradiated Tissue. A. J. Welch and M. J. C. van Gemert. New York, Plenum Press**:** 609-618.

96. Madsen, S. J., E. A. Chu and B. J. Wong (2000). Optical Property Measurements in Mammalian Cartilage. Laser-Tissue Interaction XI: Photochemical, Photothermal, and Photomechanical, San Jose, CA, SPIE **3914**: 305-311.

97. Beek, J. F., P. Blokland, P. Posthumus, M. Aalders, J. W. Pickering, H. J. C. M. Sterenborg and M. J. C. van Gemert (1997). "In Vitro Double-Integrating Sphere Optical Properties of Tissues between 630 and 1064 Nm." Physics in Medicine and Biology **42**: 2255-2261.

98. Tuchin, V. V. (2000). Tissue Optics: Light Scattering Methods and Instruments for Medical Diagnostics. Bellingham, WA, SPIE Press.

99. Descalle, M.-A., S. L. Jacques, S. A. Prahl, L. T. J and W. R. Martin (1998). "Measurements of Cartilage and Ligament Optical Properties at 315nm, 365nm, and in the Visible Range (400-800nm)." Proceedings of SPIE **3195**: 280-286.

100. Hecht, E. (1998). Optics. Reading, MA, Addison-Wesley.

101. Tuchin, V. V. (1999). Controlling of Tissue Optical Properties. Saratov Fall Meeting 1999: Optical Technologies in Biophysics and Medicine, Saratov, Russia, SPIE **4001**: 30-53.

102. Maier, J. S., S. A. Walker, S. Fantini, M. A. Franceschini and E. Gratton (1995). "Possible Correlation between Blood Glucose Concentration and Reduced Scattering Coefficient of Tissues in the near-Infrared." Optics Letters **19**(24): 2062-2064.

103. Bashkatov, A. N., E. A. Genina, Y. P. Sinichin, N. A. Lakodina, V. I. Kochubey and V. V. Tuchin (1999). Estimation of Glucose Diffusion Coefficient in Scleral Tissue. Saratov Fall Meeting 1999: Optical Technologies in Biophysics and Medicine, Saratov, Russia, SPIE **4001**: 345-355.

104. Bruulsema, J. T., J. Hayward, T. Farrell, M. Patterson, L. Heinemann, M. Berger, T. Koschinsky, J. Sandahl-Christiansen, H. Orskov, M. Essenpreis, G. Schmelzeisen-Redeker and D. Böcker (1997). "Correlation between Blood Glucose Concentration in Diabetics and Noninvasively Measured Tissue Optical Scattering Coefficient." Optics Letters **22**(3): 190-192.

105. Vargas, G., K. F. Chan, S. L. Thomsen and A. J. Welch (2001). "Use of Osmotically Active Agents to Alter Optical Properties of Tissue: Effects on the Detected Fluorescence Signal Measured through Skin." Lasers in Surgery and Medicine **29**(3): 213-220.

106. Genina, E. A., A. N. Bashkatov, N. A. Lakodina, S. A. Murikhina, Y. P. Sinichin and V. V. Tuchin (1999). Diffusion of Glucose Solution through Fibrous Tissues: In Vitro Optical and Weight Measurements. Saratov Fall Meeting 1999: Optical Technologies in Biophysics and Medicine, Saratov, Russia, SPIE **4001**: 255-261.

107. Berg, J. M., J. L. Tymoczko and L. Stryer (2002). Biochemistry. New York, W H Freeman and Company.

108. Karlsson, J. O. M. and M. Toner (1996). "Long-Term Storage of Tissues by Cryopreservation: Critical Issues." Biomaterials **17**(3): 243-256.

109. Koshimoto, C. and P. Mazur (2002). "The Effect of the Osmolality of Sugar-Containing Media, the Type of Sugar, and the Mass and Molar Concentration of Sugar on the Survival of Frozen-Thawed Mouse Sperm." Cryobiology **45**: 80-90.

110. Tomford, W. W., G. R. Fredericks and H. J. Mankin (1984). "Studies on Cryopreservation of Articular Cartilage." The Journal of Bone and Joint Surgery. American Volume **66**(2): 253-259.

111. Kawabe, N. and M. Yoshinao (1990). "Cryopreservtion of Cartilage." International Orthopaedics **14**(3): 231-235.

112. Erickson, G., L. Alexopoulos and F. Guliak (2001). "Hyper-Osmotoc Stress Induces Volume Change and Calcium Transients in Chondrocytes by

Transmembrane, Phospholipid, and G-Protein Pathways." Journal of Biomechanics **34**: 1527-1535.

113. Xu, X., R. Wang and J. B. Elder (2003). "Optical Clearing Effect on Gastric Tissues Immersed with Biocompatible Chemical Agents Investigated by near Infrared Reflectance Spectroscopy." Journal of Physics D: Applied Physics **36**: 1707-1713.

114. Vargas, G., E. K. Chan, J. K. Barton, H. G. Rylander, 3rd and A. J. Welch (1999). "Use of an Agent to Reduce Scattering in Skin." Lasers in Surgery and Medicine **24**(2): 133-141.

115. Davies, M. J. (2003). "Singlet Oxygen Mediated Damge to Proteins and Its Consequences." Biochemical and Biophysical Research Communications **305**: 761-770.

116. Spikes, J. D. (1988). Photochemotherapy: Molecular and Cellular Processes Involved. Selected Papers on Photodynamic Therapy. D. Kessel, (reprinted from Proceedings of SPIE Vol. 997, Advances in Photochemotherapy) SPIE**:** 412-420.

117. Davies, M. J. and R. Truscott (2001). "Photo-Oxidation and Its Role in Cataractogenesis." Journal of Photochemistry and Photobiology B: Biology **63**: 114-125.

118. Kohen, E., R. Santus and J. Hirschberg (1995). Photobiology. San Diego, Academic Press.

119. Bonnett, R. (2000). Chemical Aspects of Photodynamic Therapy. Amsterdam, The Netherlands, Gordon and Breach Science Publishers.

120. Michaeli, A. and J. Feitelson (1994). "Reactivity of Singlet Oxygen toward Amino Acids and Peptides." Photochemistry and Photobiology **59**(3): 284-289.

121. Dubbelman, T., A. De Goeij and J. Van Steveninck (1978). "Photodynamic Effects of Protoporphyrin on Human Erythrocytes: Nature of the Crosslinking of Membrane Proteins." Biochimica et Biophysica Acta **511**: 141-151.

122. Michaeli, A. and J. Feitelson (1995). "Reactivity of Singlet Oxygen toward Large Peptides." Photochemistry and Photobiology **61**(3): 255-260.

123. Shen, H.-R., J. D. Spikes, C. J. Smith and J. Kopecek (2000). "Photodynamic Crosslinking of Proteins V.: Nature of the Tyrosine-Tyrosin Bonds Formed in the Fmn-Sensitized Intermolecular Crosslinking of N-Acetyl-L-Tyrosine." Journal of Photochemistry and Photobiology A: Chemistry **133**: 115-122.

124. Verweij, H., T. Dubbelman and J. Van Steveninck (1981). "Photodynamic Protein Crosslinking." Biochimica et Biophysica Acta **647**: 87-94.

125. Sionkowska, A. (2000). "The Influence of Methylene Blue on the Photochemical Stability of Collagen." Polymer Degradation and Stability **67**: 79-83.

126. Menter, J. M., A. M. Patta, R. M. Sayre, J. Dowdy and I. WIllis (2001). "Effect of UV Irradiation on Type I Collagen Fibril Formation in Neutral Collagen Solutions." Photodermatology, Photoimmunology, & Photomedicine **17**: 114-120.

127. Kakehashi, A., J. Akiba, N. Ueno and B. Chakrabarti (1993). "Evidence for Singlet Oxygen-Induced Cross-Links and Aggregation of Collagen." Biochemical and Biophysical Research Communications **196**(3): 1440-1446.

128. Fujimori, E. (1989). "Cross-Linking and Fluorescence Changes of Collagen by Glycation and Oxidation." Biochimica et Biophysica Acta **998**(2): 105-110.

129. Au, V. and S. A. Madison (2000). "Effects of Singlet Oxygen on the Extracellular Matrix Protein Collagen: Oxidation of the Collagen Crosslink Histidinohydroxylysinonorleucine and Histidine." Archives of Biochemistry and Biophysics **384**(1): 133-142.

130. Venkatasubramanian, K. and K. T. Joseph (1977). "Action of Singlet Oxygen on Collagen." Indian Journal of Biochemistry & Biophysics **14**(3): 217-220.

131. Musser, D. A., J. M. Wagner and M. Datta-Gupta (1982). "The Interaction of Tumor Localizing Porphyrins with Collagen and Elastin." Research Communications in Chemical Pathology and Pharmacology **36**(2): 251-259.

132. Kato, Y., K. Uchida and S. Kawakishi (1994). "Aggregation of Collagen Exposed to UVA in the Presence of Riboflavin: A Plausible Role for Tyrosine Modification." Photochemistry and Photobiology **59**(3): 343-349.

133. Yowa, D., V. Hovhannisyan and T. Theodossiou (2001). "Photochemical Effects and Hypericum Photosensitized Processes in Collagen." Journal of Biomedical Optics **6**(1): 52-57.

134. Milne, P. J. and R. G. Zika (1992). "Crosslinking of Collagen Gels: Photochemical Measurements." SPIE Proceedings: Ophthalmic Technologies **1644**: 115-124.

135. Pandey, R. K. (2003). Chapter 37: Synthetic Strategies in Designing Porphyrin-Based Photosensitizers for Photodynamic Therapy. Biomedical Photonics Handbook. T. Vo Donh. Boca Raton, CRC Press**:** 37.1-37.22.

136. Arrondo, J. L. R., A. Muga, J. Castresana and F. M. Goni (1993). "Quantitative Studies of the Structure of Proteins in Solution by Fourier-Transform Infrared Spectroscopy." Prog. Biophys. Molecular Biol. **59**: 23-56.

137. Chittur, K. K. (1999). "FTIR and Protein Structure at Interfaces." BMES Bulletin **23**(3): 3-6.

138. Camacho, N. P., P. West, P. A. Torzilli and R. Mendelsohn (2001). "FTIR Microscopic Imaging of Collagen and Proteoglycan in Bovine Cartilage." Biopolymers **62**(1): 1-8.

139. Kaminska, A. and A. Sionkowska (1996). "Effect of UV Radiation on the Infrared Spectra of Collagen." Polymer Degradation and Stability **51**(1): 19-26.

140. Chang, M. C. and J. Tanaka (2002). "FTIR Study for Hydroxyapatite/Collagen Nanocomposite Crosslinked by Glutaraldehyde." Biomaterials **23**: 4811-4818.

141. Camacho, N. P., P. West, P. Torzilli and R. Mendelsohn (2001). "FTIR Microscopic Imaging of Colalgen and Proteoglycan in Bovine Cartilage." Biopolymers **62**: 1-8.

142. Payne, K. J. and A. Veis (1988). "Fourier Transform IR Spectroscopy of Collagen and Gelatin Solutions: Deconvolution of the Amide I Band for Conformational Studies." Biopolymers **27**: 1749-1760.

143. Adams, R. D. (1984). Structural Adhesive Joints in Engineering. New York, Elsevier Applied Science.

144. DiMicco, M. A., S. N. Waters, W. H. Akeson and R. L. Sah (2002). "Integrative Articular Cartilage Repair: Dependence on Developmental Stage and Collagen Metabolism." Osteoarthritis and Cartilage **10**(3): 218-225.

145. Anderson, T. L. (1995). Fracture Mechanics: Fundamentals and Applications (Second Edition). Boca Raton, CRC Press.

146. Chivers, R. A. (2000). "In Vitro Tissue Welding Using Albumin Solder: Bond Strengths and Bonding Temperatures." International Journal of Adhesion and Adhesives **20**(3): 179-187.

147. Chandra, N. and H. Ghonem (2001). "Interfacial Mechanics of Push-out Tests: Theory and Experiments." Composites Part A: Applied Science and Manufacturing **32**: 574-584.

148. Hunter, C. J. (2001). Mechanical Stimulation of an in Vitro Cartilage Defect Repair Model. (PhD Thesis) School of Biomedical Engineering. Atlanta, Georgia Institute of Technology.

149. ASTM-D-3893-98 Standard Test Method for Measuring Strength and Shear Modulus of Nonrigid Adhesives by the Thick -Adherend Tenslie-Lap Specimen. Book of Standards, Volume 15.06, ASTM International.

150. Goland, M. and E. Reissner (1944). "The Stresses in Cemented Joints." Journal of Applied Mechanics **11**: A17-A27.

151. Oplinger, D. W. (1994). "Effects of Adherend Deflections in Single Lap Joints." International Journal of Solids and Structures **31**(18): 2565-2587.

152. Tsai, M. Y. and J. Morton (1994). "An Evaluation of Analytical and Numerical Solutions to the Single-Lap Joint." International Journal of Solids and Structures **31**(18): 2537-2563.

153. Tsai, M. Y., D. W. Oplinger and J. Morton (1998). "Improved Theoretical Solutions for Adhesive Lap Joints." International Journal of Solids and Structures **35**(12): 1163-1185.

154. ASTM-D-4896-01 (2003). Standard Guide for Use of Adhesive-Bonded Single Lap-Joint Specimen Test Results. Book of Standards, Volume 15.06, ASTM International.

155. Gorbatkina, Y. and V. Ivanova-Mumjieva (1997). "Adhesive Strength of Fiber/Polymer Joints Upon Loading in Liquids: Effect of Liquid Surface Tension." International Journal of Adhesion and Adhesives **17**(4): 329-332.

156. Bowditch, M. (1996). "The Durability of Adhesive Joints in the Presence of Water." International Journal of Adhesion and Adhesives **16**(2): 73-79.

157. Wu, G. and A. D. Crocombe (1996). "Simplified Finite Element Modelling of Structural Adhesive Joints." Composites & Structures **61**(2): 385-391.

158. Crocombe, A. D. (1989). "Global Yielding as a Failure Criterion for Bonded Joints." International Journal of Adhesion and Adhesives **9**(3): 145-153.

159. Williamson, A. K., A. C. Chen, K. Masuda, E. J.-M. A. Thonar and R. L. Sah (2003). "Tensile Mechanical Properties of Bovine Articular Cartilage: Variations with Growth and Relationships to Collagen Network Components." Journal of Orthopaedic Research **21**(5): 872-880.

160. Armstrong, C. G., W. M. Lai and V. C. Mow (1984). "An Analysis of Confined Compression of Articular Cartilage." Journal of Biomechanics, England **106**: 165-173.

161. Williamson, A. K., A. C. Chen and R. L. Sah (2001). "Compressive Properties and Function-Composition Relationships of Developing Bovine Articular Cartilage." Journal of Orthopaedic Research **19**(6): 1113-1121.

162. Mobley, J. and T. Vo-Dinh (2003). Chapter 2: Optical Properties of Tissue. Biomedical Photonics Handbook. T. Vo Donh. Boca Raton, CRC Press**:** 2.1-2.73.

163. Bos, P. K., J. DeGroot, M. Budde, J. Verhaar and G. van Osch (2002). "Specific Enzymatic Treatment of Bovine and Human Articular Cartilage." Arthritis and Rheumatism **46**(4): 976-985.

164. Quinn, T. M. and E. B. Hunziker (2002). "Controlled Enzymatic Matrix Degradation for Integrative Cartilag Repair; Effects on Viable Cell Density and Proteoglycan Deposition." Tissue Engineering **8**(5): 799-806.

165. Hunziker, E. B. and E. Kapfinger (1998). "Removal of Proteoglycans from Surface Defects in Articular Cartilage Transiently Enhances Coverage by Repair Cells." The Journal of Bone and Joint Surgery. British Volume **80-B**(144-150).

166. Li, K. W., T. Ahsan and R. L. Sah (1996). Effect of Trypsin Treatment in Integrative Cartilage Repair in Vitro. Proceedings of the 42nd Annual Meeting of the Orthopaedic Reserch Society, Atlanta, GA **21**: 101.

167. Chen, J., S. Maniwa and M. Ochi (2000). "Influence of Trypsin on the Biological Bonding of Cartilaginous Surface to Bone in Rabbits." Archives of Orthopaedic Trauma and Surgery **120**: 587-591.

168. Enzyme Nomenclature (1992). San Diego, Academic Press.

169. Eyre, D. (2002). "Articular Cartilage and Changes in Arthritis: Collagen of Articular Cartilage." Arthritis Research **4**: 30-35.

170. Knudson, C. B. and W. Knudson (2001). "Cartilage Proteoglycans." Cell and Develepmental Biology **12**: 69-78.

171. Albertini, R., S. Rindi, A. Passi, A. Bardoni, R. Salvini, G. Pallavicini and G. De Luca (1996). "The Effect of Cornea Proteoglycans on Liposome Peroxidation." Archives of Biochemistry and Biophysics **327**(2): 209-214.

172. Campo, G. M., A. Avenoso, S. Campo, A. Ferlazzo, D. Altavilla, C. Micali and A. Calatroni (2003). "Aromatic Trap Analysis of Free Radicals Production in Experimental Collagen-Induced Arthritis in the Rat: Protective Effect of Glycosaminoglycans Treatment." Free Radical Research **37**(3): 257-268.

173. Reinholz, G. G., L. Lu, D. B. F. Saris, Y. M. J and S. W. O'Driscoll (2004). "Animal Models for Cartilage Reconstruction." Biomaterials **25**: 1511-1521.

174. von Rechenberg, B., M. K. Akens, D. Nadler, P. Bittmann, K. Zlinsky, A. Kutter, A. R. Poole and J. Auer (2003). "Changes in Subchondral Bone in Cartilage Resurfacing - an Experimental Study in Sheep Using Different Types of Osteochondral Grafts." Osteoarthritis and Cartilage **11**: 265-277.

175. Montgomery, D. C. (1991). Design and Analysis of Experiments (Third Edition). New York, John Wiley and Sons.

176. Nelson, P. R. Design and Analysis of Experiments. Handbook of Statistical Methods for Engineers and Scientists (Second Edition). H. M. Wadsworth. New York, McGraw-Hill**:** 15.1-15.143.

177. Peltier, M. R., C. J. Wilcox and D. C. Sharp (1998). "Technical Note: Application of the Box-Cox Data Transformation to Animal Science Experiments." Journal of Animal Science **76**: 847-849.

178. Hayter, A. J. (2002). Probability and Statistics for Engineers and Scientists (Second Edition). Pacific Grove, CA, Duxbury (Wadsworth Group).

179. Ochsner, M. (1997). "Photophysical and Photobiological Processes in the Photodynamic Therapy of Tumours." Journal of Photochemistry and Photobiology B: Biology **39**(1): 1-18.

180. Li, K. W. and R. L. Sah (2003). Biomechanical Implications of Implant Press-Fit in Cartilage Repair. Proceedings of the 49th Annual Meeting of the Orthopaedic Research Society, New Orleans, LA **28**: 653.

181. Aeshlimann, D., P. Lyons, T. Masterlark, K. Hyashi, B. Graf and R. Vanderby (2000). Repair of Cartilage Defects with Autogenous Osteochondral Transplants (Mosaicplasty) in a Sheep Model. Proceedings of the 46th Annual Meeting of the Orthopaedic Research Society, Orlando, FL **21**: 183.

182. Hunziker, E. B. (1999). "Articular Cartilage Repair: Are the Intrinsic Biological Constraints Undermining This Process Insuperable?" Osteoarthritis and Cartilage **7**(1): 15-28.

183. An, H. and R. Friedman (1999). Animal Models in Orthoeaedic Research, CRC Press.

184. Dell'Accio, F., J. Vanlauwe, J. Bellemans, J. neys, C. DeBari and F. P. Luyten (2003). "Expanded Phenotypically Stable Chondrocytes Persist in the Repair Tissue and Contribute to Cartilage Matrix Formation and Structural Integration in a Goat Model of Autologous Chondrocyte Implantation." Journal of Orthopaedic Research **21**(1): 123-131.

185. Hunziker, E. B. (2001). "Growth-Factor Induced Healing of Partial-Thickness Defects in Adult Articular Cartilage." Osteoarthritis and Cartilage **9**(1): 22-32.

186. Hunziker, E. B. and I. M. K. Dreisang (2003). "Functional Barrier Principle for Growth-Factor-Based Articular Cartilage Repair." Osteoarthritis and Cartilage **11**(5): 320-327.

187. Mainil-Varlet, P., S. Grogan, W. Mueller, C. Saager and R. Jakob (2001). "Articular Cartilage Repair Using a Tissue-Engineered Cartilage-Like Implant: An Animal Study." Osteoarthritis and Cartilage **9**: S6-S15.

188. Pufe, T., K. Scholtz-Ahrens, A. Franke, W. Peterson, R. mentlein, D. Varoga, B. Tillman, J. Schrezenmeir and C. Gluer (2003). "The Role of Vascular Endothelial Growth Factor in Glucorticoid-Induced Bone Loss: Evaluation in a Minipig Model." Bone **33**(6): 869-876.

189. Han, C. W., C. R. Chu, N. Adachi, A. Usas, F. F. H, J. Huard and Y. Pan (2003). "Analysis of Rabbit Articular Cartilage Repair after Chondrocyte Implantation Using Optical Coherence Tomography." Osteoarthritis and Cartilage **11**(2): 111-121.

190. Rahfoth, B., J. Weisser, F. Sternkopf, T. Aigner, K. von der Mark and R. Brauer (1998). "Transplantation of Allograft Chondrocytes Embedded in Agarose Gel into Cartilage Defects of Rabbits." Osteoarthritis and Cartilage **6**(1): 50-65.

191. Reddi, E. and G. Jori (1988). "Steady-State and Time-Resolved Spectroscopic Studies of Photodynamic Sensitizers: Porphyrins and Phthalocyanines." Reviews of Clinical Intermediates(10): 241-268.

192. Rosenthal, I., C. M. Krishna, P. Riesz and E. Ben-Hur (1986). "The Role of Molecular Oxygen in the Photodynamic Effect of Phthalocyanines." Radiation Research **107**: 136-142.

193. Kimel, S., B. J. Tromberg, W. G. Roberts and M. W. Berns (1989). "Singlet Oxygen Generation of Porphyrins, Chlorins, and Phthalocyanines." Photochemistry and Photobiology **50**(2): 175-183.

194. Mechanic, G. L. (1998). Process for Crosslinking Collagenous Material (Patent Number 5,854,397). United States, University of North Carolina at Chapel Hill.

195. Sullivan, L. G., T. Hasan, M. Wright, H. J. Mankin and C. A. Towle (2002). "Photodynamic Treatment Has Chondroprotective Effects on Articular Cartilage." Journal of Orthopaedic Research **20**(2): 241-248.